Antibiotic-Loaded Drug Delivery Platforms: Theory, Structural Evolution, and Elution Characteristics

by

Lydia Marilyn Mensah

A dissertation submitted in partial fulfillment
of the requirements for the degree of
Doctor of Philosophy
(Materials Science and Engineering)
in the University of Michigan
2021

Doctoral Committee:

Professor Brian J. Love, Chair
Assistant Professor Aidin EslamPour
Assistant Professor Ashwin Shahani
Assistant Professor J. Scott VanEpps

Lydia Mensah

lymensah@umich.edu

ORCID iD: 0000-0003-3238-2712

Dedication

This dissertation is dedicated in loving memory of Ifedapo Adebamiji, Dr. Ella Kelley, and Charles Barnes Acquah Quaigraine. I am so grateful and thankful to have had you all in my life. Though you were not here to start this journey with me, the constant thought of you has comforted me going through; it is only right that I have you with me in the end.

Acknowledgements

My matriculation through graduate school has been impacted and influenced by so many and for that I am so grateful. The love, support, and encouragement from my family, friends, and colleagues made the easy days, a cake walk, and the hard days, bearable.

I thank God for giving me wisdom, understanding, knowledge, counsel, fortitude, piety, and fear of the Lord. These seven virtues have given me a sense of serenity in what felt like constant chaos. My journey has been a true testament of God's faith and mercy in my life.

I sincerely want to thank my advisor, Brian Love, for his mentorship and friendship throughout this time. I thank you for welcoming me into your group and being invested in my success. Your patience, understanding, and willingness to be invested in my success along with me has been instrumental in my personal growth and professional development. I also like to thank my committee members, J. Scott VanEpps, Aidin Esalm Pour, and Ashwin Shahani. This work would not have been possible without your guidance, direction, and resources. A special thanks to Dr. Esalm Pour and Dr. VanEpps. Whether it was bringing me bags of antibiotic in the hospital to allowing me to come into your lab during a pandemic to figure things out, I am grateful that you allowed me to learn from you.

Additionally, special thanks to Dr. Andre Thompson who has cheered me from the lab to the court. Thank you for always being one call or text away and being the greatest teammate! I also like to thank other current and former members of The Love Group, notably, Julie Rieland, and Jed Forester without your help running what appeared to be endless DSC samples, fixing equipment, and trying our hand in pandemic horticulture.

There are not enough words to express my gratitude for my family and friends. Thank you to my parents, Patrick and Elizabeth Mensah, for providing me with life and showing me how to be a servant leader. Thank you to my siblings, Paula, Patricia, and Patrick for being my first friends and always providing joy and laughter to my life. Thank you to my three God-children Adriana, Alex, and Ava, for bringing so much light into my life and once again making me the odd letter out. Thank you to Rev. J. Asare-Dankwah for always being there for me and praying for and with me. Thank you to my best friend Faith Benford for reminding me to stop dance and enjoy the music. Thank you to my roommate Sadé Richardson for always being there for support from day one and always willing to go on an adventure with me. The escapes from what felt like a never-ending journey, gave me motivation to get through, and anticipate the next adventure. Lastly, to the group chat that kept me, I have come a long way from that first BBQ shaming, and you all have never turned your back on me. Thank you for serving as an inspiration for me to keep going and as the fuel to my everything in Michigan. When I came to this school, I barely knew one person, and now I can say I have a whole new family. I am in awe of all of y'alls accolades and accomplishments. I pray that I am as good a friend to y'all, as y'all have been to me.

"Asem papa bia mate, Oye Oye,

Asem papabia mate ne se Yesu ye odo,

Oye, Oye Ampa,

Oye, Oye, Oye

Oye, Oye, Me kra sore na to ndowm se oye

Agya Nyame ye, Oye Ampa

Oye, Oye, Oye…"

Table of Contents

List of Tables

List of Figures

List of Equations

Abstract

The occurrence of periprosthetic joint infections (PPJI), a major complication of joint arthroplasty, is rising. Current treatment involves the use of antibiotic-loaded bone cement (ALBC) intraoperatively and postoperative intravenous drug delivery. Amphiphilic block copolymers can be a localized drug delivery system for prophylactic and supplementary treatment of PPJI when loaded with antibiotics to overcome the limitations of ALBC and systemic drug delivery. In this thesis, current PPJI treatments were evaluated, and the structural evolution and bacterial growth inhibition characteristics of antibiotic-loaded Polyoxyethylene-polyoxypropylene-polyoxyethylene (PEO-PPO-PEO) triblock copolymers were investigated.

A number of clinical studies were examined to identify those in which controlled drug release or mechanical behavioral assessments were conducted on ALBC. Anecdotal evidence suggests that ALBC can help eradicate or delay the onset of infections, but quantifying the response functionality is challenging. The ALBC study focused on vancomycin (VAN)—which is more commonly proscribed for staphylococcal osteomyelitis—in part due to its higher potency relative to gentamycin. The studies indicate that large fractions (>99%) of loaded VAN are sequestered in the bulk matrix of cement and are not labile once the cement has set due to high molecular weight (1449.3 g/mole) and glassy behavior. VAN fluence measurements ranged from 1 to 283 $\mu g/cm^2 hr$. The initial strength of the samples ranged from 52 to 96 MPa. Efforts to raise the elution rate by increasing drug loading reduced cement strength. Smaller drug molecules and more gel-like immobilization matrices with lower glass transition temperatures offered higher potential for larger and more comprehensive drug elution.

Differential scanning calorimetry was used to probe the thermophysical properties of 25% F127 gels loaded with ciprofloxacin (CIPRO) (0.05-0.2%), VAN (0.8-5%), gentamicin (GM) (0.2-0.8%), and cefepime (CEFE) (2-10%). CEFE had the greatest effect on $T_{micelle}$ with a range of ~3-8 ºC with respect to decreasing concentration. GM showed the smallest effect with a range of 8.5-10.5 ºC. CIPRO had an invariant effect over the concentrations tested, but decreased $T_{micelle}$ by ~2.5 ºC. CIPRO also showed an invariant effect on the endotherm energy between concentrations after the initial decrease to 3.4 $J*mol^{-1}$. CEFE showed an athermal micellization process as the concentration of CEFE increased. Additionally, GM and VAN showed an invariant effect on the endotherm energy. Dynamic mechanical analysis of 25% F127 loaded with CIPRO were investigated to probe the kinetics of the gel transition, which occurred up to 7 ºC lower than the neat sample.

Cell culture assays were used to probe whether antibiotic-loaded amphiphilic gels act as a functional antimicrobial. Additionally, modification of the traditional bacterial plate culture assay by introducing a void within the agar allowed insight on the properties of an injectable plug. Zone of inhibition (ZoI) and bacterial growth inhibition were used as qualitative and quantitative assessments. VAN and GM loaded amphiphilic gels had a range of 3.00-3.90 cm and 3.50-5.70 cm, respectively. Bacterial growth inhibition curves showed that VAN decreased maximum optical density (OD) by 70-80%. Gompertz growth model was used to summarize the OD curves and determine the growth rates and lag times for 0-5% VAN.

This dissertation yielded a characterization of the changes in thermophysical properties and insight on elution and antimicrobial activity of antibiotic-loaded F127 gels. A greater understanding of the interactions between amphiphilic copolymer solutions and dissolved solutes was achieved to probe their use as a localize drug delivery vehicle.

Chapter 1 Introduction

1.1 Overview/Motivation

These days most medicines are administered orally in the form of mass manufactured capsules or tablets. Some drugs are produced in an array of steps that start with research and development (R&D) and end with a final pill, while others, such as solubilized ampoules, injectables, compound mixtures, and compound dispersions, are administered via other means. Current drug manufacturing practices are costly and can take years to progress from beginning to final stages. However, recent work by The Human Genome Project has resulted in a push to design individualized pharmaceuticals, which require expedited development periods when treating diseases like cancer due to shorter patient lifespans.

The ideal drug delivery system should be an inert system that is biocompatible, mechanically sound, comfortable, durable, simple to use, low cost, and easy to fabricate. As such, research is needed to (1) help change the way common pharmaceuticals are produced, (2) process individualized drug development to reduce the amount of time and money spent on developing medicines, and (3) increase the number of patients who can be treated. The key challenge to developing the ideal drug delivery system is aqueous drug solubility. Many drugs since they are organic molecules are fat soluble; however, they also need to be bioactive in a system that is largely ionic and aqueous. If the aqueous solubility of a drug is low, causing it to be non-functional at its solubility limit, then other methods should be employed to solubilize the drug while maintaining its activity.

Hydrogels are three-dimensional cross-linked networks of water-soluble polymers, and they can be formed from natural or synthetic sources. They can be formulated into a variety of physical forms due to their high water content, mechanical compliance, and biocompatibility [1]. Hydrogels can be physically or chemically cross-linked, which are two methods used to fine-tune their mechanical properties. The porous 3D structure of hydrogels resembles that of living tissue, which allows these gels to have many uses as cell-immobilized tissue engineered matrices, biodegradable structures in regenerative medicine, and barrier materials such as hydrophilic absorbent wound dressings, among others [2]. Hydrogels are also used in sustained-release drug delivery systems where pharmaceuticals can be more soluble when encapsulated into hydrogel than when dissolved in saline.

The Love research group has worked on several different forms of hydrogel structures including those based on amphiphilic polyether-based copolymer micelles, those based on alginates, and those created from photopolymerized resins (e.g., methacrylate grafted hydrogels based on hyaluronic acid, reactive dimethacrylates and diacrylates). The group's focus has been on understanding the structural evolution of these gels and creating kinetic models to describe gel formation and gel performance.

The goal of this dissertation was to construct porous 3-D biocompatible architectures that would facilitate the formations of micelles within hydrogels. In particular, I engineered hydrogels designed to keep drugs contained within these structures until they reached localized delivery at an active treatment site. At the active site, the drug can then elute into the system to prevent whatever infection is present. I addressed this goal by focusing on functional characterization and process development to make better use of effective—but poorly solubilized—pharmaceuticals.

1.2 Periprosthetic Joint Infection

Targeted drug delivery, also called smart drug delivery, affects only a small, specified area rather than exposing the entire body. The goal of this delivery approach is to prolong, localize, and maintain a protected drug interaction with the diseased tissue or bone, as in the case of osteomyelitis and periprosthetic joint infections. Periprosthetic joint infection (PPJI) is one of the major challenges currently faced in orthopedic surgery [3–7]. Yearly, the complications and infections are on a rise after joint arthroplasty procedures, as well as the cost associated and treatment time [5]. The current method of treatment involves arthroplasty implant resection, thorough surgical debridement of synovial tissue, and a period of 6 to 8 weeks of intravenous (IV) antibiotic therapy. For IV therapy to be successful, the area needs to be highly vascularized to maintain the local antibiotic dose and to maintain a concentration of drug above the minimum inhibitory concentration (MIC). A current treatment protocol for PPJI involves the use of antibiotic-loaded bone cements.

There are commercial formulations of certain drugs—some of which have been successful—that formulate at specific concentrations into bone cement. However, the dosage or type of the antibiotics in these premade antibiotic bone cements are often insufficient for the treatment of the infections. For example, most premade antibiotic cement combinations include aminoglycosides, such as gentamicin or tobramycin, as 1 g per one bag of cement. Most osteomyelitis or periprosthetic infections require antibiotics that have stronger gram positives coverage, such as cephalosporins or vancomycin, with higher dosages (3-4 g per bag). The premade antibiotic cement combinations are generally inadequate for the treatment of osteomyelitis or periprosthetic joint infection. The antibiotic release from antibiotic cement combination is also unpredictable. Another problem is insufficient blood supply to the infection

area due to additional harmful conditions such as arteriosclerosis, diabetes, or microvascular thrombi. There is a need to consider new paradigms and quantitative assessment tools to optimize drug/material combinations that offer more relief in addressing PPJI and other deep bone infections.

1.2.1 Challenges in PPJI

A challenge in infection treatment is ensuring that the drug therapy ends up in the right place and remains effective to treat for an adequate amount of time to eradicate the infection. Current PPJI treatment protocols rely on systemic or local drug administration routes. The choice of either route is influenced by many factors, including convenience, patient status (stable/unstable), nature of drugs used for treatment (e.g., some drugs, like insulin, are only effective by one route), age, and gastric pH. Local drug delivery is the simplest administration route because the drug is delivered and localized at the active site [8]. In comparison, systemic administration has two routes for drug absorption, and there are two options for delivery, which are shown in Figure 1.1. Enteral routes involve drug absorption through the gastrointestinal tract and parenteral routes are routes around the gastrointestinal tract [8]. Systemic systems are more commonly used due to the ease of use; however, systemic delivery may result in suboptimal drug concentration and may be ineffective in treatment [9]. Systemic drug delivery systems based on oral ingestion or IV spike introduction often result in the concentration of the drug to peak, plateau, or decrease depending on the pharmacokinetic (PK) and pharmacodynamics (PD) observed.

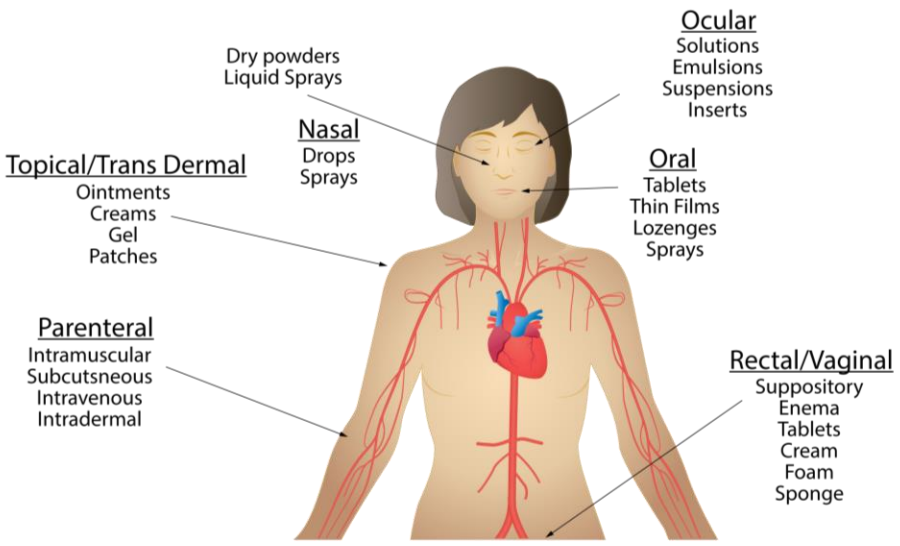

Figure 1.1 Some commons routes and methods for drug administration. Injections can be parenteral or subcutaneous, etc. Some routes, like enteral (not listed), overlap. For example, oral and a feeding tube are both types of enteral. Additionally, vaginal could be local (e.g., cream for yeast infection) or systemic (e.g., estradiol tablets for menopause).

PD can be described as what a drug does to the body and PK can be described as what the body does to a drug. PD/PK is the study of effects of drugs on the body and the movement of drugs into, though, and out of the body. The two help explain a drug's effects on the body through the relationship between dose and response. Drug effects can be viewed as a function of dose and time, where dose and potency simultaneously increase, reaching a maximum efficacy overtime. Drug dosing guidelines take into consideration PD and PK so that antibiotic dosing can be personalized to ensure bacterial death. PD also involves the pathogen, where the susceptibility of a pathogen to antibiotic killing/inhibition varies. The concentration of a drug at the site of infection determines the drug's effect. For example, the minimum concentration of a drug needed to inhibit bacterial growth is referred to as *minimum inhibitory concentration (MIC)*, which is a PD parameter. In systemic drug delivery, a maximum concentration needs to be maintained in the blood so that the local site is above MIC. Contrarily, local delivery requires a lower concentration of drug to maintain MIC.

Drug solubility plays an important role in both drug delivery routes. When drugs enter the body via either route, they can be effectively absorbed and used for treatment at the active site. Some drugs are dispersed in their salt formation to improve solubility and dissolution and/or are packaged with other additive to help improve their stability, such as dextrose and saline [10,11]. When delivering antibiotics, often a systematic approach is taken by delivering drug via intravenous delivery (IV) [12]. Through the IV administration route, the circulatory system of the entire body is affected. In addition, delivery using IV often causes alteration of the natural microbiome depending on its susceptibility to the antibiotic used.

1.2.2 Controlled Drug Delivery as an Alternative

Controlled drug delivery allows the delivery of a drug at a pre-determined rate, locally or systemically, for a specific period and integrates drug-encapsulating devices that allow the pharmaceuticals to be released at set rates for delivery times ranging from days, months, or years. Amphiphilic copolymers, such as those from Polyoxyethylene-polyoxypropylene-polyoxyethylene (PEO-PPO-PEO) triblock copolymers, can form micelles and encapsulate both hydrophobic and hydrophilic drugs, thus increasing solubility and facilitating targeted delivery. Amphiphilic copolymers are also comprised of a controlled release mechanism.

1.2.2.a Amphiphilic copolymer gels for localized treatment

I aimed in this dissertation to investigate the use of an antibiotic-gel drug delivery system that undergoes colloidal crystallization to study the antibiotic release from the crystalized gel form. This drug delivery system can be optimized to perform without the use of intravenous catheters by introducing a localized injection to self-assembly into a soft gel *in vivo* as depicted in Figure 1.2. A localized injection allows for free range of joint motion because the gel is soft and allows the affected area to be loaded with a lower concentration of antibiotic for effective

treatment. Compared to ALBC, localized injection makes it easier to achieve MIC and does not require as high of a concentration as an intravenous system that would negatively affect other systems in the body. These effects can include alterations in the microbiome (e.g., gut, skin, oral, vaginal), opportunistic infections (difficile), an increase potential for development of antibiotic resistance, and off-target effects of antibiotics (renal and hepatic toxicity, allergic reactions, etc.). If additional doses are needed, a physician or mid-level provider with expertise in the field can administer an injection.

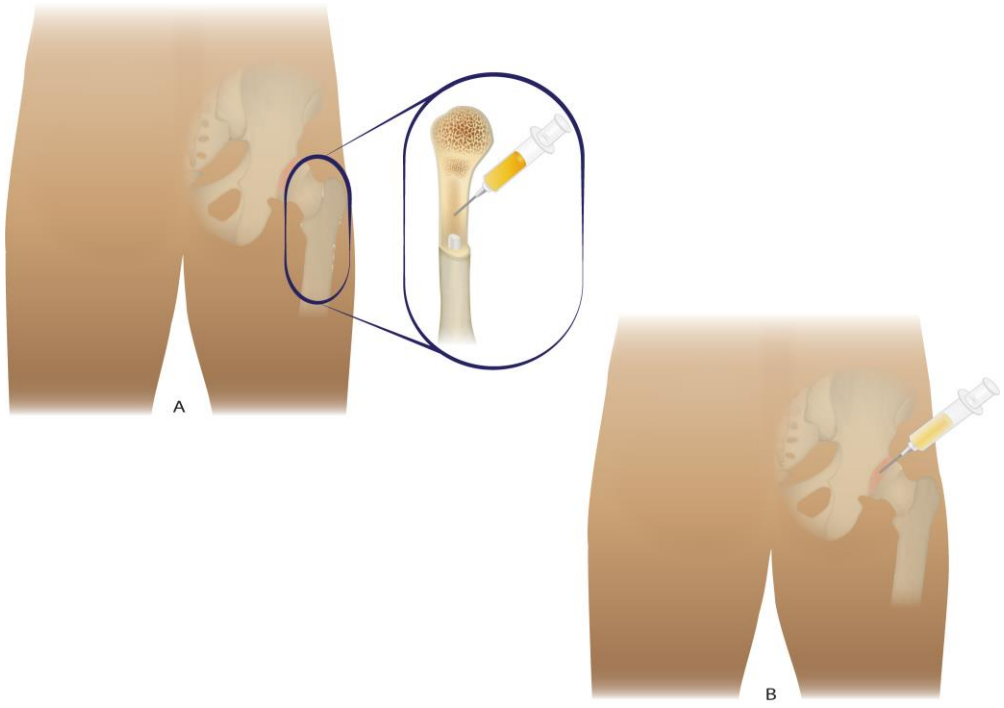

Figure 1.2 Illustration of localized injection of amphiphilic copolymer. The injection can be delivered in two locations (A) into the bone marrow canal (B) into the joint space.

Chapter 2 Meta-Analysis of Bone Cement

2.1 Introduction

Methacrylate-based powder/liquid bone cements have revolutionized orthopedic treatment and have long been part of clinical practice linked with total joint arthroplasty procedures and in vertebral compression fracture stabilization [13–16]. Co-formulating bone cements with antibiotics and other drugs has also allowed for their use as passive drug delivery systems. The use of these systems has resolved infections, albeit without standards on either the amount of antibiotic in the cement or the mixing and insertion conditions [17]. Some commercial antibiotic-loaded cements are available, but only in specific concentrations. As a result, surgeons must formulate their own mixtures in the operating room if the desired antibiotic/cement combination is not available.

When co-formulating antibiotics within bone cements, there are instances where the antibiotic interferes with cement performance. First, it is possible that the antibiotic could react with the radicals and lead to a slower polymerization rate [18–20]. Second, the antibiotic could plasticize the cement thereby softening it, reducing its glass transition temperature, and increasing its viscoelastic response. Lastly, as the antibiotic diffuses through the matrix, voids and pores could form that could coalesce resulting in lower cement strength the longer it is installed. These viscoelastic and structural changes are more pronounced at higher mass loadings of antibiotics. The cement is likely weaker with increasing drug concentration and will likely

worsen with immersion time *in vivo*, although not every drug infused cement mixture has a strength requirement.

There are published clinical studies in which antibiotic-loaded bone cement (ALBC) spacers have released sufficient amounts of antibiotic to contain or eradicate raging infections often in poorly vascularized and other infection prone local regions *in vivo* [7,21]. The inclusion of antibiotics in the cement allows the cement to be both a controlled drug release system and structural stabilizer. Studies using commercial formulations of gentamicin- (GM) loaded cements and off-label uses of GM, tobramycin (TM), vancomycin (VAN), and combinations thereof, among others, have shown success [6,7,16,8–15]. In terms of joint infections, the preferred protocol has used VAN as the pathogens found in these infections have commonly shown methicillin resistance, and VAN has proven effective [30]. More generally, the choice of antibiotic is determined by a clinical assessment of the infection before identifying a treatment, and combination treatments are often also prescribed. It is hard to argue with clinical outcomes, but the size, virulence, and type of infection require decisions about (a) spacer location and shape, (b) the antibiotic type, (c) loading concentration, and (d) drug distribution in the cement; all which affect efficacy. MIC is a regulatory standard with respect to antibiotics and corresponding pathogens; however, there is a need to determine the effective dose of the antibiotic administrated to achieve concentrations above MIC. Relatedly, the protocols for performing such assays require an assessment of the antibiotic distribution in the cement.

2.1.1 Controlled Release from Antibiotic-Loaded Bone Cements (ALBCs)

An integral feature of antibiotic-loaded cements is localized antibiotic release to eradicate a nearby infection. Higher drug mobility (diffusivity) and higher antibiotic concentration correlate with a higher overall flux [22-25]. It is plausible that surface versus bulk effects are

important if antibiotics are not bioavailable deep in the bone cement. The cement could be filled with higher levels of antibiotic, but much of it could remain sequestered.

In quantitatively probing cement-based antibiotic mass transfer, several features need to be considered. For a specific mass of polymerized antibiotic-infused cement, the dimensions of the specimen regulate the surface area presented for mass transfer to occur. Mass transfer from a cube is different from mass transfer from a sphere of the same mass due to surface area. The time element also needs consideration. If permeability is mostly derived from the surfaces, then the mass transfer of antibiotic decreases as they are depleted relative to the bulk. The rate of mass transfer of drug release with time follows from Mircioiu et al. [32] as shown in Equation 2.1,

$$V(t) = J(t)A(t) \qquad \text{Equation 2.1}$$

where *V* is the drug flow rate (mass/time) from the cement into the medium, *J* is a time dependent mass flux, and *A(t)* is the surface area of the cement. The surface area can be dynamic as well, particularly for dissolving matrices. For bone cements, the dimensions are invariant. The total dose, D released [32], is identified in Equation 2.2.

$$D = A * \int_0^\infty J(t)dt \qquad \text{Equation 2.2}$$

Embedded in the determination of a drug's flux is (a) its size, (b) its relative permeability within the polymer matrix, (c) the distribution within both the cement and the surrounding medium, and (d) the presence of any pores or cracks in the cement allowing drug leakage.

Smaller antibiotic molecules might have higher molecular mobility as compared to large, bulkier molecules migrating through the cement. The molecular mobility of the cement is regulated by the glass transition temperature of the cement that is typically higher than body temperature. Comparing antibiotic size, vancomycin (MW = 1485 g/mole) might be less mobile than gentamycin (MS = 478 g/mole) within the cement [33–35].

As shown in Equation 2.3, if X is the mass of antibiotic in the cement, a relative mass transfer efficiency, E, is defined as,

$$E = \frac{D}{X} \qquad \text{Equation 2.3}$$

where *E* represents the ratio of total drug conveyed (*D*) relative to what's formulated (*X*) into the cement. The antibiotic release from gentamicin loaded at 1 g in 40 g of cement (a 2.5% loading) might not have the same efficiency as at 10% loading.

Figure 2.1 represents an idealized response of antibiotic elution exposed to an inert receiver solution. The antibiotic-loaded bone cement sample has volume, V, a corresponding surface area, SA, and loaded at fractional antibiotic mass/cement mass ratio. The receiver solution collects dispersed antibiotic either from its surface or from bulk diffusion from the ALBC.

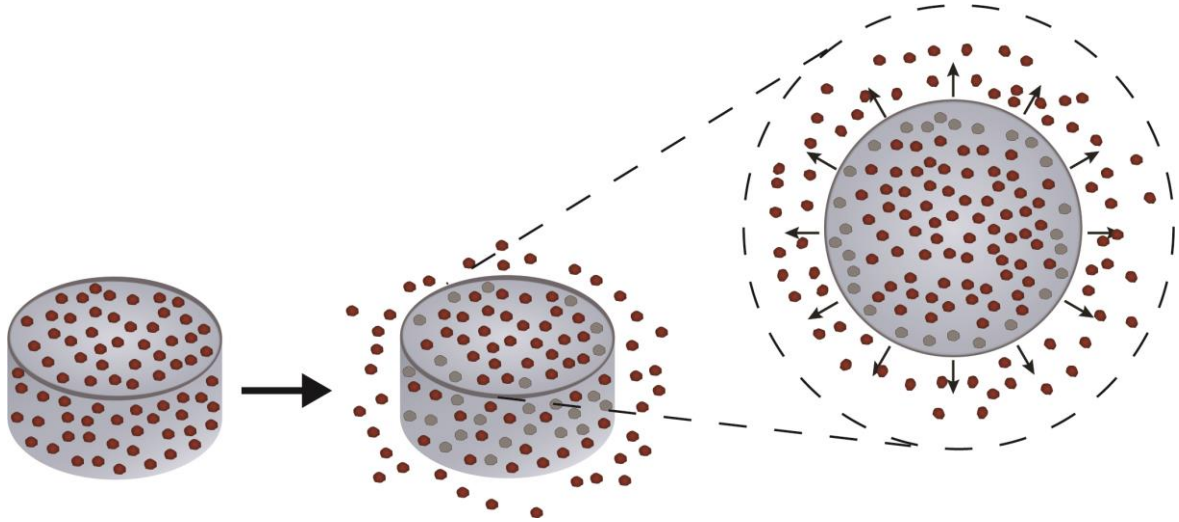

Figure 2.1 Illustration of antibiotic release from a drug-eluting bone cement (Red corresponds to antibiotic elution out and grey to the remaining voids in the cement). When the ALBC is introduced, small molecule antibiotics percolate from the cement surface and convey into the surrounding medium. While release can come from crevices and cracks on the ALBC surface, most of the antibiotic is sequestered in the bulk of the cement.

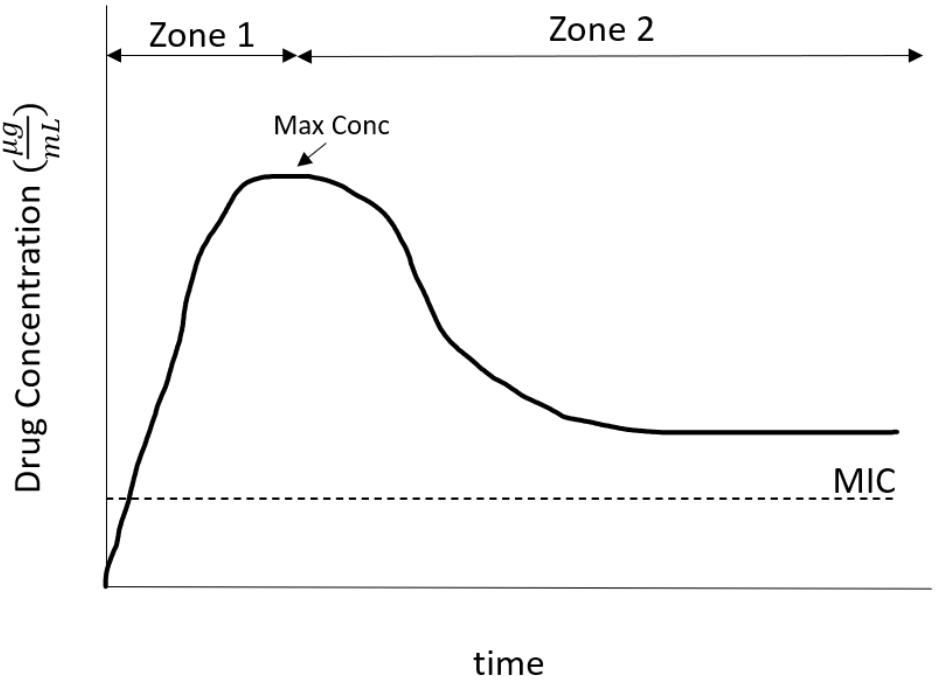

Figure 2.2 This shows idealized dynamic drug elution from an ALBC. The rise in the concentration in the tissue is regulated by the antibiotic release. A burst release corresponds to a steeper slope of initial drug release. The goal is to release enough antibiotic (Zone 1) to overcome the minimum inhibitory concentration (MIC). In a real tissue, the antibiotic concentration is also reduced by dispersion and metabolism. At the peak, the release is balanced by metabolism and dispersion. In Zone 2, the exhaustion of the ALBC release reduces local drug availability.

Regardless of the sample dimensions, there is a threshold dose to eradicate an infection, referenced as a minimum inhibitory concentration (MIC) [36–38] as shown in Figure 2.2. Engineering the dimensions of the plug can optimize the surface area/volume ratio for appropriate drug dosing. Ideally, a constant antibiotic flux is achieved overtime to account for the balance between release and metabolism.

The ideal flux profile releases enough drug above the MIC long enough to eradicate infection. The antibiotic release conceptually can be one of several dynamic responses as shown in Figure 2.3. The antibiotic could release as a burst (the red dashed curve), with further release blocked by the cement structure. If the antibiotic is permeable in the cement, then diffusion-related dosing is achievable (the green solid line). It is also possible that a soluble shell allows for a delayed release resulting in an induction time for core-level release (blue dotted curve). The

outer shell layer can be made up of a material susceptible to physical and/or chemical degradation. Once the outer shell erodes, the drug in the core can release.

Factors that regulate controlled release antibiotic flux include the drug size; the glass transition temperature of the cement; the temperature of the release response; and the presence of holes, cracks, and other surface asperities [3,39–41]. For example, Masri et al. correlated the surface area and elution of tobramycin from bone cement blocks [42]. They also showed that increased roughness raised TM release [42].

Many efforts have assessed infection clearance by ALBCs [6,15,43–45]. Other studies have probed how drug concentration, mixing quality, and polymerization conditions affect drug release [14,29,46,47]. The current study compiles strength and permeability assessments based on prior published work and derives prevailing conclusions based on the results.

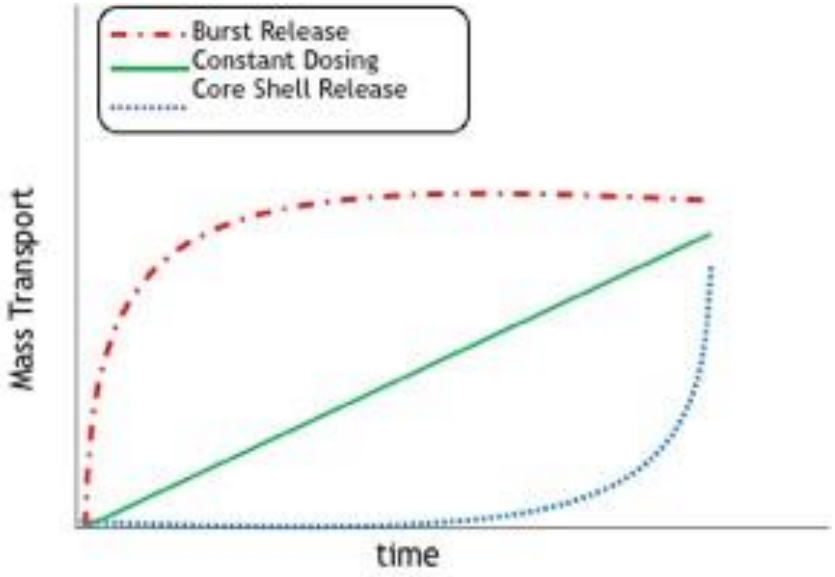

Figure 2.3 Shows three proposed mass release (V(t)) mechanisms. One is where there is an initial rapid “burst” where most drug is released rapidly (red dashed curve). It is also possible that the flux is constant, (green solid line) or a delayed core-shell release that is followed by a burst as cracks form (blue dotted curve).

2.1.2 Orthopaedic Infection Treatment

As the number of orthopaedic surgeries has risen, so has the number of infections [4,6,13]. The rate of infection in hip and shoulder is <1%, ~2% for knee replacement, and 2-10% for the elbow [6]. These surgeries are open procedures where a large incision allows the surgeon space to operate. Size of the incision is important for the infection, but the most important issue with arthroplasty is the foreign material in the body, which increases the possibility for infection. Bacteria can enter the blood stream and sit on the foreign material, which does not have blood flow. Then bacteria begins to grow and multiply creating biofilm and causing infection. Most arthroplasty infections develop from bacterial growth and are hematogenous.

PPJI is one of the most common reasons for revision surgery, accounting for ~15% of hip and 25% of knee total joint revisions [4]. Currently, two approaches exist for treating joint infections: incision and drainage (I & D), which occurs in a single step, and a more involved two-step procedure that includes (a) resection of all the foreign material including the arthroplasty implants, (b) infection control via systemic and local antibiotic therapy, and (c) revision surgery to place the new implants after infection eradication. Infections occur at various time points perioperatively and are classified as early (0 to 2 months), delayed (3 to 24 months), or late (any time after 24 months). I & D can be completed with or without exchange of the hardware, and is more conservative and traditional among PPJI options with only 50% success rate [6]. When infections are found early, bacterial biofilm formation is incomplete on the prosthetic implant and a thorough I & D can resolve joint infections. When infections are found later, biofilm formation is more complete, and treatment requires hardware removal. New paradigms and quantitative assessment tools are needed to optimize drug/material combinations that address PPJI [4,6,15,44,45,48].

Orthopaedic-related infections involve several common pathogens including *Staphylococcus aureus* (Gram-positive) and *Enterobacteria* (Gram-negative) [15]. Once pathogens are identified, a corresponding antibiotic therapy is prescribed. For example, vancomycin and cephalosporins inhibit growth of gram-positive bacteria and clindamycin is more effective for both Gram-positive and Gram-negative bacteria [15]. However, more antibiotic-resistant strains of bacteria require other agents for effective eradication [24,44,49,50].

There are many elements relating to exploring new modalities in treating joint infection, including what antibiotics are available, what loading level is needed, and what type of release mechanism is used. This meta-analysis compares studies where ALBCs are loaded with several antibiotics commonly used to eradicate periprosthetic joint infection (PPJI) both in terms of potential drug release and residual strength of the spacer as it releases antibiotic.

The content covered in this chapter was submitted and published in *Materials Science and Engineering: C* [51].

2.2 Research Paper Selection Criteria and Protocol

Papers were identified that evaluated quantifiable measurements of dynamic drug elution combined with strength assessments by tension, compression, or shear for antibiotic/bone cement combinations. The primary drug of interest was vancomycin given its common use for joint infections, although to gauge the effect of drug size, data from other papers were used that showed similar elution results using gentamicin, a much smaller drug. Papers using a clinical infection grading of *in vivo* studies were omitted in addition to those focused on combination therapies including multiple antibiotics to enhance eradication.

The elution and compressive strength data were extracted from Bitsch et al. [25], Lee et al. [52], Bishop et al. [22], and Galvez-Lopez et al. [18]. Next, determinations of surface area,

flux, and mass release rates were made. The goal was to resolve whether differences in antibiotic release depended on formulation, concentration, or other observables. When comparing to mechanical strength, links between formulation, flux, and strength were also made. Four articles contained relevant data that could be used for vancomycin, and three more were linked with gentamicin to assess strength. The resulting papers and their formulations are showcased in Table 2.1.

Research Group	Drug Tradename	Cement Type	Surface Area	Drug Loading	Cement Mass	Elution Sample Geometry
Bitsch et al.	Vancomycin Hydrochloride (VAN-HCl) / Aminoglycoside Gentamicin Sulphate (AGS)	Copal Spacem	17.66 cm^2	2 g, 4g, 6 g	60	Disk
Lee et al.	Vanco	Simplex P	9.42 cm^2	1 g, 4 g	60	Cylinder
	Lyo-Vanco	Palacos R	9.42 cm^2	1 g, 4 g	60	Cylinder
	Sterile	CMW	9.42 cm^2	1 g, 4 g	60	Cylinder
Bishop et al.	VAN-HCl	Palacos R	0.84 cm^2	0.50 g, 1 g, 2 g	60	Disk
Galvez-Lopez et al.	VAN / Gentamicin (GM)	Depuy	0.785 cm^2	1 g, 2 g	10	Spherical Beads
De Belt et al.	Gentamicin Sulphate (GS)	Palacos R / CMW3	1.17 cm^2	$8.3*10^{-4}$ g / $1.6*10^{-3}$ g	0.1	Disk

Table 2.1 Highlights the details on the construction of elution specimens. Included are the suppliers of vancomycin, gentamicin, loading amounts, and cement types used. All elution studies were done at 37 °C [18,22,25,52,53].

2.3 Antibiotic Release Profiles

From the studies with published relevant results, dynamic dose was extracted and presented in Figure 2.4 to showcase vancomycin elution overtime. For all drug/matrix combinations, vancomycin initially has a comparatively large release from the cement. Within

hours, there is a decay of vancomycin release into the receiver solution. An example dataset is shown in Figure 2.4 produced by Lee et al.; this ALBC combination conveyed only 0.15% (E = 0.0015) of the total fraction of vancomycin [52]. The initial burst of vancomycin is attributed to antibiotic adsorbed on or near the cement surface [22,52,54–56].

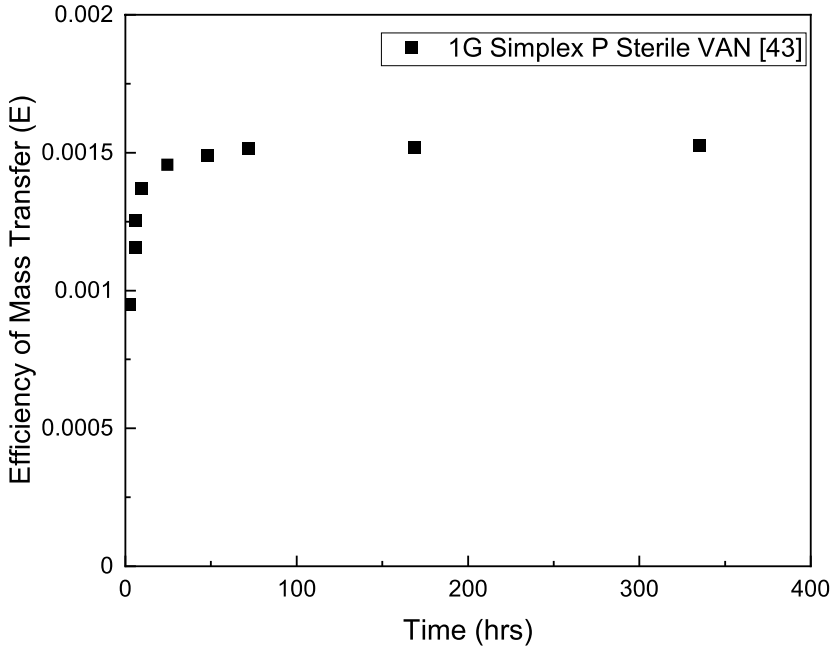

Figure 2.4 This representative graph shows the efficiency of mass transfer of VAN over 400 hours of drug release. Most release occurs over the first 20 hours and plateaus at a dose not much larger than the burst release [52]. This data was extracted from datasets captured from Lee et al. [52].

A typical depletion of antibiotic profile from ALBC results in a terminal plateau dose over the time scale of hours to days, shown in Figure 2.4. What is remarkable is the small total release of antibiotic overall. When the dose data is represented as a dynamic flux (see Figure 2.5), even after 10 days of release, the residual flux is ~10% of the peak flux. Whether the release rate is sufficient to be above the minimum inhibitor concentration in the surrounding medium is a challenge due to the difficulty in determining the efficacy of ALBC in patient specific infections without a standardized assay to address biofilm eradiation and other localized infections.

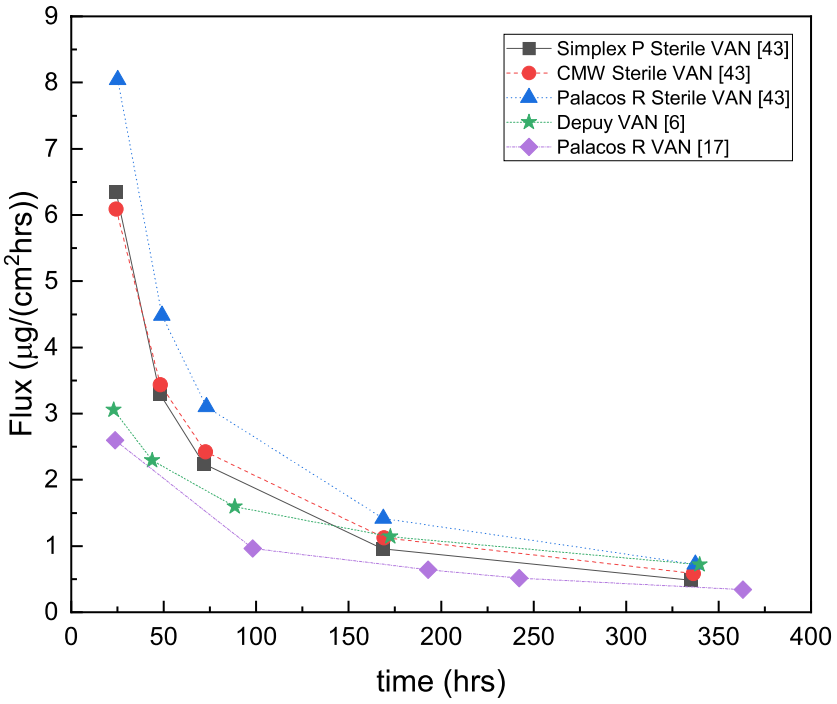

Figure 2.5 Selected data from 1G VAN ALBC elution studies comparing dynamic flux, J(t) [18,22,52]. When the spacer is introduced into the blank receiver solution at time zero. The first measurement always shows the peak release, followed by a sharp decay [18,22,52].

Loading the antibiotic at higher concentrations results in more antibiotic on the outer surfaces of the cement when implanted and higher total dose. The flux datasets were modeled as a two-phase exponential decay model based upon the sum of releases coming from two different regions in the cement as shown in Equation 2.4. The first decay represents the surface-bound vancomycin, and the subsequent drug release is lumped into the more retarded, sub-surface release influenced by voids created by the first decay.

$$J(t) = J_1 e_1^{-t/\tau_1} + J_2 e_2^{-t/\tau_2} \qquad \text{Equation 2.4}$$

Here, J_1 is the flux tied to the initial burst coming from the outer surfaces, J_2 is linked with drug release in the sub-surface, and τ_1 and τ_2 are the relaxation constants linked with each response. Figure 2.6 shows the vancomycin release decay for one representative dataset.

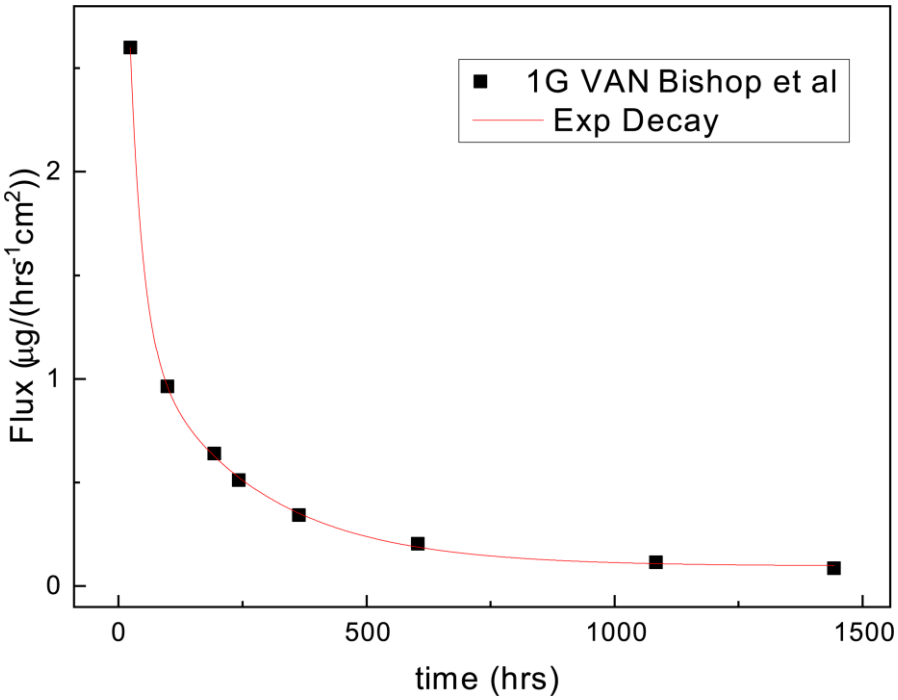

Figure 2.6 Representative dynamic flux measurements vs time for 1G Vancomycin in Palacos R cement used by the Bishop et al. group (datapoints) [22]. The curve represents a two-phase exponential decay based on Equation 2.4 (curve). The model adequately represents the changes in dynamic flux that arise with elution time. Initially, there is a large burst release. As the burst dissipates, a non-zero release is evident.

2.3.1 Burst Release Assessment

Table 2.2 summarizes average vancomycin release including the peak flux incorporating the sample geometry, total dose, and efficiency over the time frame of the elution experiments. When the efficiency of mass transfer is determined, drug release is very modest, at most 0.8% of the loaded drug eluted from the cement.

Paper	**Cement Type**	**Vancomycin Type & Content**	**Avg Max Flux, J(t)** $(\frac{\mu g}{cm^2 hr})$	**Avg Total Dose, D(t)** (μg)	**Avg Efficiency of Mass Transfer**	**#**
Bitsch et al. [25]	Copal Spacem	2G VAN-HCl	8.7	$5.3*10^3$	0.003	1
		4G VAN-HCl	14	$1.6*10^4$	0.004	2

		6G VAN-HCl	34	$2.9*10^4$	0.005	3
Lee et al. [52]	Simplex P	1G Vanco UCS	48	$1.3*10^3$	0.001	4
		1G Lyo-Vanco	125	$1.0*10^3$	0.001	5
		1G Sterile Vanco	38	$1.5*10^3$	0.002	6
		4G Vanco UCS	119	$5.4*10^3$	0.001	7
		4G Lyo-Vanco	144	$7.2*10^3$	0.002	8
		4G Sterile Vanco	138	$8.2*10^3$	0.002	9
	Palacos R	1G Vanco UCS	40	$1.8*10^3$	0.002	10
		1G Lyo-Vanco	208	$2.1*10^3$	0.002	11
		1G Sterile Vanco	36	$2.3*10^3$	0.002	12
		4G Vanco UCS	81	$1.7*10^4$	0.004	13
		4G Lyo-Vanco	108	$3.1*10^4$	0.008	14
		4G Sterile Vanco	144	$2.2*10^4$	0.006	15
	CMW	1G Vanco UCS	38	1.2*103	0.001	16
		1G Lyo-Vanco	43	$1.4*10^3$	0.001	17
		1G Sterile Vanco	29	$1.9*10^3$	0.002	18
		4G Vanco UCS	241	$1.6*10^4$	0.004	19
		4G Lyo-Vanco	283	$2.8*10^4$	0.007	20
		4G Sterile Vanco	273	$2.0*10^4$	0.005	21
Bishop et al. [22]	Palacos R	0.50G	1	$5.9*10^1$	0.0001	22
		1G	2.6	$1.0*10^2$	0.0001	23
		2G	2.4	$1.0*10^2$	0.0001	24
Galvez-Lopez et al. [18]	Depuy	1G	3.1	$2.6*10^2$	0.0003	25
		2G	4.2	$3.7*10^2$	0.0002	26

Table 2.2 This table displays features of vancomycin from ALBCs including average max flux, J(t), average total dose, D(t), mass transfer efficiency, E, and # for sample number. The values were determined from data extracted from selected papers that met the established parameters for paper consideration [18,22,25,52].

There are some general trends seen from Table 2.2. One is that when formulated with more vancomycin, both the average peak flux J and the average total dose delivered, E, rise. Since release is a burst response, the analysis for flux is tied to first measurement period and the total dose is biased by how long the experiments were executed. It is possible that incrementally more release can occur, and the flux decay model could predict a total dose if extrapolated. All elution curves resulted in plateau of total release. There were few instances where different researchers analyzed a similar formulation but measured different release features.

Comparing the different elution studies, peak flux is both resin supplier and vancomycin form specific. Generally, adding more antibiotic in the formulation correlates with higher release. There is an overlap between the studies of Bishop et al. (study 23) [57] and Lee et al. (studies 10-12) [52], who evaluated 1 g of different vancomycin forms in Palacos R cement, and the peak flux and total dose both vary by 2 orders of magnitude. If antibiotic forms and resins supplied are truly equivalent, then the same release profiles would be expected within some margin of error. Perhaps there are also nuances and differences in sample preparation as well. More consistency in protocols here could help resolve either the randomness of the formulation or confirm an individual experiment as a potential outlier. A similar evaluation was done at 4 g of vancomycin comparing the Bitsch et al. results (study 2) [25] and the Lee et al. results [52] using the different resins and a greater than one order of magnitude difference in average flux was noted.

Within the Lee et al. study [52], lyo-vancomycin releases more than ~3 times the level of antibiotic than the other forms of vancomycin when formulated in Palacos and Simplex B, while

all forms of vancomycin release similarly in the CMW resin. If the resins were equivalent, one would expect smaller differences for antibiotics formulated at the same level in bone cement. Average peak flux determinations were compared to controlled dye permeation experiments through dialysis tubing using malachite green [58]. The dye release can be modelled to fit the elution from the bone cement. With the dye diffusion coefficient determined (~$1x10^{-6}$ cm^2/s) and concentrations (10 μg/ml) and wall thickness (~30 μm) defined, the flux for dye permeation was ~10 $\mu g/cm^2$-hr, similar to the average peak fluence for vancomycin from ALBC [58]. The comparison shows that while vancomycin elution is modest, its release is linked with surface release and less by diffusion from the bulk of the cement.

Paper	Cement Type	Gentamicin Type & Content	Avg Max Flux, J(t) ($\frac{\mu g}{cm^2 hr}$)	Avg Total Dose, D(t) (μg)	Efficiency of Mass Transfer	#
Bitsch et al. [25]	Copal Spacem	Aminoglycoside Gentamicin Sulphate (AGS)-2G	6.6	$2.8*10^2$	0.0001	1
		AGS-4G	15	$1.7*10^4$	0.004	2
		AGS-6G	30	$3.8*10^4$	0.006	3
De Belt et al. [53]	Palacos R	Gentamicin Sulphate (GS)-4.4 mg	6.6	79	0.08	4
	CMW	GS-2.0 mg	9.9	70	0.05	5
Galvez-Lopez et al. [18]	Depuy	Gentamicin (GM)-1G	0.79	$1.7*10^2$	0.0001	6
		GM-2G	1.2	$2.5*10^2$	0.0001	7

Table 2.3 This table shows gentamicin elution from bone cements including average max flux, J(t), average total dose, D(t), and mass transfer efficiency, E. The values were determined from data extracted from selected papers that met the established parameters for paper consideration [18,25,53].

Separate studies were found on the elution of gentamicin (GM) to determine whether a smaller drug was more extractable from bone cement (see Table 2.3). GM (molar mass = 478 g/mole) is much smaller than vancomycin (1449 g/mole), yet total release as a ratio of what is

loaded, E, is similar for both drugs sequestered in bone cement. Thus, ALBCs are limited to surface drug depletion and have minimal elution potential from the bulk matrix.

2.3.2 Mechanical Response of Drug-Loaded Bone Cements

The presence of antibiotics in ALBCs reduces their initial strength once polymerized. Strength is further reduced as drug releases forming voids and stress concentrations. Table 2.4 shows cement strengths for a subset of these studies with exposures ranging from 300-1200 hours testing both pre- and post-elution. Elution reduced cement strength by ~5-25%. Voids in the specimen amplify the variability in strength after drug elution with strength-based measurements. The current ASTM F451 standard for acrylic bone cement strength is 70 MPa and most of the antibiotic-loaded specimens initially satisfied this threshold. In some instances there was no strength reported after elution [59]. Perhaps the strength standard is not applicable.

Paper	Cement Type	Vancomycin Type & Content	Average Initial Strength (MPa)	Retained Strength Ratio	#
Bitsch et al. [25]	Copal Spacem	2G VAN-HCl	Undisclosed	N/A	1
		4G VAN-HCl	Undisclosed	N/A	2
		6G VAN-HCl	Undisclosed	N/A	3
Lee et al. [52]	Simplex P	1G Vanco UCS	86	0.97	4
		1G Lyo-Vanco	82	0.96	5
		1G Sterile Vanco	81	0.89	6
		4G Vanco UCS	84	0.97	7
		4G Lyo-Vanco	84	0.722	8
		4G Sterile Vanco	74	0.84	9
	Palacos R	1G Vanco UCS	85	0.96	10

		1G Lyo-Vanco	79	0.93	11
		1G Sterile Vanco	84	0.92	12
		4G Vanco UCS	86	0.84	13
		4G Lyo-Vanco	80	0.74	14
		4G Sterile Vanco	80	0.85	15
	CMW	1G Vanco UCS	96	0.91	16
		1G Lyo-Vanco	84	0.92	17
		1G Sterile Vanco	79	0.93	18
		4G Vanco UCS	96	0.81	19
		4G Lyo-Vanco	76	0.81	20
		4G Sterile Vanco	77	0.79	21
Bishop et al. [22]	Palacos R	0.50G	63	N/A	22
		1G	65	N/A	23
		2G	52	N/A	24
Galvez-Lopez et al. [18]	Depuy	1G	Undisclosed	N/A	25
		2G	Undisclosed	N/A	26

Table 2.4 Reported initial strength values extracted from selected papers, of antibiotic bone cements and #, for sample number. The strength ratio was derived from the compressive yield strength of bone cements before and after elution, where the elution periods ranged from 14-60 days [18,22,25,52]. Not all authors reported compresssive yield strength or collect data before and after elution.

2.4 Discussion

In evaluating the breadth of responses dynamic vancomycin release, Lee et al. and Bishop et al. show a plateau in total drug release within 10 days of initial release [18,22,25,52]. Galvez et al. and Bitsch et al. show a similar trend; however, the plateau period is longer [18,52]. There is a perception that commercially loaded ALBCs are better mixed with antibiotic. Aside from including the antibiotic, there are separate issues of degassing and dispensing, relative to the conversion of monomer to polymer. Details in these papers did not include these processing

variations in the overall assessment of drug availability and strength, but variations in processing could have been affected by mixing.

What is striking is that over all the studies presenting dynamic release data on both antibiotics, the relative amount of release was very low. E ranged from 0.0001 to 0.008, for vancomycin regardless of drug loading. E was higher in one study where much smaller samples were made. As the loading increases, there are more near-surface sites from which drug can elute, but only a small amount is bioavailable. For example, when loading 6 g of drug in a 60 g pack of bone cement, only tens of milligrams of vancomycin are available.

None of the studies showed a linear release rate for either drug from ALBCs. Burst release into the receiver solution was common. Longer elution times showed a plateau in total drug release typically within 10 or more days.

The average vancomycin flux released varied from 1 to 283 $\mu g/cm^2$ *hr. The variation is attributed in part due to when the first measurement was taken. Gentamicin release features were similar. Antibiotic size is not a factor in regulating bulk diffusion in ALBCs. The meta-analysis has only considered antibiotic release into an inert solution. Duey et al. showed in a related study that larger zones of bacterial inhibition around an antibiotic releasing plug were observed when the concentration of vancomycin rose from 10 μg/ml to ~1000 μg/ml [60]. Clinically, the rise in vancomycin release from an ALBC will be tempered by the metabolic clearance where it is placed. Several studies also show the same burst response clinically and some authors reported antibiotic levels upon implantation and after showing similar results as the papers analyzed for this review [17,18,21,22,25,27,61,62]. In cases where metabolism is slow, sufficient amounts of antibiotic could accumulate in the affected area. Anagnostakos and Meyer compiled data on a variety of ALBCs tracking dynamic serum concentrations [62]. They showed serum

concentrations in the joint fluid of 30-1500 μg/ml in the first several days post-operatively from installation [62]. The burst might be enough to inhibit infections, but the volume of infection is important. Also, when infections are localized, a longer sustained flux may be needed.

The best antibiotic is one that clears infections without affecting the healthy microbiome or leading to antibiotic resistance. There are many studies that suggest that ABLCs reduce infection, but what constitutes a sufficient dose and period is unresolved. In addition, there is a mechanical penalty paid for loading bone cement with high antibiotic doses. Lower cement strength correlates to lower structural stability. Singh et al. showed that adding >3 g of vancomycin lowered both the bending strength and the stiffness of ALBCs [46].

The co-formulation of active drug elements within a liquid methacrylate and powdered polymethyl methacrylate bone cement mixtures has proven viable for localized drug delivery. The use of drug eluting spacers from relatively rigid bone cement mixtures are proven release systems. If spacers have no structural requirement, then the cement matrix may be loaded with more antibiotic without structural concerns for the spacer.

In the clinical realm, the ALBC release is assessed qualitatively by observing an infection response, or by measuring drug transport [63]. These use a spacer interacting on a bacterial culture plate and result in *a zone of death* emanating from the spacer. For transfers not assessed on live cultures, aliquots of solution can be taken for analysis by either fluorescence-based assays or by liquid chromatography. There exists promise to consider bacterial cell culture assays as objective tests for adequate and sufficient drug release from ALBC platforms, using adaptations from traditional bacterial cell culture assays of antibiotic efficacy.

2.4.1 Alternative Strategies to Address Periprosthetic Joint Infection

Gaps seem to exist between loading and realistic dosing levels releasing from the cements. Perhaps, more regulated, and controlled release systems could achieve similar dosing levels, without retaining vast amounts of antibiotic in the cement. Biodegradable cements and gels increase the fraction of drug contained in the therapy that is bioavailable. Prior work by Veryies et al. suggests that colloidal crystal gels loaded with vancomycin at 20 μg/ml might accommodate both a burst release and a sustained release measurable quantities of μg/ml of vancomycin after 7 days sufficient to eradicate infection [64]. Similar degradable controlled release systems could be developed that account for a dissolving sequestration matrix.

There is also a need to identify bacterial responses of specific pathogens of interest. Appropriate bacterial culture assessments are needed. Nandi et al. mention that osteomyelitis evolves naturally, and as an outcropping of invasive pathogen exposure that can occur from diabetic foot ulcers and surgical intervention for joint replacement and fracture fixation [63]. Pathogens more likely to be found organically include *Staphylococcus aureus*, while those from foot ulcers evolve from microbial exposure. For joint replacements, *Staphylococcus epidermis* is the most common pathogen [65]. With Gram-positive pathogens like staphylococci, drug release from antibiotics potent to Gram-positive bacteria is key [66]. Other attributes that might allow for some grading of specific antibiotics might be related to their size or molecular weight, their overall potency, and the potential for antibiotic resistance. Similar studies are needed for other antibiotics given that both Gram-positive and Gram-negative bacteria can colonize to form an infection.

A separate issue is the age of an infection, as formed biofilms can reduce antibiotic effectiveness. Bacterial cell culture assays should assess how permeable vancomycin, or any

other antibiotic is in piercing the biofilm. Here, a smaller molecular weight antibiotic-loaded into the cement or combinations of antibiotics might be more potent.

Others have added antibiotics to bio-degradable carriers as localized drug delivery vehicles [54,63,64,67–70]. These have included, but are not limited to, antibiotics within packaged resorbable salts, bioactive glasses, and bone tissue [70–74]. Softer biodegradable matrices have been proposed including collagen or hydrogels [71,75,76]. Zhou et al. integrated the use of other fillers formulated with antibiotics and PMMA bone cements [77]. They showed that when PMMA cements loaded with a mixture of vancomycin, tobramycin, and 10% calcium polyphosphate (CP), a much lower burst release occurred and sustained release was extended up to 24 weeks [77]. The larger pore sizes influenced by the CP addition led to higher release rates while maintaining similar mechanical strength of the unfilled bone cement [77]. Alternatively, Inzana et al. used biodegradable polymers incorporating antibiotics [70,78,79]. In their review, they considered hydrogels, including polylactic acid, and polyglycolic acid that dissolve by hydrolysis, copolymers, and polycaprolactone, shaped into solids incorporating the antibiotics and then installed. The formed hydrogels could also be used as sustained-release drug delivery systems. This was an added feature when the antibiotics are more soluble when encapsulated into a hydrogel than when dissolved in saline alone. Particularly, aqueous solutions of polyethylene oxide-polypropylene oxide-polyethylene oxide (PEO-PPO-PEO) copolymers form micelles and crystallize into cubic lattices when introduced into a warm bodied creature [78,80]. When different solutes are added, the kinetics and structural evolution of these colloidal crystals shift [78,80–82], but allow for controlled release [58]. In comparison to using antibiotic-loaded bone cements for infection, softer gels could allow for a diffusion-based mechanism and release more antibiotic in non-cemented joint infections. There is a need to also resolve whether other

biodegradable antibiotic-loaded drug delivery systems could be used as a lavage at the I & D stage. Presenting antibiotic into the bone cavity before bacterial colonization is most likely effective in staving off joint infections.

2.5 Trends and Conclusions

The meta-analysis has confirmed that antibiotic-loaded bone cements can release antibiotics, though dose efficiency is low. The cited studies show a common initial burst, and then a decay in the elution rate for the antibiotics and some decrease in spacer strength after elution, typical of a core-shell structure with little to no release from the core. The reported doses may be high enough to achieve the minimum inhibitory concentration, noted as 0.5-2.0 μg/ml [83] for vancomycin. A large portion of formulated drug in the cement is not bioavailable. In addition, comparisons in mass transfer were possible since the elution sample shapes were included.

Formulating ALBCs with higher concentrations of antibiotics allows for more mass transfer, but also leads to more surface voids that risk the cement's long-term mechanical integrity. From the burst response, the drop-off in elution rate follows an exponential decay. Further experimentation is needed to determine whether the variations in elution response are due to experimental error or a function of attributes of the drug and resin elements making up the ALBC. Alternative matrices that release a larger fraction of what is formulated also warrant consideration.

When considering alternative methods, resins that allow for more antibiotic to diffuse from the core, or that dissolve and/or disperse to expose more core-located antibiotic, are appropriate to consider. Softer, gel-like structures have many of those attributes and could be co-formulated for release in infected joint regions.

Chapter 3 Thermophysical and Viscoelastic Properties of F127 with Added Pharmaceuticals

3.1 Introduction

Block copolymers are macromolecules compromised to two or more chemically different chains bound together by covalent bonds. Polyethylene oxide-polypropylene oxide-polyethylene oxide (PEO-PPO-PEO) triblock copolymers—as shown in Figure 3.1—are a class of ABA amphiphilic triblock copolymers, commercially known as Pluronics (non-propriety name "poloxamers"). These amphiphilic triblock copolymers can be made into thermoreversible solutions and potentially formulated as injectables for use as drug delivery vehicles [1,64,84–86].

BASF first introduced *Poloxamer* in 1973 with corresponding nomenclature that identified the morphology of each Pluronic at room temperature, as pictured in Figure 3.2 below: liquids (L), pastes (P), and solid flakes (F) [87]. These three leading characters are then followed by one or two numbers which reference each Pluronic on the grid. Copolymers on the same horizontal line moving to the right indicate an increase in the weight percent of the hydrophile arms (PEO), and those on the vertical line moving upwards indicate an increasing weight percent of the hydrophobe center block (PPO). The center number or two (if four characters) represents 1/300 of the molar mass of the PPO block. The last value represents one-tenth of the mass fraction of the PEO block. For example, the Pluronic with characters P105 is a paste ("P") at room temperature with a PPO block molar mass of 3000 g/mol and is 50% by weight PEO. The total molecular weight of P105 would be approximately 6,500 g/mol with a chemical formula of $PEO_{37}PPO_{56}$ PEO_{37}.

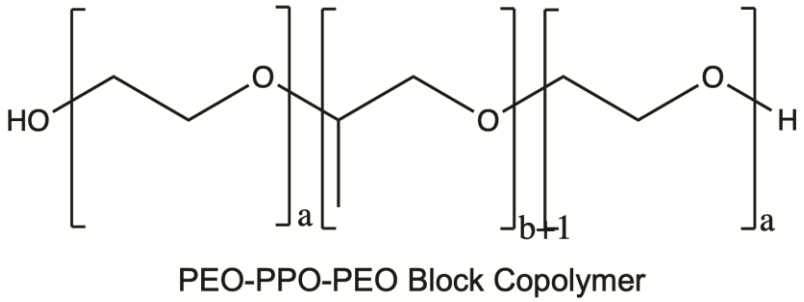

Figure 3.1 Structure of Pluronic block copolymers.

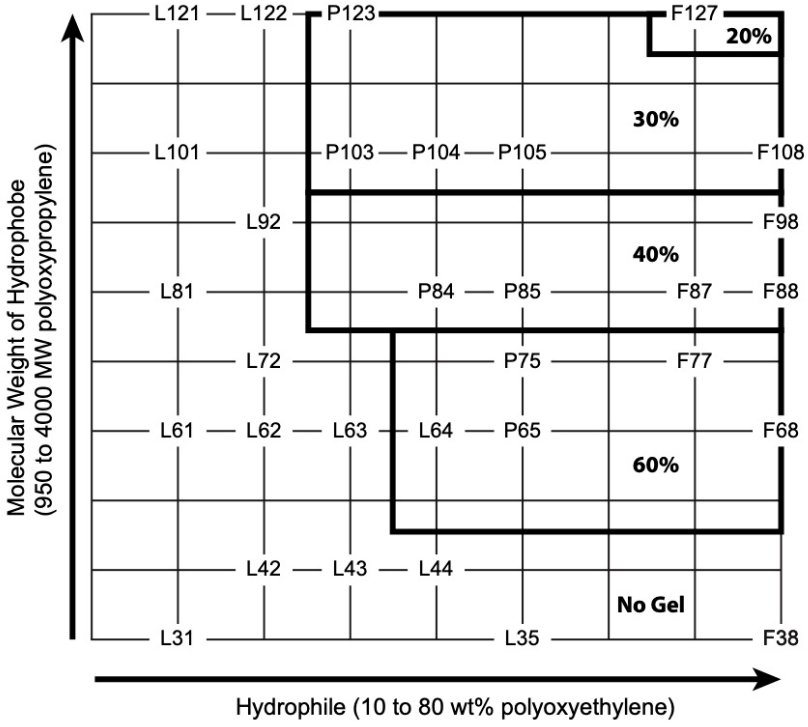

Figure 3.2 Pluronic gel formation grid. The first letter of each Pluronic indicate the phase of the Pluronic at room temperature: Liquid (L), pastes (P), and solid (F). The bolded region and percentages represent the minimum concentration needed for the Pluronic to gel at room temperature. F127 has the best gelation abilities of all the Pluronics. Figure reproduced from Schmolka [87].

3.1.1 Micellization and Gelation of Amphiphilic Block Copolymers

The physical and chemical properties of Pluronics can be modified by changing the molar mass ratio between PEO:PPO blocks. The differences in molar mass ratio affect properties such as physical state, thermophysical, and mechanical properties. The minimum weight percent concentration of PEO-PPO-PEO triblock copolymer needed to achieve a gel state at 25 ℃ is

indicated by bold lines in Figure 3.2. At those corresponding weight fractions and temperatures, aqueous solutions of PEO-PPO-PEO copolymers will first form micelles, and with sufficient driving force, organize the micelles into various self-assemblies. Figure 3.3 shows a schematic of this process.

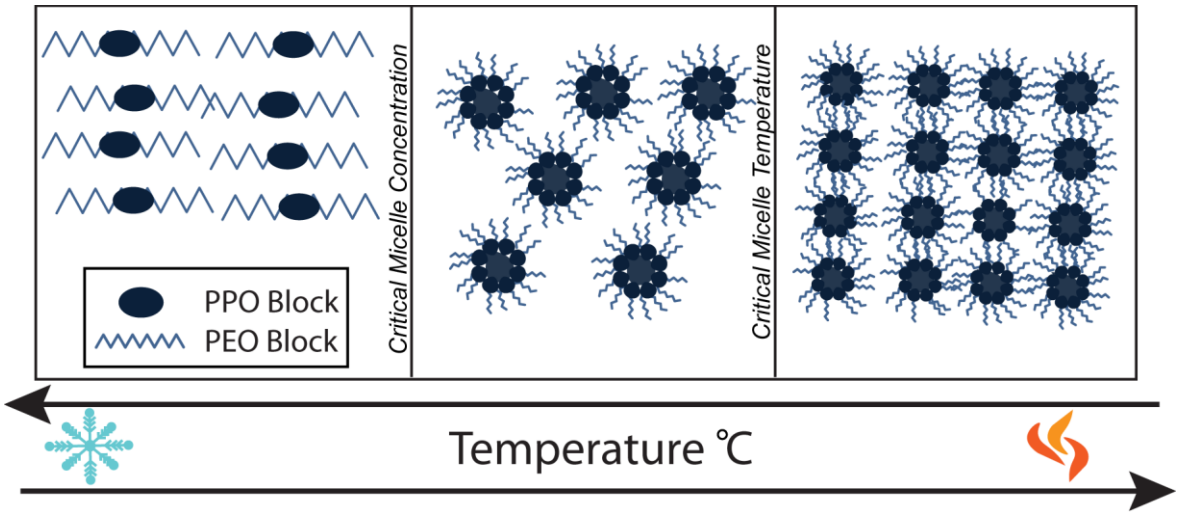

Figure 3.3 Illustration of temperature-dependent micellization and gelation of PEO-PPO-PEO block copolymers. PPO and PEO unimers are initally present in solution. When the solution is heated above critical micelle temperature, micelle formation begins. As the solution is further heated and reaches above the critical gel temperature, the micelles order into a collodial crystalline structure.

At low concentrations the unimers are dispersed in the solution and randomly organized. If more unimers are added at a low temperature, the driving force for clustering may still be insufficient. If at higher concentrations the aqueous mixtures are heated above the *critical micelle temperature (cmt),* also identified as $T_{micelle}$, there is an enthalpic payoff for self-excluding some regions of hydrophobicity into clusters through a nucleation and growth response of the unimers in solution. If the energy is a large enough driving force for the self-organization of the hydrophobic segments, this will trigger micelles to spontaneously form. This driving force is due to the hydrophobic effect, where hydrophobic PPO block aggregates with

others to exclude water molecules [88]. Goldstein suggests the contributions to the driving force for forming micelles can be idealizes as a spherical core that has hydrophobic sections that bind together to form a mass with constant density [89]. The resulting spherical micelles are disordered micelles present within the solution [90–93]. After heating through the *cmt* and the temperature increases further, the micelles can arrange into more organized structures representative of colloidal crystals. The unit cell dimensions of micelles organized at lattice points are much larger than atomic crystals and they do not appear to act as hard spheres. This gel formation is driven by the increase in the aggregate of the Pluronic micelles and the phase transition from liquid to crystalline [90,93]. The disordered to ordered transition to crystalline lattices is driven by the increase in micelle volume fraction and the repulsive force between micelles. As the temperature increases, (a) the volume fraction of micelles increases, (b) the repulsive interactions between the nearest micelle neighbor occurs, and (c) the micelles form ordered phases to maximize the distance from one micelle to another.

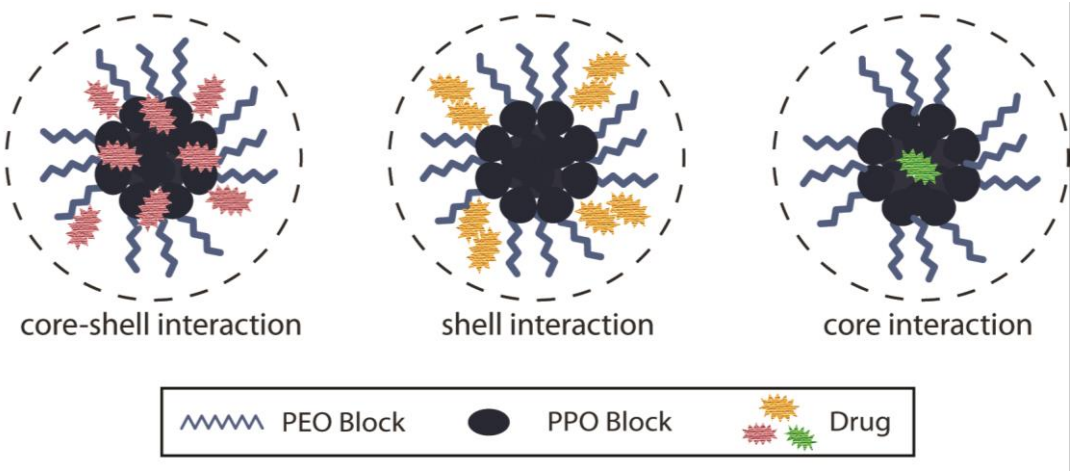

Figure 3.4 Illustration of three micelle interactions. Core-shell interaction where the additive interacts with the hydrophobic micelle core and hydrophilic shell. Shell interaction where the additive interacts with the hydrophillic shell. And core interaction where the additive interacts with the hydrophobic micelle core.

In addition, the presence of dissolved solutes affects Pluronic micelle formation by influencing the thermophysical and mechanical properties [94–100]. For example, in 10% F127 with 0.5% and 1% of methylparaben (MP) added, Meznarich et al. saw $T_{micelle}$ shift from ~18 ℃ for the neat sample to ~5 ℃ and ~-2 ℃ respectively [81]. There are several potential interactions with the micelles that could take place with ternary additives. The first, as depicted in Figure 3.4, is a core-shell interaction where the additive interacts with the hydrophobic core and the hydrophilic shell of the polymer. Second, is a shell interaction where the additive interacts with the hydrophilic shell of the polymer. Third, is a core interaction where the additive interacts within the micelle core. Lastly, the additive could interact with the hydrophilic tails of the micelles. As noted by Chen et al., the micellization process can be described in two parts: (1) the "desolvation" process where the dehydration of the hydrocarbon tail of surfactant molecules occurs and (2) the "chemical" process where the aggregation of the hydrocarbon tails of the surfactant molecules forms a micelle [101,102]. It is the "desolvation" process and "chemical" process coupled with the driving force for micelle formation that gives way to variations noted as changes in in $T_{micelle}$, ΔH, and critical gel temperature (T_{gel}). In addition, the interactions affect the phase formation of amphiphiles as well, where the crystal structure changes with ternary additives [78,80]. A number of other factors could influence where the additive would interact, such as molecular weight, size, and hydrophobicity [80,99,103,104]. The hydrophobicity of an additive could potentially help define the core, shell, or core-shell interface and help organize the structure by chaperoning or delaying micelle formation. Meznarich et al. and Thompson et al. have previously investigated a rationale for how the presence of ternary additives interacts when forming micelles and how interactions between drug and micelle influence the thermophysical and structural changes in F127 micelles by several methods [81,82,105]. Additionally, for use in

drug delivery, further investigation of the thermophysical properties of micelles in which colloidal crystals form is an important aspect to consider when determining the bioavailability and efficacy of pharmaceuticals added.

3.1.2 Amphiphilic Triblock Copolymers Facilitating Drug Solubility and Delivery

The biocompatibility and the colloidal gel formation potential of amphiphilic triblock copolymers allow their consideration for injectable drug delivery systems. Previous work has evaluated the use of Pluronic triblock copolymers for targeted drug delivery of a range of molecules including cisplatin, docetaxel, and anesthetics [1,98,99,104–107]. Researchers have shown that when co-formulating pharmaceuticals with triblock copolymers they raise drug solubility [103,104], treat infections locally [107], are used in gene therapy [84], and can be used as a tool in the creation of injectable scaffolds [108]. Pluronic F127, a solid flake, is a common formulation co-constituent given its wide availability and its ability to form solid phase structures at concentrations as low as 20% in aqueous solution. PEO-PPO-PEO in the form of F127 has low toxicity which makes it an ideal candidate for use in medicine [90]. Sharma et al. studied the gelation behavior of Pluronic F127 in the presence of hydrophobic pharmaceuticals to determine the correlation between gelation and physicochemical parameters of drug solutes [99]. Their results showed that the presence of common pharmaceutical additives, such as methylparaben and ethylparaben, tends to reduce the sol-gel transitions for F127 solutions, relative to the neat solutions, and was drug-concentration dependent with as much as a 10ºC decrease from the initial ~10 ºC for 30% F127. The amphiphiles also raise drug solubility, which is a separate consideration for dispensing drugs of low solubility in blood.

3.1.2.a Sample selection

In this dissertation, I studied the interaction of 25% F127 with four antibiotics commonly used to eradicate pathogenic bacteria, depicted in Figure 3.5: vancomycin (VAN), cefepime (CEFE), ciprofloxacin (CIPRO or CIP), and gentamicin (GM). Though all are antibiotics, their use varies based on the type of bacteria present, infection type, and cost. Vancomycin (1449.3 g/mol) is a hydrophobic antibiotic. It is commonly used for treatment of serious infections by Gram-positive bacteria unresponsive to other antibiotics, often considered as a last resort. Cefepime (571.5 g/mol) is a hydrophobic fourth-generation cephalosporin that has an extended spectrum of use against Gram-positive and Gram-negative bacteria. Ciprofloxacin (331.3 g/mol) is a hydrophilic antibiotic that is also used for a broad spectrum of Gram-positive and Gram-negative bacteria. Gentamicin (477.6 g/mol) is another hydrophilic antibiotic used for treatment of Gram-positive and Gram-negative bacteria. There are standard dosing guidelines associated with each of the drugs based on potency, *MIC*, toxicity, and other factors as mentioned in Chapter 1. In clinical settings there is no one-size-fits-all playbook to treat infections. A physician would consider the *MIC,* as well as other factors described in Chapter 1, to determine a protocol to treat an infection. The goal of this thesis was not to probe new types of antibiotic potency, but to evaluate drug in package systems that might offer more effective distribution. However, by adding pharmaceutical additives, the chemical potential of the solution containing water, amphiphilic copolymer, and drug is different without the drug and perturbing where $T_{micelle}$ and T_{gel} occur and require characterization.

The goal of an antibiotic-loaded gel system is to (a) allow a clinician to inject cold dispersions of liquid below the critical micelle, the gel formation, and body temperatures; and (b) allow metabolic heat to trigger solidification. These micelle-based gels are unusual in that they

are less viscous at lower temperatures. A separate issue also arises in considering how drug co-formulation might affect how micelles interact with the drug or destabilize it. These antibiotics are commonly dispensed in a range of forms and are available as reagent grade chemical. Clinically, they are often already solubilized in saline and other sterile and dispensable forms in pharmacies, thus providing another variable beyond simple formulation conditions. However, VAN is typically lyophilized and solubilized at the time of administration and CEFE is in powder form. Therefore, I decided to incorporate the amphiphilic copolymers with medical grade samples, rather than reagent grade, to investigate their thermophysical and viscoelastic properties *in vitro.* In addition, reagent grade ciprofloxacin was also studied as a comparison packaged in amphiphilic copolymers.

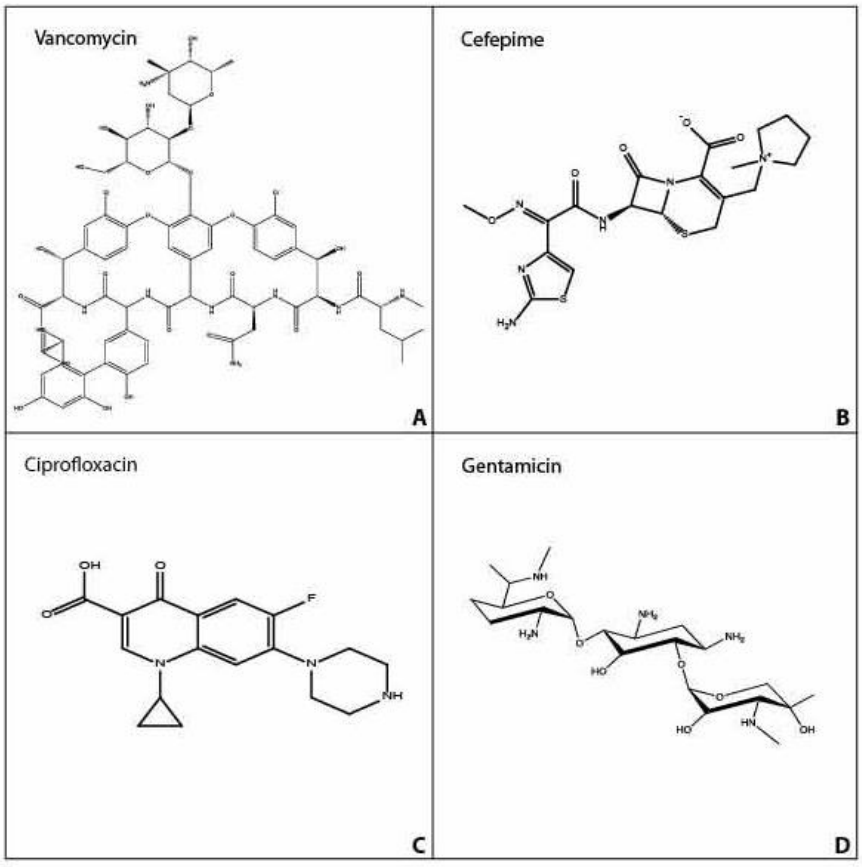

Figure 3.5 Structure of antibiotics used for the study. (A) Vancomycin (B) Cefepime (C) Ciprofloxacin (D) Gentamicin.

3.1.2.b Overview

In the previous chapter, I discussed treating deep bone infections with antibiotic-loaded bone cements and investigated their efficacy. The implication from that work was that the formulations mixed with bone cement were quite inefficient and potentially expensive given that there is so much bio-unavailable drug locked into the cement structure. Perhaps other softer and more metabolizable forms might allow for a more efficient treatment using less drug overall while still bathing the infection site with sufficient antibiotic. In this chapter, I present the results of experiments that observed how the formation of amphiphilic triblock copolymer micelles affect the thermophysical properties before gelation and assess how the gelation behavior is affected by the presence of added pharmaceuticals. These antibiotics loaded hydrogels could serve as alternative drug delivery vehicles in treating infections locally. This study aims to contribute and help build a deeper understanding of how poloxamer-based drug delivery formulation properties.

3.2 Materials and Methods

3.2.1 Sample Preparation

3.2.1.a Pluronic stock solutions

Pluronic F127 was obtained from Sigma-Aldrich (St. Louis, MO) and used as received. Aqueous solutions of Pluronic F127 were prepared according to the "cold method" as described by Schmolka [100]. Twenty-five percent was selected as the weight percent for F127 because it has a micelle and gelation temperature well below body temperature (37 ℃). Therefore, gel formation would trigger when introduced at body temperature based upon the limit from the Pluronic grid [100]. Solutions were prepared using deionized (DI) water, 0.9% sterile saline, and

5% dextrose. Sterile saline was obtained from Baxter Healthcare Corporation (Deerfield, IL) and used as received. Dextrose was obtained from Becton Dickinson (Franklin Lakes, NJ). Weighed amounts of F127 were added slowly to DI water, 0.9% sterile saline, or 5% dextrose, and stirred gently to avoid foaming. Once all the dry F127 was added, the solution was kept at 4 °C to dissolve quiescently. In the pharmaceutical trials, the F127 concentration was fixed at 25%. This concentration was selected because of the need to trigger micelle formation for an injectable antibiotic therapy that gels.

3.2.1.b Drug/Pluronic mixtures

Cefepime (CEFE) was obtained from Apotex Corp (Toronto, CA) and used as received. Solutions containing CEFE were prepared by first making a stock of 10% (wt/v) CEFE in 25% F127. Aliquots of the CEFE and F127 stock were taken and diluted to 2%, 4%, 6%, and 8% using a neat stock solution of 25% F127. Ciprofloxacin (CIPRO) in 5% dextrose was obtained from Claris Lifesciences Inc. (New Brunswick, NJ) and used as received. Solutions containing CIPRO were prepared by first making a stock of 0.2% Cipro in 25% F127. Aliquots of the Cipro in 5% dextrose in 25% F127 stock was then diluted to 0.05%, 0.075%, 0.1%, and 0.15% using a neat stock solution of 5% dextrose and 25% F127.

Gentamicin (GM) was obtained from Fresenius Kabi USA (Lake Zurich, IL) and used as received. Solutions containing GM were prepared by first making a stock of 0.8% GM in 25% F127. Aliquots of the 0.8% GM and 25% F127 stock were taken and diluted to 0.6%, 0.4%, and 0.2% using a neat stock solution of 25% neat F127. Vancomycin Hydrochloride (VAN) was obtained from Alvogen (Pine Brook, NJ) and used as received. Solutions containing VAN were prepared by first making a stock of 5% VAN in 25% F127. Aliquots of the VAN and 25% F127 stock were taken and diluted to 0.8%, 1%, 2%, 3%, 4%, and 5% using a neat stock solution of

25% neat F127. The concentrations for the antibiotics used were prepared following instructions given by the manufacture. For each antibiotic, the maximum concentration was selected to be tested as the upper limit based on the preparation instructions and diluted into smaller concentrations as added variables. The dosing guidelines take into consideration the antibiotic, dose, and duration of treatment to maximize efficacy and minimize toxicity. The dosing guidelines have variations based upon the pharmacokinetic and pharmacodynamic properties. The maximum concentration was prepared and then diluted to be able to determine what variations occur with lower concentrations. Table 3.1 lists all concentrations prepared.

Sample	Prepared Concentrations (wt%)
Cefepime (CEFE)	2%, 4%, 6%, 8%, 10%
Ciprofloxacin (CIPRO)	0.05%, 0.075%, 0.1%, 0.15%, 0.2%
Gentamicin (GM)	0.2%, 0.4%, 0.6%, 0.8%
Vancomycin (VAN)	0.8%, 1%, 2%, 3%, 4%, 5%

Table 3.1 Details of the samples and the concentrations prepared for the study.

3.2.2 Differential Scanning Calorimetry (DSC)

The DSC experiments were conducted on a TA Instruments (New Castle, DE) Q2000 series DSC with an RCS90 refrigerating unit for cooling. An empty aluminum TZero^{TM} pan was placed onto a micro balance, weighed, and tared to zero to prepare each dispersion batch for analysis. Approximately 10 µl was pipetted into the sample pans. The mass of the pipetted solution was recorded, and a press was used to hermetically seal the sample pan.

Tests included a heating ramp starting at a temperature below the known *cmt* of the neat 25% F127 solution; however, to ensure that all potential changes were captured, tests were started well below the *cmt* at -5 °C or 0 °C. Samples were heated at a rate of 1 °C/min from 0-40

°C under nitrogen purge. In addition, CIP and VAN samples were run at a higher heating rate of 10 °C/min.

3.2.3 Dynamic Mechanical Analysis

Dynamic mechanical experiments were carried out on a TA Instruments Discovery Hybrid Rheometer-3 (DHR-3) rheometer in dynamic oscillatory mode. A Peltier attached to the rheometer stage controlled the temperature and heating rate. Parallel plate geometry was used with a 20 mm diameter stainless-steel upper tool and the Peltier stage as the lower plate. Figure 3.6 below shows the experimental set up for the rheometer.

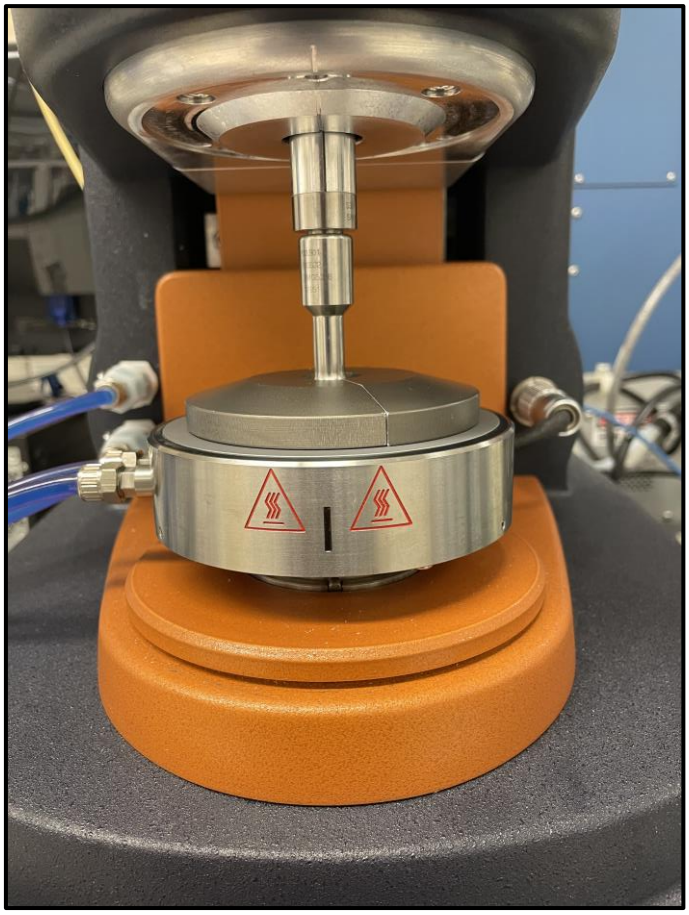

Figure 3.6 This is the rheometer setup with the Peltier thermal controller on the bottom. The upper shaft is capable of controlled rotational motion and the torque on the shaft to regulate those motions is also measurable. The sample is placed onto the Peltier stage and upper shaft lowered onto the sample to a set gap length and then covered with a humidity shield.

The rheometer was operated in dynamic oscillatory mode with a frequency of 10 rad/s and an applied strain of 1%. Data was collected at 1 Hz for the 1 °C/min and 10 °C/min tests as the temperature was ramped from 0-70 ºC to fully capture the liquid-to-gel transition of the solutions. The experimental condition was $n = 3$, with the results being the average of the replicates and standard deviation calculated. The temperature range tested was between 0 °C and 70 °C to fully capture the liquid-to-gel transition of the solution. The test protocol allowed for (1) the solution to be heated from the starting temperature at the preset heating rate until the final temperature, and (2) a 10-minute incubation period at the final temperature to capture any transient lagging gel formation.

3.2.4 Data Analysis

All data generated by the calorimeter was saved in individual files, which were then analyzed using the TA Instruments Universal Analysis software for quantitative analysis of the resulting thermogram curves. Typical experimental results showed in a single endothermic peak being detected during the programmed heating. Three main values were extracted from this peak as shown in Figure 3.7: (a) the onset temperature ($T_{micelle}$, intersection between the baseline and the tangent of the maximum slope in the initial region of the curve), (b) the peak temperature (T_{peak}, temperature at which maximum deviation from the baseline is achieved), and (c) the enthalpy of the transition *(*ΔH, integrated area between the baseline and the experimental curve).

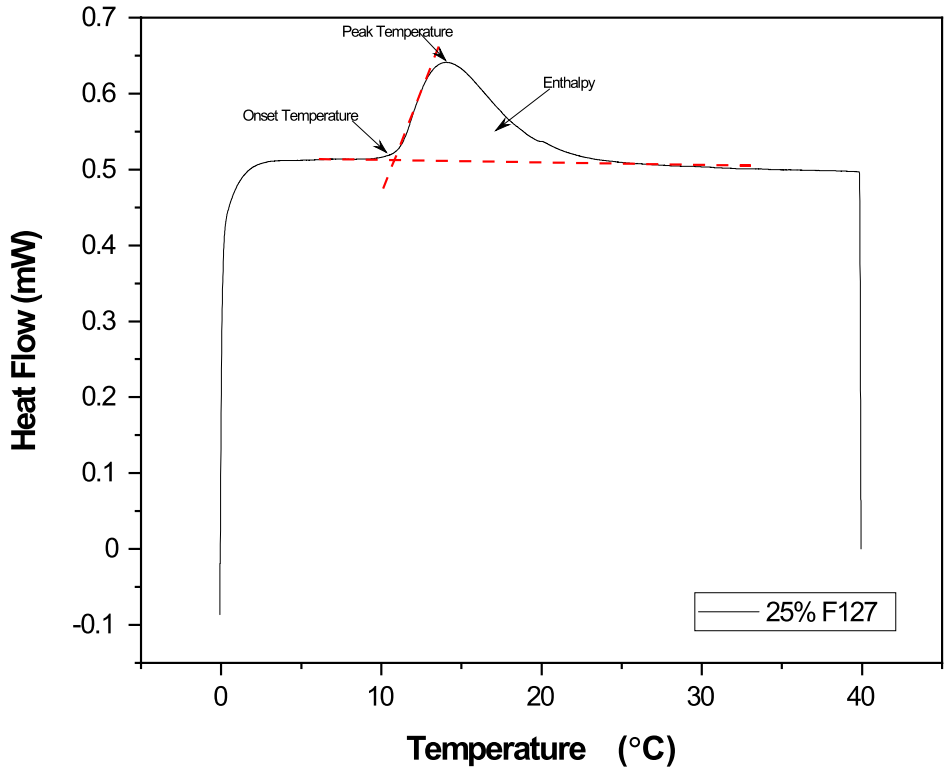

Figure 3.7 An example DSC thermogram of 25% F127 heated at 1 ºC/min. The labels depict the extracted values from each thermogram. The onset temperature is the intersection of the baseline and the maximum slop of the initial portion of the peak. This is interpreted as $T_{micelle}$. The maximum peak temperature is the maximum deflection from the baseline. The enthalpy is the total area under the curve from the baseline, indicated by the shaded lines. For clarity the number of data point has been reduced.

Oscillatory rheometric experiments were used to investigate the time dependence of the viscoelastic changes in the samples. The data generated by the rheometer was saved as individual files and analyzed using MATLAB™. The critical gel temperature, T_{gel}, was quantified using *G' vs. G''* crossover [109]. The storage modulus, *G'*, represents the elastic portion describing the solid-state behavior of the sample. The loss modulus, *G''*, represents the viscous portion describing the liquid-state behavior of the sample. Figure 3.8 shows an output of oscillatory rheometric experiments. At the start of each controlled heating experiment, the loss modulus is higher than the storage modulus due to the liquid-like consistency of the dispersion. As temperature increases at the set angular frequency, the storage modulus (solid-state) dominates the loss modulus (liquid-state) and crosses over the modulus [109,110]. The point at which this

crossover occurs is characterized as T_{gel}, where the colloidal fluid has transitioned into a colloidal gel.

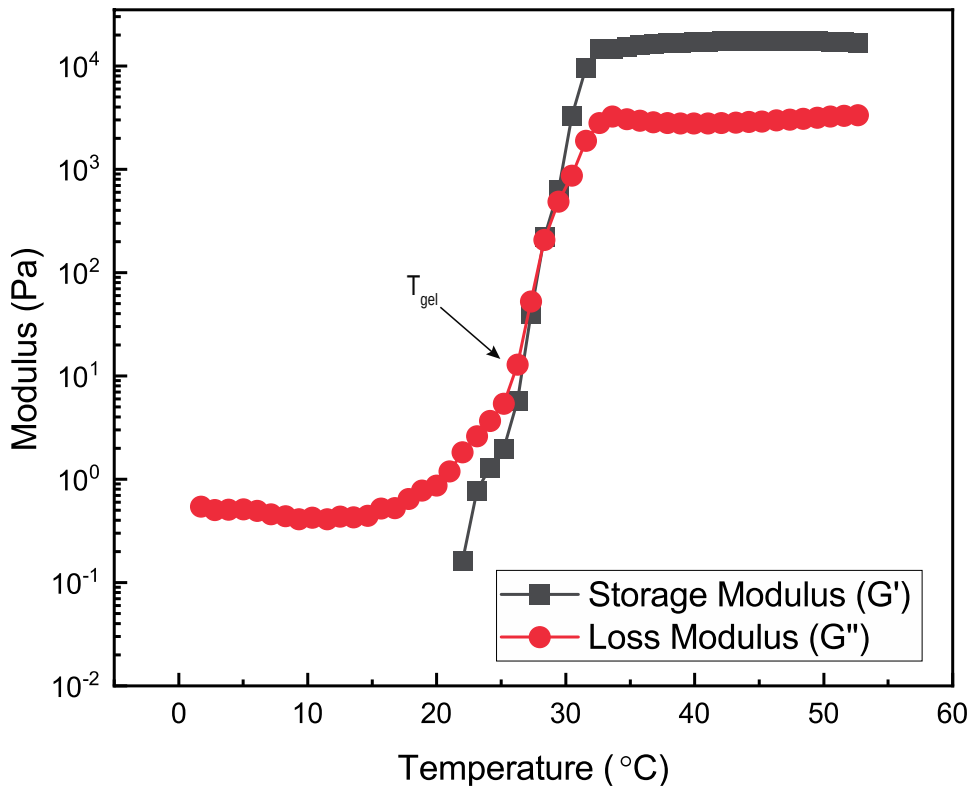

Figure 3.8 Modulus vs. Temperature for 0.2% CIP in 25% F127 solution heated at 10 °C/min and rad/sec at 1% strain. T_{gel} indicates the point at which the storage and loss moduli cross each other, marking a transition from liquid-like to solid-like behavior.

3.3 Results

3.3.1 Effect of Increasing Ternary Additive Concentration

Figure 3.9 depicts a series of DSC thermograms for a solution of 25% F127 with increasing amounts of different antibiotics added. For the CEFE and GM dispersions, as the amount of antibiotic added is increased, the $T_{micelle}$ and T_{peak} shift to lower temperatures. There is a linear dependence on the temperature for the increasing amounts added. CEFE shows the greatest effects on $T_{micelle}$, additionally the largest concentration range was used for CEFE. The

values for testing were based upon the antibiotic dosing guidelines set by the manufacturer; however, if the concentrations evaluated were molecularly equivalent, the results could show more granular details in relation to antibiotic differences. The results for VAN show that there is a slight decrease; however, the values are not statistically significant.

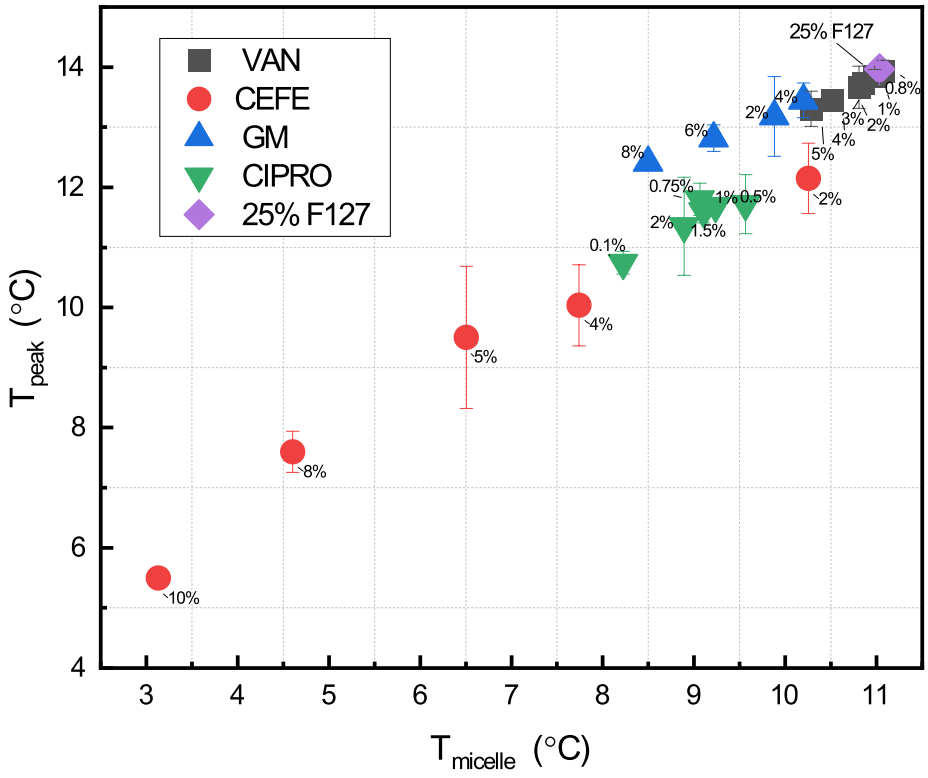

Figure 3.9 Twenty-five percent F127 with increasing amounts of various antibiotics added. There is a general trend observed showing the decrease of $T_{micelle}$ and T_{peak} with the addition of antibiotic of various concentrations. However, VAN does not produce statistically significant changes to $T_{micelle}$.

There were two formulations of CIPRO investigated in this study, neat CIPRO in 25% F127, and neat CIPRO with 5% dextrose in 25% F127. When initial experiments were with neat CIPRO in 25% F127, it was observed that the solubility in solution was very low. Additionally, the resulting DSC measurements (see Figure 3.10) showed some suppression of the endotherm; however, the results were not statistically significant and showed no systematic changes to

$T_{micelle,}$ in regard to concentration of CIPRO, which was not seen in the literature. Subsequently, neat CIPRO was prepared with 5% dextrose in 25% F127. The results showed statistically significant results for $T_{micelle}$ and ΔH with a $p \leq 0.001$ and $p \leq 0.05$, respectively. CIPRO with 5% dextrose showed an initial suppression of the endotherm and decrease of $T_{micelle}$; however, there was an invariant effect on the endotherm and $T_{micelle}$ between concentrations (see Figure 3.10). The results indicate that dextrose may play a role in the micellization in antibiotic-loaded amphiphilic gels when packaged with CIPRO. Perhaps dextrose is interacting with the PPO core formation while CIPRO is in the periphery with limited interactions, which could potentially account for the small variation in endotherm energy and large $T_{micelle}$ differences.

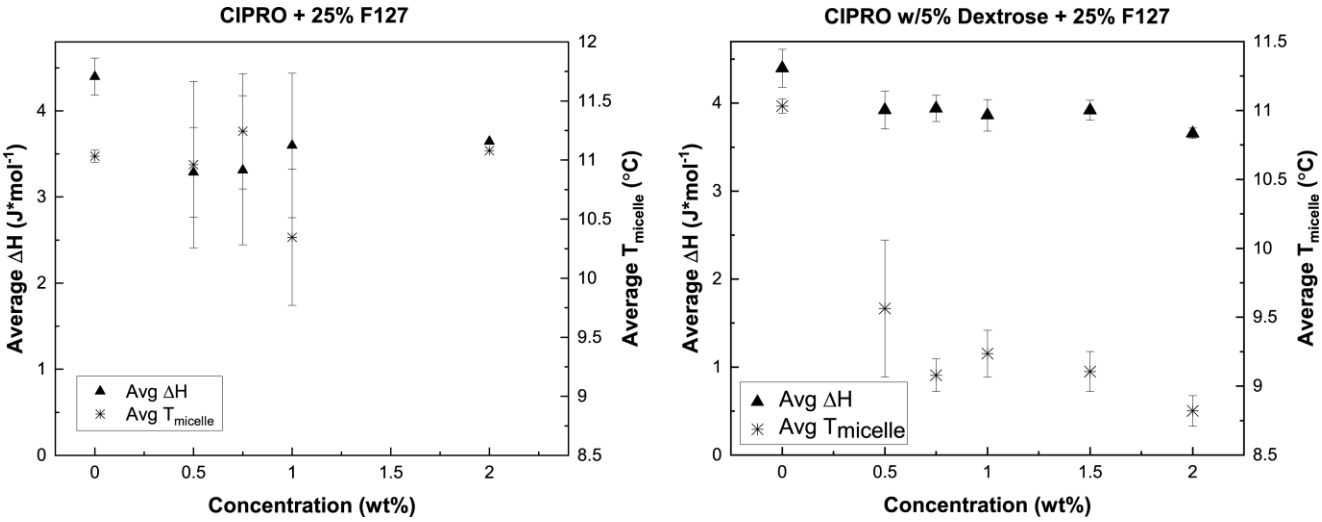

Figure 3.10 Comparison of average CIPRO without dextrose and CIPRO with dextrose resolved through DSC measurements and analysis of the endotherms. Any concentration of CIPRO in 25% F127 reduces $T_{micelle}$ and suppresses the endotherm though not statistically significant. However, CIPRO with 5% dextrose in 25% F127 is statistically significant.

Figure 3.11 shows the effect of increase concentration of VAN in 25% F127 solutions that affected ΔH and $T_{micelle}$. The resulting values indicate that VAN does not have a statistically significant effect on micellization. Perhaps there is a solubility limit for VAN in these mixtures

and if it is not soluble, it likely is not capable of migrating within the micelles. If VAN were to directly interact with the PPO core, a more enthalpic effect would likely be seen, resulting in a more pronounced decrease in ΔH, which is similar to results seen with other drugs in this study or as Sharma et al. saw with lidocaine [99].

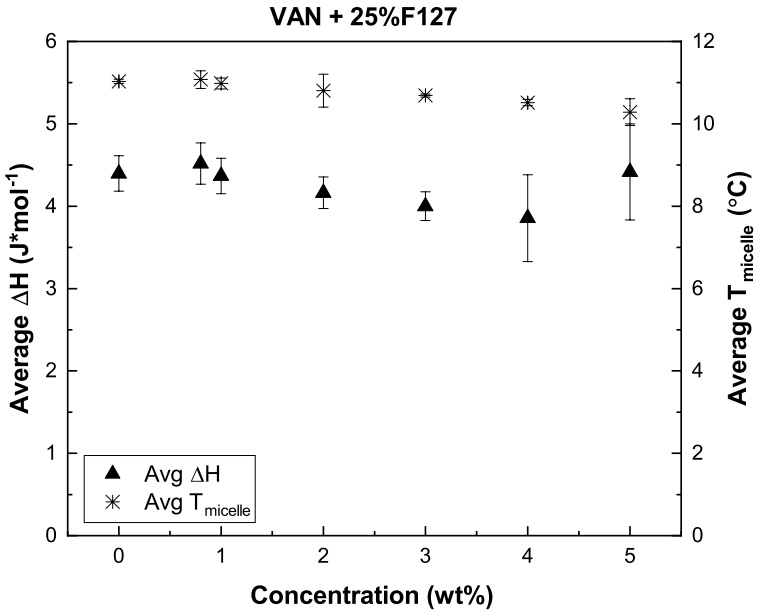

Figure 3.11 Averages of increasing concentrations of VAN in 25% F127. Results show a statistically insignificant effect on the $T_{micelle}$ and dH.

Figure 3.12 shows how adding CEFE to 25% F127 solutions affected ΔH and $T_{micelle}$. The results showcase an athermal micellization process that as more CEFE is added, the size of the endotherm decreases with concentration of solution. Bouchemal et al. and Meznerich et al. found similar findings in their characterization of 1,2 propanediol in F127, also noting athermal micellization [81,111]. Micelles form in the athermal micellization trend, but the energetics for formation are increasingly poor. The formation of micelles has an association energy cost, but the payoff is reduced due to the presence of additives in solution that interfere with packing.

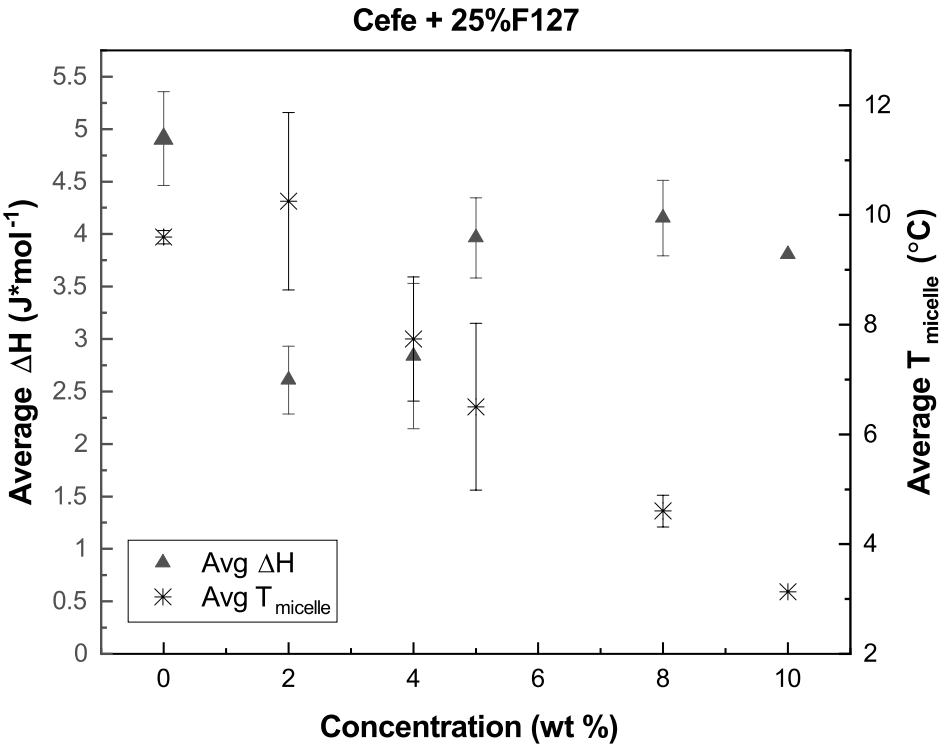

Figure 3.12 Increasing concentrations of CEFE in 25% F127 reduce the $T_{micelle}$ and a weak suppression of the endotherm dH.

Figure 3.13 shows how adding GM to 25% F127 solutions with increasing amounts of GM affected ΔH and $T_{micelle}$. The figure shows related changes in the endotherm and $T_{micelle}$ as concentration is increased. The endotherm changes are marginal, but a decrease in $T_{micelle}$ was observed. Sharma et al. also noted a reduction in $T_{micelle}$ in their study of anti-inflammatory agents as did Gilbert et al. in their study of para-hydroxy-benzoate esters [99,112].

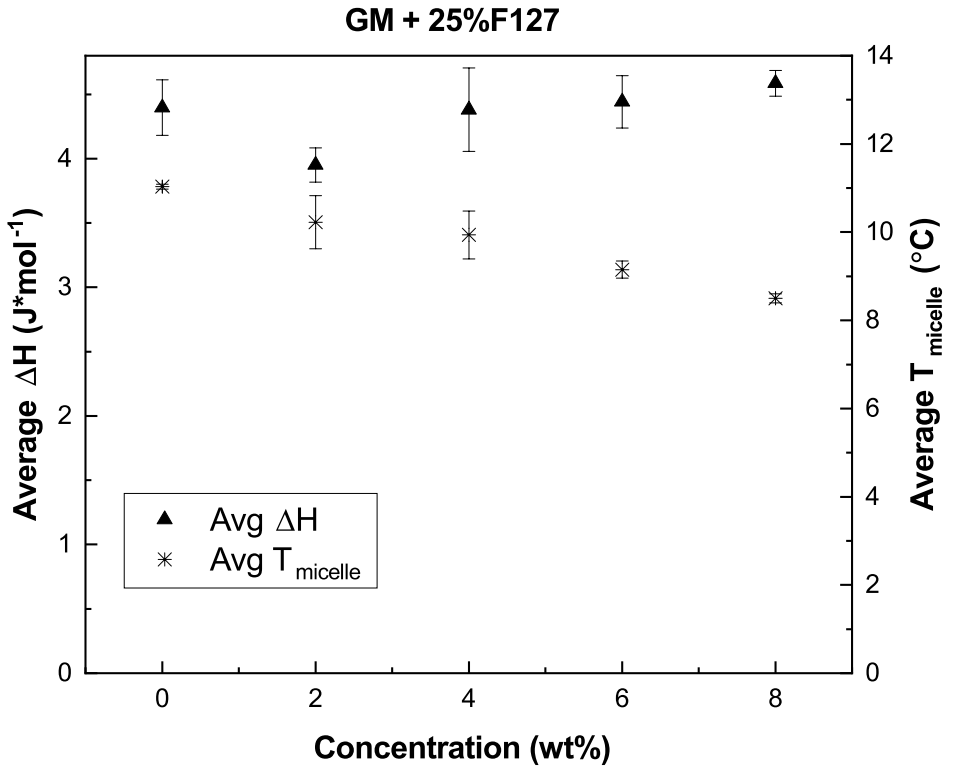

Figure 3.13 Average increasing concentrations of GM in 25% F127. There is an invariant effect on ΔH with respect to the neat and other concentrations. However, as concentration of GM increases there is a decrease in the $T_{micelle}$.

3.3.2 Effect of CIPRO on T_{gel}

To further understand the effects of antibiotics in amphiphilic gel formation, dynamic mechanical analysis using a rheometer was used to probe gelation. Previous work has shown the presence of dissolved solutes affects the gelation behavior of Pluronic solutions [103]. Figure 3.14 shows the addition of CIP up to 0.075% decreases the T_{gel} when compared to neat F127. Though CIPRO concentration has an invariant effect on micelle formation as concluded from the DSC measurements, the addition of CIPRO does appear to drive the T_{gel} formation temperature to lower temperatures. In a clinical setting, this would mean that the formulated drug in amphiphile would need to be further chilled to allow for liquid-like injection. However, at

loading concentrations above 0.075%, this effect is lost. Perhaps this is due to thermal lag on the Peltier stage or sample dehydration.

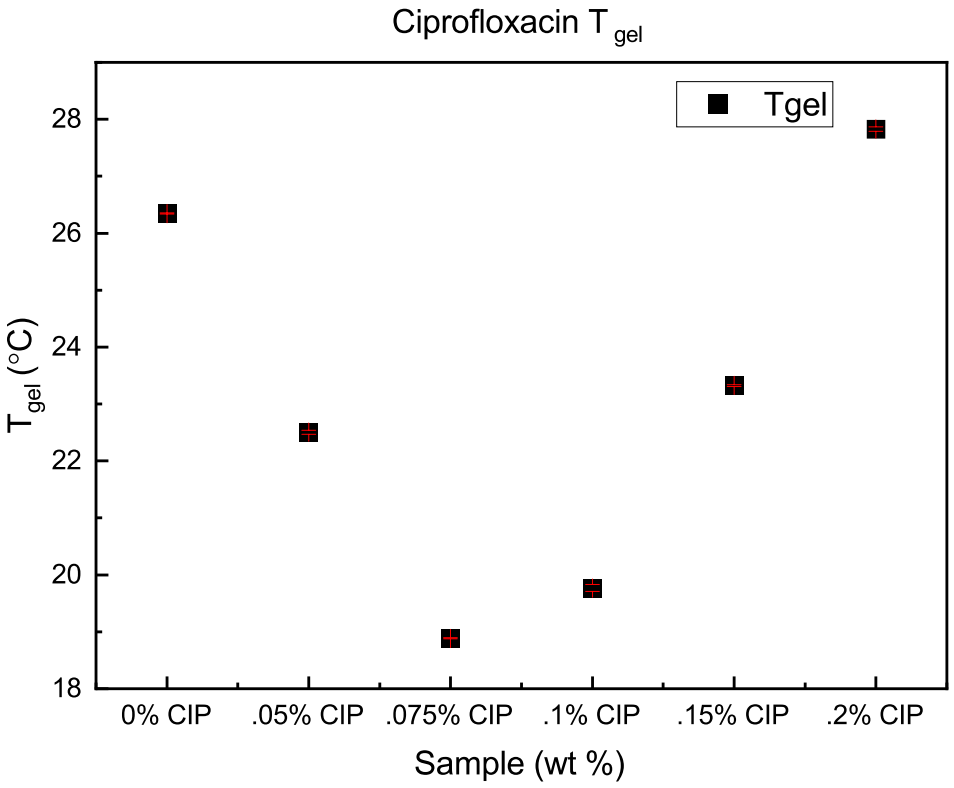

Figure 3.14 T_{gel} of CIP determine by G' vs G" cross over analysis. T_{gel} was determined from each concentration dependent parametric study performed at 1 Hz [109,110]. The results show that upon introduction of CIP there is a decrease in T_{gel} and is most reduced at 0.075% CIP. STDev <0.05 ºC for all points therefore error bars are too small to be show given the scale of the y-axis.

3.4 Discussion

Adding antibiotic additives to 25% F127 has shown several trends that are supported in the literature [28,81,93,99,103,105,112,113]. The disorder-to-order transition of Pluronics to form thermoreversible gels is regulated by intermolecular interactions between the dispersed organic drugs and the amphiphiles. Meznarich et al. showed methylparaben and other hydrophobic additives localize or associate themselves with the PPO core in Pluronic surfactants, which contributes to a suppression of $T_{micelle}$ and ΔH [81]. The lower ΔH is likely to lead to

increased imperfections as colloidal crystals form. A similar effect is noted with $T_{micelle}$ and ΔH with CIPRO. Given the similar trend, hydrophilic drugs could also be interacting with the PEO shell. Though micellization is primarily controlled by the PPO block length and concentration, the PEO block is of less importance [93]. However, there could be potential interactions between hydrophilic drugs and the hydrophilic PEO blocks, which could also lead to an increase in the $T_{micelle}$ onset temperature. The greatest effect on the thermophysical properties could potentially occur when an additive is interacting throughout the core-shell interface. In this study, the hydrophilic drugs CIPRO and GM showed $T_{micelle}$ changes that could be attributed to interactions with the PEO shell.

It is important to note that even though CEFE begins to have an increased effect on the endotherm at higher concentrations, it is still influencing micellization as indicated with a corresponding decrease of $T_{micelle}$. The influence is not seen in VAN, though both drugs are hydrophobic. However, VAN's size is a confounding factor. Therefore, it was more energetically favorable for the PPO core to not interact with VAN. Importantly, as Thompson et al. noted, if ternary compounds raise structural disorder, the enthalpy contribution to micelle formation should be reduced [82,105]. However, though not investigated in this study, the solute-solvent interactions could provide deeper understanding of the micelle formation energetics of VAN, GM, CEFE, and CIP. A component in the solute-solvent interactions is solubility. The solubility of CIPRO, CEFE, GM, VAN, and dextrose are shown in Table 3.2.

Drug	**Solubility**
CIPRO	30 mg/ml
CEFE	40 mg/ml
GM	50 mg/ml
VAN	> 100 mg/ml

Dextrose	450.5 mg/ml

Table 3.2 Solubility in water for additives.

If hypothesizing results based upon solubility values, the effect of the additives on the amphiphilic copolymer gel could be ranked from lowest to highest as presented in Table 3.2. However, solubility is not an independent factor when hydrophobicity/hydrophilicity and molecular size introduce variants on endotherm energy and $T_{micelle}$.

Additionally, solubility plays a role in gelation. Basak et al. showed that PPO-rich hydrophobic domains can incorporate hydrophobic drugs, such as Erythromycin, Aspirin, and Ibuprofen, and raise their solubility [103] when packaged accordingly. When there is a favorable free energy change, a hydrophobic solute is localized within the PPO blocks of the micelle core [114,115]. Bodratti et al. noted that in the context of drug delivery, one of the most useful features of Pluronics is their ability to solubilize hydrophobic drugs, raising their bioavailability while still allowing for thermoreversible gelation [104].

At concentrations >0.075% CIPRO, it was observed that dextrose began to precipitate out of solution. This resulted in the solution becoming a dispersion with different viscoelastic behavior that was evident in T_{gel} determinations. The question then arises, what role does dextrose play? Mathew et al. showed that dextrose acts as a stabilizer within the Pluronic solution with CIPRO and is commonly formulated with other pharmaceuticals [11]. When the T_{gel} of 5% dextrose in 25% F127 was investigated, there was a ~16 °C decrease in T_{gel} observed. Potentially, dextrose additionally acts as a chaperone in coordination with CIPRO within the copolymer system to induce micellization and an early gel formation. The gel formation refers to the transition from disorder to ordered state where the F127 micelles arrange into a crystalline-like lattice. The ordered state is based upon the repulsive forces between micelles. Consequently,

CIPRO likely interacts with the PEO shell, given its hydrophilic nature during micellization, and VAN interacts with the PPO shell of the micelle core.

3.5 Conclusions

In this chapter the micellization and gelation properties of antibiotic-loaded amphiphilic hydrogels were investigated to determine $T_{micelle}$ and ΔH via DSC. The suppression of the micellization endotherm and global trends as a function of concentration were investigated for VAN, CIPRO, GM, and CEFE. Overall, CEFE showed the greatest effect on $T_{micelle}$ ~7 °C decrease with the addition of 10% CEFE. GM showed the smallest statistically significant change in $T_{micelle}$ of 2.5 °C for 0.8% GM. Additionally, CIPRO, VAN, and GM had an invariant effect on the micellization endotherm, while CEFE reduced the size of the endotherm with respect to increasing CEFE content. Additionally, the viscoelastic response of CIPRO was investigated using oscillatory dynamic mechanical experiments using a rheometer. The variations in T_{gel} were concentration dependent. However, the influence of a quaternary additive, dextrose, also contributed to the gelation properties.

The data suggests that CEFE is modifying the energetic contributions to the micelle core formation, whereas VAN, GM, and CIPRO do not. However, the latter findings also show that size and solubility also play an important role in antibiotic-loaded hydrogel micellization.

Chapter 4 Elution of Pharmaceuticals from 25% F127 Hydrogel

4.1 Introduction

Amphiphilic copolymer-based gels and materials have been studied for a variety of pharmaceutical and biomedical applications, such as scaffolds for tissue engineering and nanotechnology based drug delivery [108,113]. Pluronics have been approved for FDA use in the human body at set concentrations due to some of their properties such as water-solubility and low toxicity. Their ability to dissolve hydrophobic solutes and thermoreversible properties have made F127 favorable for use in drug delivery and controlled release systems [99,116,117]. Though there are studies investigating the material properties of antibiotic elution from Callan et al. [118] and medical applications of antibiotic-loaded amphiphilic gels [64,103], there are limited studies that investigate the *in vitro* performance of drug-loaded amphiphiles.

4.1.1 Cell Culture Assays to Determine Cytotoxicity

Cell culture live/dead assays have commonly been used to assess the cytotoxicity of materials and as an extension, the potency of toxic materials [119]. Live/dead assays, which are performed *in vitro*, have been crucial in gauging antibiotic efficacy and assessing relative potency against pathogenic bacterial species. *In vivo* testing is useful in determining whether transport and contact of foreign species trigger cellular responses that could include mutation, apoptosis, signaling issues, and changes in phenotype. In assays focused on discovery antibiotic potency, the active drug or material is mixed homogeneously within the cell culture medium to ensure cellular exposure. Questions arise when antibiotic performance is not related to potency,

but more to flux and conveyance from controlled release drug delivery systems. New kinds of assays for regulated transport and controlled release toxins are needed. The current study utilized a more targeted assay called a modified Zone of Inhibition (ZoI) test where a drug-infused gel is deployed in an injectable plug form as opposed to being mixed homogeneously. Instead of using an antibiotic-loaded disc, a void was created within the agar to experimentally determine point source diffusion.

ZoI tests are cell culture assays that can be used to clinically measure antibiotic resistance [120]. In the test, the targeted compound or antibiotic is placed on media within a cell culture dish and cell/virus/bacteria is added and coats the entire exposed surface of the media. Overtime, the targeted compound is then left to diffuse in the agar plate. If the added species is susceptible to the targeted compound, then a dead region surrounding the target called a zone of inhibition forms overtime, and the diameter of the ZoI correlates with a *MIC* [121]. The test, which can take hours or days, can assess if water-soluble targets can inhibit growth of the tested bacteria strains. Typically, gauging antibiotic or antimicrobial potency is conducted with liquid antimicrobials placed as a droplet and allowed to dry or added to the agar media via a disk [120].

4.1.2 In Vitro Testing of Antibiotic-Loaded Hydrogels

If the goal is to assess targets undergoing controlled release from a controlled release matrix, then tests that resolve the potency of the target do not consider the challenges in releasing from or conveying through the matrix. The time elements associated with these tests include the permeation rate through the matrix and subsequent permeation into the agar. Variants on these tests have used dialysis assays, which involves adding the matrix within a dialysis membrane and tracking the target concentration in a receiver solution overtime [58]. Additionally, growth curve measurements based on optical density are commonly used in microbiology to evaluate potency

of solutions by monitoring microbial growth and proliferation overtime [122]. These evaluations can result in comparisons related to mass transport of drugs out of both the matrix and through the membrane. Still, it would be beneficial to use these kinds of functional assays to assess the clinical viability and release characteristics. Therefore, an alternative method, specifically one that uses antibiotics for controlled release in gels to address localized infections and sepsis, is needed to test target-loaded dissolving hydrogel systems.

4.1.3 Overview

A wide variety of sequestration matrices have been clinically deployed in controlled drug delivery including bone cements, hydrogels of a wide variety of compositions, and sutures, among others [52,58,67]. However, analysis from previous works have typically examined the physical and antimicrobial properties of matrices separately. The Love research group has been interested in injectable therapies based on amphiphilic copolymers that undergo gel formation if a high enough concentration is reached. If immersed in a system that dilutes the gel content, the gels are coerced to dissolve releasing soluble targets as they are solubilized. This chapter highlights protocols to produce a functional experiment and provides guidelines on results, analysis using two different kinetic models, the resulting interpretations, and insights.

4.2 Materials and Methods

4.2.1 Preparation of Gel

4.2.1.a Preparation of F127 hydrogel

Pluronic solutions used in these experiments were prepared in a similar manner to that described in Chapter 3. Pluronic F127 was obtained from Sigma Aldrich and used as received.

The 25% F127 solutions used in these experiments were prepared in 0.9% sterile saline and DI water.

4.2.1.b Incorporation of antibiotic with F127 hydrogel

Pharmaceutical samples used in these experiments were prepared in a similar manner to that described in Chapter 3. Sterile lyophilized vancomycin was obtained from the Alvogen Pharmaceutical Company and Gentamicin was obtained from Frenisus Kabi. Table 4.1 lists all concentrations and formulations of antibiotics prepared and used in the study.

Antibiotic	F127 Solution	Concentration (wt%)
VAN	25% F127 in 0.9% Sterile Saline	1%, 2%, 3%, 4%, 5%
	25% F127 in DI water	
GM	25% F127 in DI water	0.4%, 0.6%, 0.8%

Table 4.1 Details of the samples and formulations and concentrations used for the study.

4.2.2 Cell Culture Assay

4.2.2.a Preparation of tryptic soy agar plate

In preparing Tryptic Soy Agar (TSA) plates, 40 g of BD Biosciences nutrient agar was dissolved in 1 L Milli-Q® water. Once all powder was dissolved in water, the agar solution was autoclave sterilized at 121 °C at one atmosphere of positive pressure for 15 minutes. The agar solution was allowed to cool to 40-50 °C before being poured into plates to avoid condensation. Eight ml of the agar solution was then dispensed into 6 cm cell-culture dishes and allowed to cool until fully solidified at room temperature.

4.2.2.b Preparation of agar plate with antibiotic loaded-gel

The following procedure was used to load agar plated with antibiotic gel. Once the agar was set, a 3 mm biopsy punch was used to create a hole in the center of agar fraction (see Figure 4.1) in the dish which was then replaced by the antibiotic-loaded gel (see Figure 4.2). Approximately 30 μL of agar was removed and an equivalent amount of the antibiotic-loaded hydrogel was pipetted within the biopsy area in the dish. In addition, traditional cell culture plates were prepared where 30 μl of antibiotic gel were pipetted within the center of the plate. The gel plates were then left to set covered on the bench top at 1 and 12 hours to facilitate drug permeation within the matrix (see Figure 4.3 A-C). The experimental condition was $n = 3$.

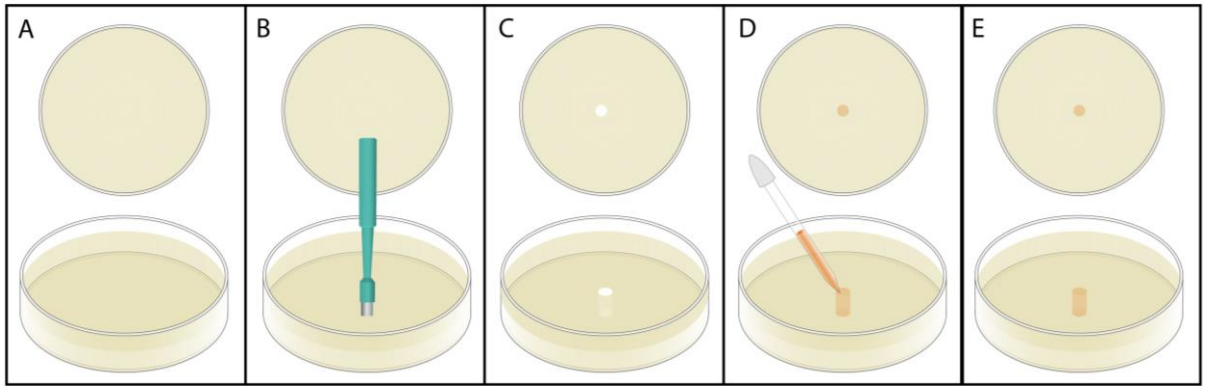

Figure 4.1 (A) A Petri dish filled with agar. (B) A biopsy punch is used to punch a hole into the agar. (C) The resulting view of the biopsy void. (D) The void is filled with the antibiotic-loaded hydrogel. (E) The resulting view of the filled void with drug-loaded gel.

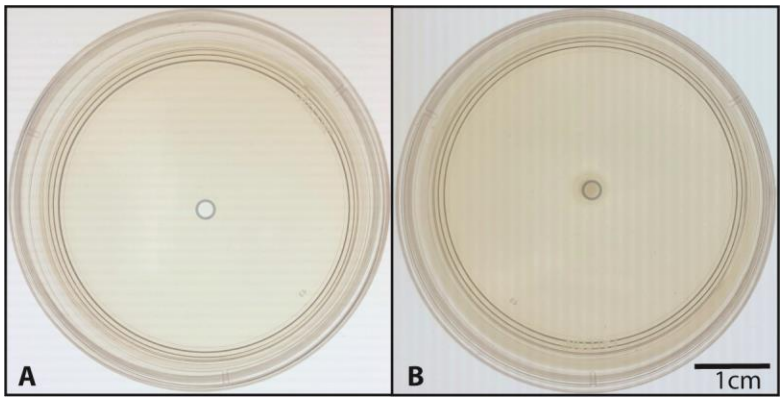

Figure 4.2 (A) After biopsy punch is used to create void, (B) the void is loaded with antibiotic-loaded hydrogel.

4.2.2.c Bacterial strain, media, and growth conditions

Methicillin-*resistant Staphylococcus aureus* (MRSA) USA300 was used in all experiments with VAN due to its prevalence in human infections and virulence. *Escherichia coli* (UTI89) was used in all experiments with GM. A glycerol stock of the strain was maintained at -80 °C. Single colony inoculates were grown in tryptic soy broth + 1% glucose w/v (TSB_G) under shaking conditions at 37 °C. Mid-log, optical density (OD) of 0.45-0.55 at 600 nm (OD_{600}) cultures were used in cell culture assay experiments and OD_{600} = 0.05 cultures for bacterial growth inhibition experiments.

4.2.2.d Introduction of bacterial media

One milliliter of bacterial-laden broth was pipetted into each gel plate (see Figure 4.3 A.1). Once the broth covered the surface of the plate, the excess broth was immediately decanted. The bacterial-loaded gel plates containing a center plug of antibiotic-loaded gel were then loaded in an incubator at 37 °C for 24 hours.

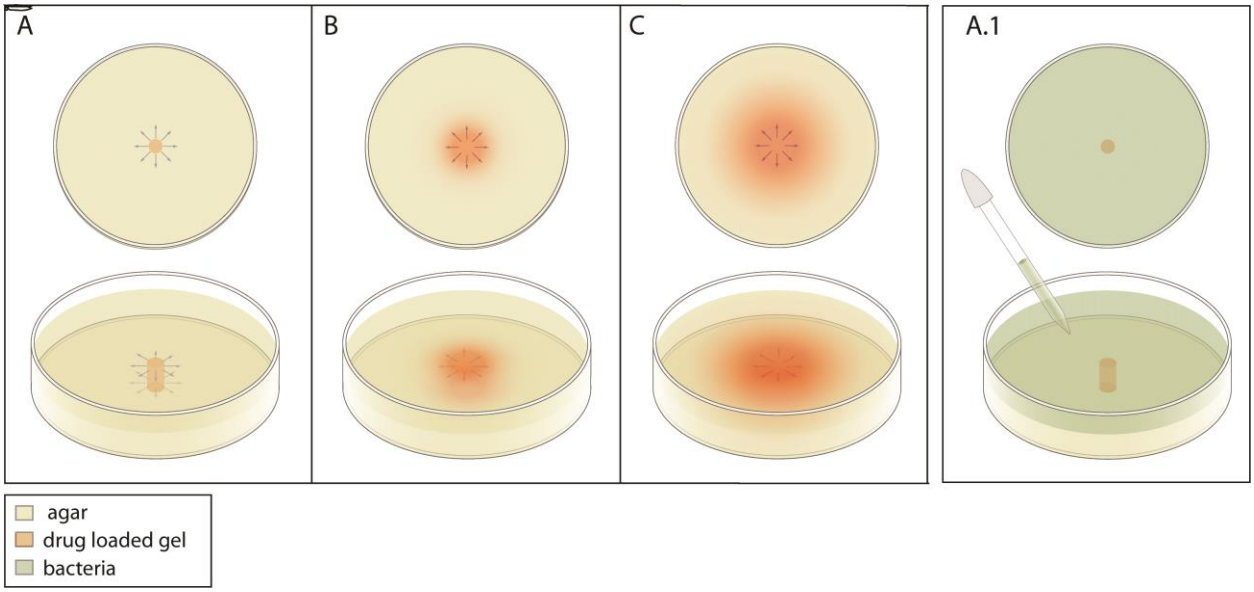

Figure 4.3 (A-C) Radial growth of the clear region as a function of time based on both the dissolution of the gel near the wet regions of the agar devoid of amphiphilic copolymer, and due to the permeability of the antibiotic in solution. (A.1) The bacteria media is pipetted onto the surface to the agar after the biopsy hole is filled with antibiotic-loaded gel. Excess media is decanted off. The bacterial-laden broth is homogenously distributed on the entire surface.

4.3 Data Analysis

4.3.1 Cell Culture Analysis

The resulting ZoI quantified how much bacterial growth was inhibited on each plate relative to the different concentrations of drug-loaded gels tested. As shown in Figure 4.4, a circular region formed corresponding to a ZoI. The darker areas near the terminal edges of each plate confirmed viable bacterial growth. The demarcation between the live and dead regions denotes a high enough concentration of antibiotic to achieve a MIC. The diameter was recorded for each culture and the mean and standard error were calculated.

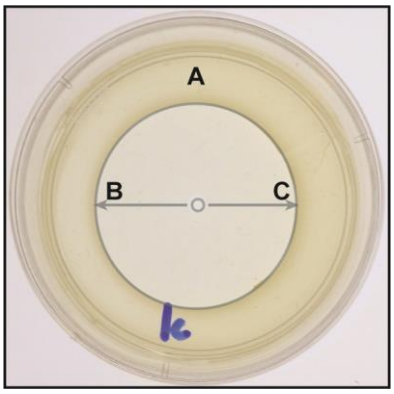

Figure 4.4 Modified cell culture plate loaded with 1% VAN in 25% F127 prepared with saline. (A) Area of bacterial growth (BC) diameter of inhibition resulting in a ZoI. Center biopsy punch is marked with circle.

4.3.1.a Minimum inhibitory concentration

The determination of ZoI provides an estimate of the susceptibility of bacteria to antimicrobial compounds. When using ZoI to determine MIC, the standard procedure uses a paper disk loaded with the antimicrobial compound of a known dose in a cell culture plate with the pathogen being investigated. To estimate the MIC of antibiotic-loaded amphiphilic gels, a correlation can be made between the ZoI and the standard value of MIC and its ZoI. Consider Equation 4.1:

$$ab = xy \qquad \text{Equation 4.1}$$

Where *a,* is the established MIC; *b,* is the established cell culture inhibition diameter; *x,* is the diameter of inhibition of antibiotic-loaded amphiphilic gel; and *y,* is the MIC of antibiotic-loaded amphiphilic gel. If the standard values of MIC and disk diffusion for a particular pathogen are known, then the resulting diameter from the modified cell culture analysis can be used to determine the MIC associated with the antibiotic-loaded gels. This study investigated the ZoI for VAN and GM. It is important to note that standard disk diffusion testing is not an entirely reliable test for VAN because it is not able to differentiate among VAN susceptible

isolates of *MRSA* [123]. Therefore, the MIC for VAN was unable to be determined using this method. The MIC values for GM-loaded amphiphilic gels were determined using the acceptable quality control ranges for susceptibility testing for gentamicin provided by the manufacturer and the CLSI document M100-S23.

4.3.2 Bacteria Growth Inhibition

As a complementary experiment, an elution study of VAN in 25% F127 was done to investigate bacterial growth inhibition. Figure 4.5 depicts the experimental process described below.

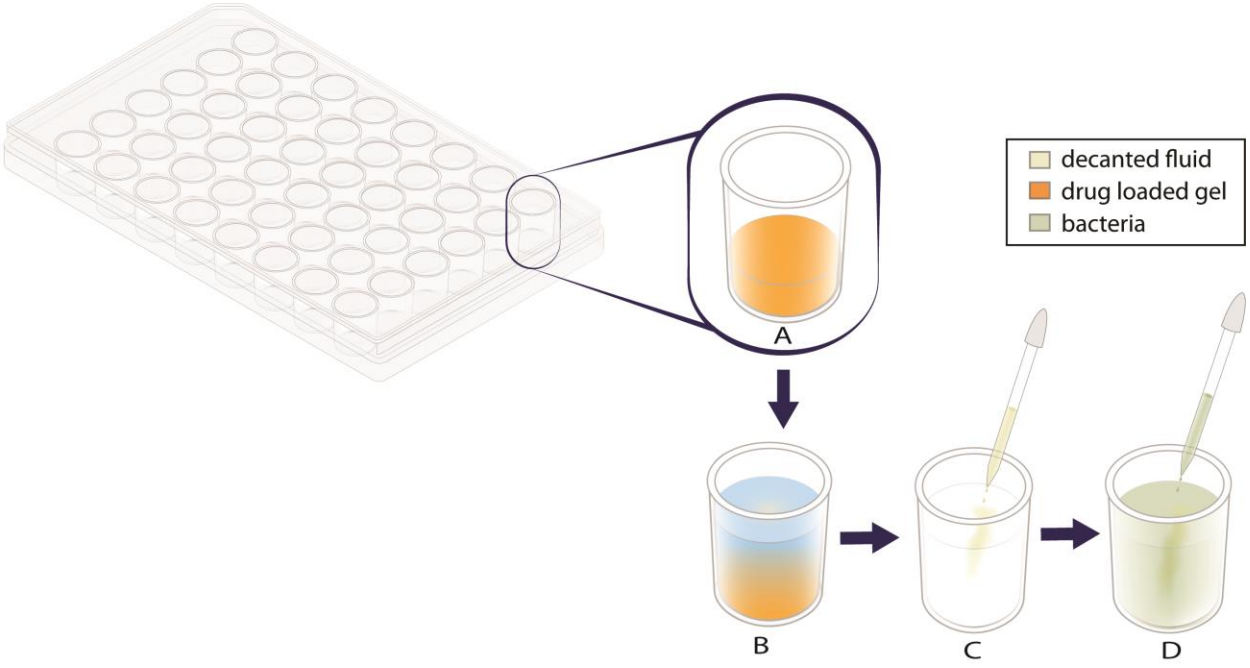

Figure 4.5 (A) 100 µl of drug-loaded gel is pipetted into 48-well plate. (B) 900 µl of milli-Q water is added after gel has set at 37 ºC for one hour. (C) At every hour 100 µl aliquots are taken from the 48-well plate. (D) The resulting aliquots are combined with bacterial media in a 96-well plate and then placed in a microplate reader.

4.3.2.a Elution Trials

In a 48-well clear bottom plate (Fisherbrand), 100 µl of 1%, 2%, 3%, 4%, and 5% VAN in 25% F127 and neat 25% F127 were plated. The gel was allowed to set for one hour at 37 ºC and then topped with 900 µl of Milli-Q water. The plates were then stored at 37 ºC for 6 hours, and at 1-hour increments 100 µl aliquots were removed and set aside. The experimental condition was $n = 3$. The mean and standard error for each sample were calculated for each time point.

4.3.2.b Bacterial growth curve measurements with a microplate reader

For the growth curve measurements with a microplate reader, 96-well clear bottom microplates (Fisherbrand) were used. To measure the growth of bacteria, 100 µl of prepared bacterial cultures (with aliquots from the elution trials) were transferred to the microplate wells. The microplates were covered with PCR film and placed in the microplate reader to monitor the OD at 600 nm of the bacteria in the wells. The plates were maintained at 37 ºC. The OD of each well was read every 10 minutes for 24 hours. The experimental condition was $n = 3$. The mean and standard error for each sample were calculated.

4.3.2.c Application of mathematical model for E. Coli growth

Data were collected in the growth experiments that allowed for the dynamic measurement of optical density of the growing bacteria through the plate reader. The plate reader allowed for kinetic analysis of the growth rates to occur while VAN was releasing from gels-relative to a neat system. There are many different models that could be applied to understand how to represent dynamic changes, such as biological growth. Halley and Mackay presented a number of different kinetic models that could be used to represent dynamic data like what has been generated in the present study [124]. Two different models were specifically used for this

analysis, one of which was a Gompertz-based model (see Equation 4.2) that yielded a growth rate constant toggling between an initial and a final measurement of optical density. The Gompertz model yields a constant, k, that broadly represents the growth rate. The Gompertz model is popular in representing biological growth data in cell culture. The model does not account for any kind of induction or latent period before growth commences. The second model that was considered for the growth is called a Boltzmann sigmoidal model (see Equation 4.3), which incorporates two separate time constants that could yield more accurate representations of the dynamic data. Calculations for the elution trial aliquots at different concentrations (1%, 2%, 3%, 4%, and 5%) for minimum (Y_0) and maximum (Y_m) optical density, specific growth rate (k), and lag coefficient (1/k) were carried out by applying the modified Gompertz equation (see Equation 4.2) using GraphPad Prism software (GraphPad Software, San Diego, CA, USA).

$$y = y_m * \frac{y_o}{y_m}^{e(-k*x)} \qquad \text{Equation 4.2}$$

The Gompertz model is one of the most frequently used nonlinear regression models used to fit growth data by microbiologists [125]. In analyzing bacterial growth, a three-parameter Gompertz model is commonly used, which has been discussed by Jeffries et al. [126]. It is important to note that there are Gompertz with other parameters [127]. Comparisons were made between the initial loading concentrations of the aliquots taken at 1, 2, 3, 4, 5, and 6 hours of elution and the control aliquots.

An alternative kinetic model called the Boltzmann sigmoidal model (see Equation 4.3) includes two time constants that allow for the determination of a latent period or induction time before growth is triggered [128–130].

$$y = \frac{A_1 - A_2}{1 + e^{(x - x_0)}/dx} + A_2 \qquad \text{Equation 4.3}$$

Here, A_1 and A_2 represent the lower and upper thresholds of optical density, respectively. There are two time constants that need resolution, x_0, represents the time required for the observable value, A, to toggle halfway from A_1 to A_2. The second time constant, *dx*, is the slope of the curve at x_0, which is assumed as the period of maximum growth. Simple math yields that there is a period of 4*dx that represents the time to toggle completely between A_1 and A_2. Thus, an appropriate induction time could be represented in the Boltzmann model as the expression x_0-2*dx as the latent period before growth occurs. If the slope of the curve is large, this occurs over a very short interval dx, so like the Gompertz model, a rapid growth rate corresponds to a short time interval during which the transformation occurs.

4.4 Results/Discussion

4.4.1 Modified Cell Culture Assay

A traditional bacterial culture was performed to compare the efficacy of the modified method for antibiotic-loaded hydrogels. As shown in Figure 4.6, 2% w/v VAN was plated via biopsy and droplet method. In the biopsy culture plate, there was a non-uniform area of inhibition that occurred. However, the droplet culture plate had complete inhibition.

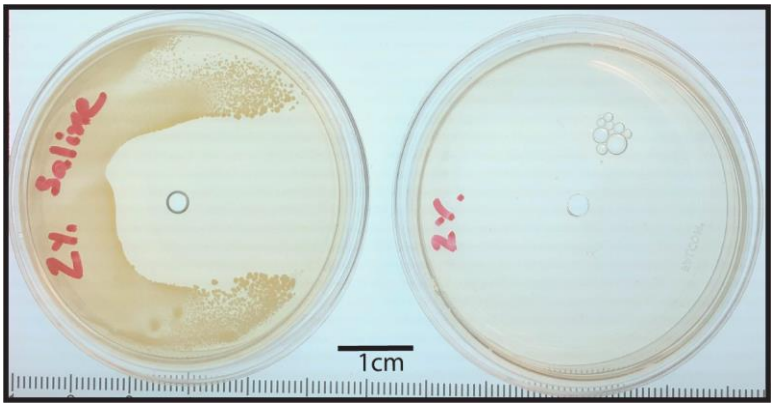

Figure 4.6 Two percent VAN in saline sans 25% F127 to the left it in the modified cell culture assay, and to the right the traditional droplet cell culture assay both after 24 hrs incubation.

The VAN loaded hydrogels in saline that were plated via the droplet method did not show complete inhibition as compared to the traditional culture. The cultures showed that as antibiotic concentration increased, the area of inhibition also increased. The results are reported in relation to the diameter of the inhibition area are shown in Figure 4.7. A similar trend was also observed in the biopsy plates for VAN in saline and DI and GM in DI, which are shown in Figure 4.7 and Figure 4.8, respectively.

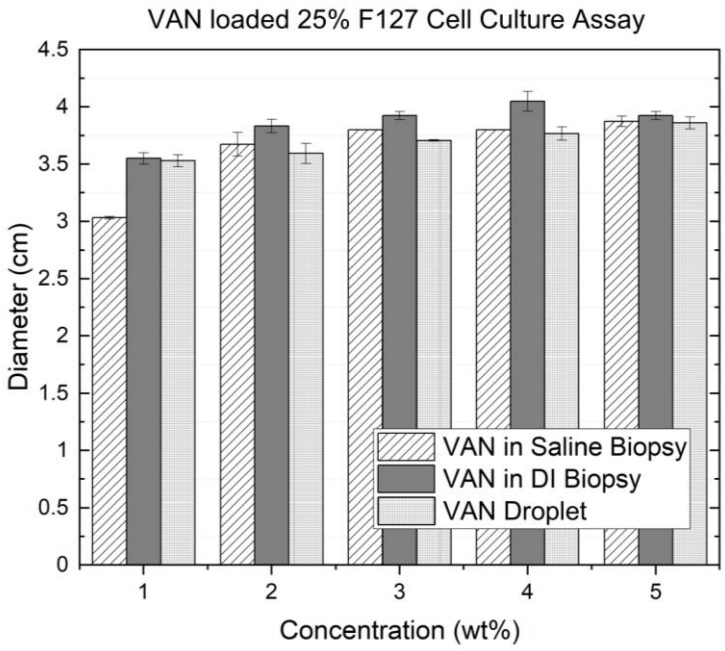

Figure 4.7 Resulting diameter of elution of VAN from 25% F127 Gel prepared in DI water via cell culture assay after 24 hrs incubation.

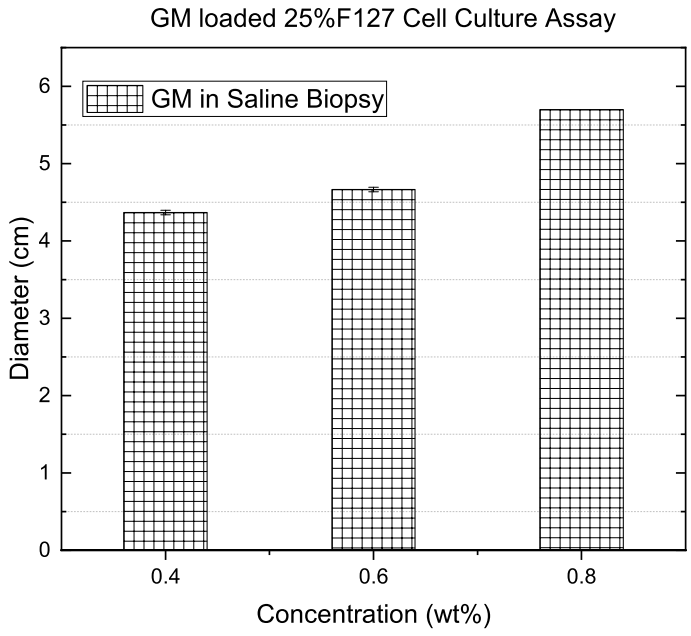

Figure 4.8 Resulting diameter of elution of GM form 25% F127 Gel prepared in DI water and tested in a modified cell culture assay after 24 hrs incubation. An increase in the inhibition diameter increased in relation to concentration with the highest concentration resulting in complete inhibition of growth.

4.4.2 Bacterial Growth Inhibition and Determination of Lag Time and Growth Rate

For a more quantitative analysis, the Gompertz growth model was used (a) to fit all of the OD curves (see Figures 4.9 and 4.10) and (b) to find the growth rate and lag times with respect to the VAN concentrations tested. Where y_0 is the starting population, y_m is the maximum population and *1/K* is the time required to achieve an inflection point during the growth phase of the bacterial cell culture experiments. K is defined as a lag coefficient.

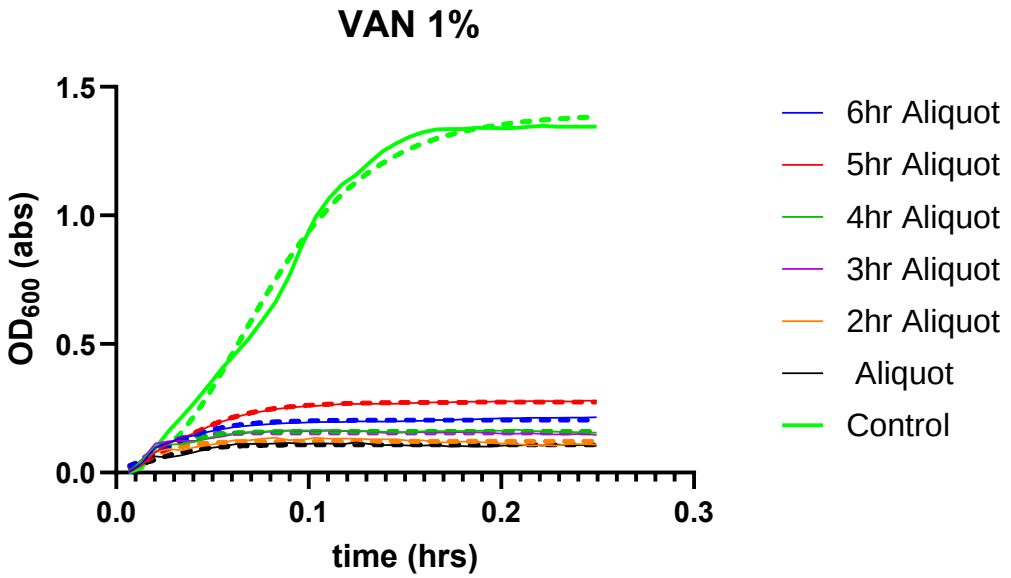

Figure 4.9 Bacterial growth inhibition results plotted with results of the Gompertz analysis of 1% VAN growth curves for 1- to 6-hr elution study before exposing the bacteria to the plate. Solid line represents time points when the elution sample was taken; dashed line represents Gompertz model fit. Results show that as time progressed less VAN eluted from the samples corresponding to an increase in bacterial growth in the samples, however growth was suppressed 70-80% less than control.

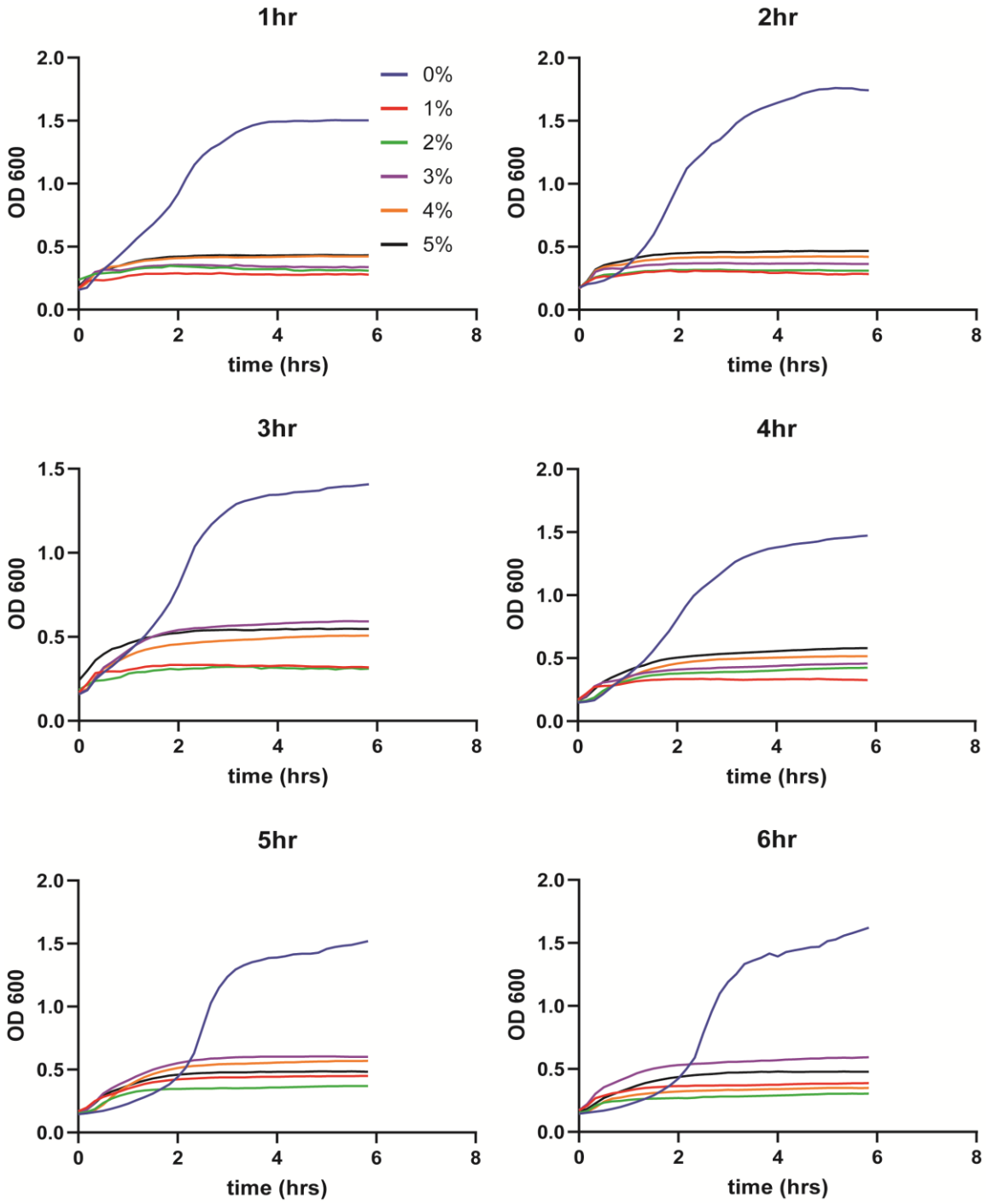

Figure 4.10 The resulting OD curves were plotted from the results of the bacterial growth experiments and categorized by time. The highest curve corresponds to the neat gel and lower curves to the gels loaded with antibiotics. Figures show the average of three measurements.

As shown in Figure 4.10, the maximum OD is plated against the growth rate. When compared against the control, the antibiotic-loaded hydrogel samples were successfully able to

inhibit bacterial growth and, in turn, decreased y_m and lag time. The results also showed that on average, the initial time points at lower concentrations of VAN were more efficient at inhibiting bacterial growth relative to the higher concentrations with respect to optical density. Additionally, when assessing a MIC, none of the VAN loaded reached the optical density of the neat bacterial growth curve or near it (see Figures 4.9 and 4.10). Further work is needed to determine the MIC of VAN- and GM-loaded hydrogels and to further refine bacterial growth inhibition results. It is important to note that although MIC is indicative of the inhibition of bacterial growth, it provides limited information about a specific bacterial resistance mechanism. Growth studies represent the earliest stage of the bacterial growth cycle and provide insight on bacterial kinetics and can also be used to infer MIC values.

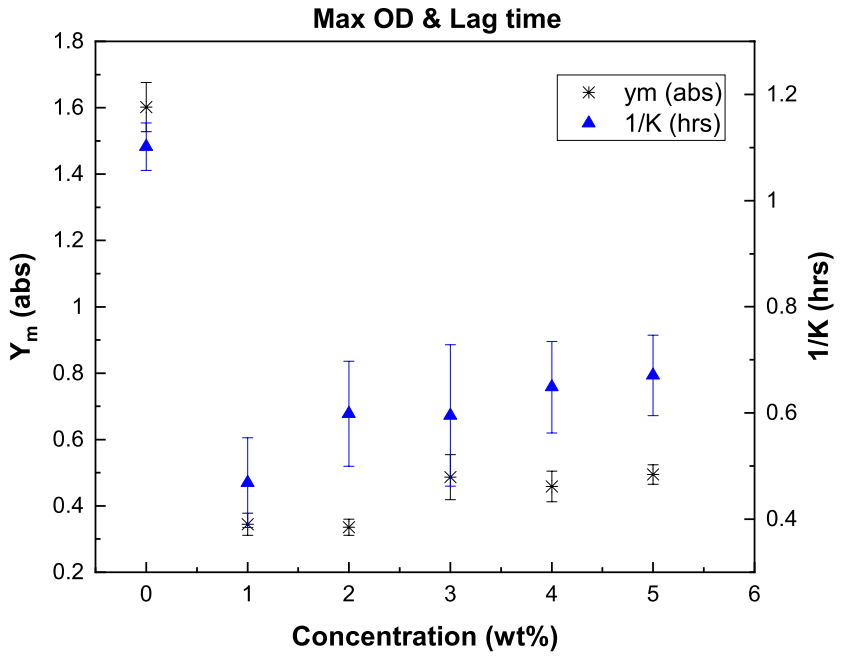

Figure 4.11 Max Optical density and lag time with respect to concentration. When compared against the control, the antibiotic-loaded F127 gels have a lower max OD (inhibition is occurring) and lower lag time (growth rate is increasing, indicating slow bacterial growth).

As the bacterial cells interact with the antibiotic present, they begin to change gene expression. Once they adapt to the new environments and begin to grow again, the physiological changes are reflected in the lag time and growth rate. The lag phase is hypothesized to be involved in fighting pathogens. For example, if there is an increase in lag time, then there is a decrease in the amount of antibiotic eluted from the amphiphilic gels available to curtail bacterial replication [128,129]. However, using the three-parameter Gompertz function does not provide a clear description of what is happening. Given that the antibiotic used is an inhibitor, its mechanism of action is different from that of other bacteriostatic and bactericidal drugs that are commonly used with the Gompertz model. Perhaps a different model would be better suited to provide insights on the growth rate of the bacteria in the presence of an inhibitor.

The Boltzmann model is essentially a sigmoidal model that remains at A_1 until sufficient time has lapsed for the transformation to occur relative to the two Boltzmann time constants. If there was a sufficient lag in the growth rate, the extra refinement in the Boltzmann model should result in a better fit.

As shown in Figure 4.12, the Boltzmann model and the Gompertz model were deployed using Origin. The value of the Boltzmann model compared to the Gompertz model is that it can accommodate a latency period before growth occurs. Figure 4.12 only shows positive times in the Boltzmann model. The growth rate of the neat bacteria by the two models were compared with and without antibiotic, and were compared to a neat copolymer plug devoid of inhibitor. The growth rate based on OD goes from 18.7 hrs^{-1} and the 1-hour aliquot rate was 12.8 hrs^{-1} using the Boltzmann model. The reduced growth rate shows that the bacterial in the control were proliferating much faster than in the presence of the inhibitor. The Gompertz model is unable to deliver the type of insight provided by the Boltzmann model. The growth rate as determined by

Gompertz went from 25.7 hrs^{-1} for the control to 63.6 hrs^{-1} for the samples loaded with VAN, which seems a little counterintuitive.

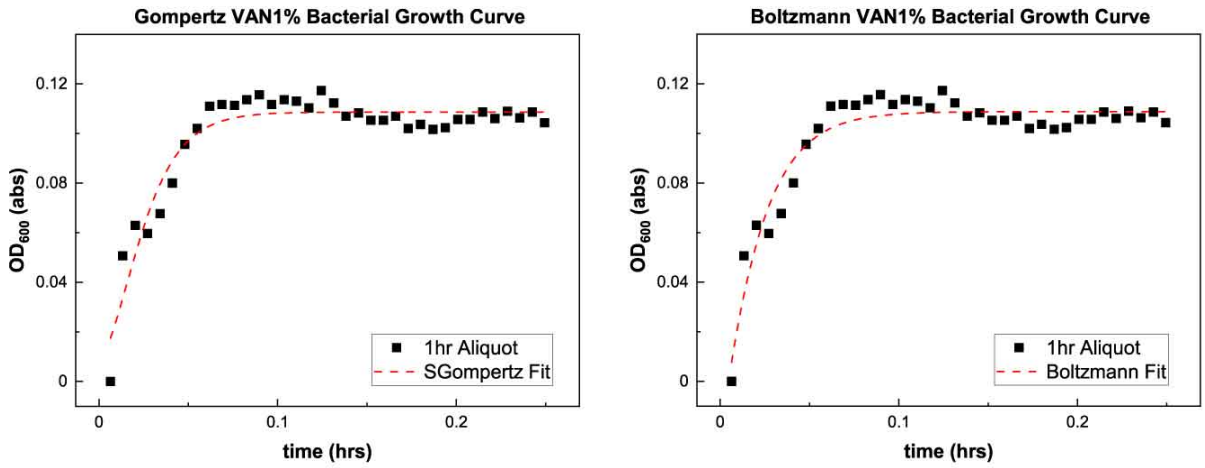

Figure 4.12 The Gompertz and Boltzmann models run on 1% VAN 1-hour Aliquot data. The dashed line represents the models fitted and black squares represent the data.

A separate question that arose was whether the Boltzmann model could extract a lag time from the analysis for a very effective inhibitor. Taking the slope of the fitted curves and resolving the value of time at x_0-2dx, the deviations in the curves from the initial optical density are occurring almost instantaneously. Both models seem to fit the data well (see Appendix). The Boltzmann model's kinetic parameters appear to be following the model of inhibition intuitively. The fact that inhibited growth might be occurring in some fraction of the dish probably makes the distinction between the models somewhat moot.

4.4.2.a Considerations

There are two different types of issues with a new form of assay: one in the experimental details of producing samples and one in the analysis of the data. In modifying the traditional cell culture assay for use with an antibiotic-loaded hydrogel, there were challenges involved in the protocol. One challenge was determining how to introduce the gel into the cell culture dish. After

biopsy, the antibiotic amphiphilic gel was pipetted into the dish. However, due to the gelation properties, the gel was not set after initial introduction. As the gel set, elution of antibiotic to the surface and/or agar matrix occurred with the droplet and biopsy dishes, respectively. The gel plates via droplet and biopsy were initially set for 10 minutes before adding the bacterial broth. When the bacterial media was pipetted onto plates that were set for an hour, the inhibition regions did not form concentric circles, but rather varied nonuniform inhibition regions, as shown in Figure 4.13. Since the gel was not set at the time interval, the F127 would "drag" and streak VAN that had eluted from the gel when the liquid bacteria broth was introduced. When the gel was allowed to set longer (>1 hour), these variances did not occur. A similar pattern occurred with VAN (see Figure 4.6) in saline without F127; however, complete inhibition was observed in the droplet because the VAN was completely soluble in the bacterial broth, and a misshapen area was observed in the biopsy where the VAN "spilled" out and mixed with broth. These challenges were noted, and the protocol was adapted to gather the results presented in this chapter.

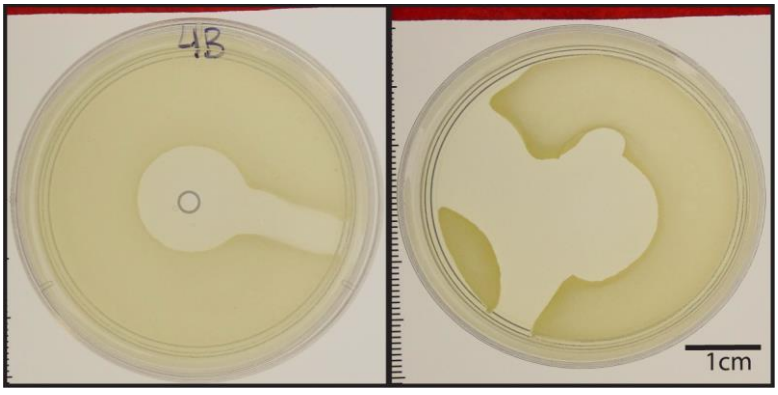

Figure 4.13 (Left) Gel is not set within biopsy before bacteria introduction. (Right) Gel not set with droplet before bacteria intro.

Additionally, determining how to quantitatively assess bacterial growth inihibition was challenging. Due to the physical structure of the antibiotic-loaded gel, it was not feasible to use as prepared to perform a growth curve study. Therefore, an elution study was needed to assess the efficacy of the eluted VAN. However, there were potential sources of error with the method employed, such as mixing the gel with the aliquot, which caused a misreading of the absorbance. Also, it is inconceivable that drug permeation is too fast to be fully released during the time scale of the experiments. Alternative experiments are needed to correlate the bacterial growth inihibition curves to a concentration to determine MIC, but the initial effort looks promising. More experimentation is needed to replicate these results and to develop a figure of merit, such as the rate constant from the Boltzmann model. The best that can be expected is a reduced growth rate, not complete inhibition.

4.5 Trends and Conclusions

Adapted bacterial culture assays have been used as a standard *in vitro* experiment to determine a zone of inhibition of an antibiotic to assess antimicrobial activity and potency. The modified *in vitro* method using a cut out to load the antibiotic-loaded drug can help assess the diffusion of antibiotics loaded in amphiphilic gels by assessing a zone of inhibition following insertion and incubation. VAN produced a ZoI range of 3.0-3.9 cm for the biopsy method and 3.5-3.9 cm for the droplet method for the 1-5% concentrations. GM ranged from 3.5 cm to complete inhibition within the cell culture plate. When compared against a traditional droplet method, the biopsy method more precisely sensed a concentration dependent inhibition for concentration ranges of vancomycin studied. Incorprating the Gompertz model in the bacterial growth inihibition experiment allowed for a quantitaive assessment of the relative growth rate of bacteria when exposed to antibiotic-loaded gel. In the case of the Boltzmann model, the growth

rate in the neat samples, as evidenced by the analysis, is clearly higher than those containing VAN. Additional refinement using a more informed perspective on the analysis of this data is needed to quantify the effects in a more controlled way.

Adding antibiotics in the plug-in-plate model reduces the overall amount of bacterial proliferation as noted by both analytical models. There were some noted reductions in the inflection time as well when antibiotics were included, which ranged from 0.469-1.102 hrs for 1-5% VAN, and the control had the highest values increasing with respect to VAN concentration. This study illustrates a new approach to monitior antimicrobial properties and kinetics by providing a quantiative and mechanistic evaluation.

Chapter 5 Conclusions and Future Works

5.1 Summary

The aim of this dissertation was to survey and probe how antibiotic-loaded drug delivery platforms could potentially be used to treat deep bone infections and develop schemes to investigate the antimicrobial properties of similar antibiotic-loaded amphiphilic gels that could be more effective. Investigations to establish the baseline efficacy of current drug-loaded platforms using bone cements, to address thermophysical changes in gelation formation of drug-loaded 25% amphiphilic copolymer F127 gels, and to assess their antimicrobial elution characteristics were completed.

A survey of the literature identified studies in which both controlled drug release and mechanical behavioral assessments on samples submerged for periods of time had been conducted on drug-infused cements. The drug of choice was vancomycin (VAN) in part due to its (a) higher potency relative to other antibiotics; (b) common usage for staph infections; and (c) direct relation to high concern infections, such as those linked with periprosthetic joint infections. The literature review evaluated the controlled release of vancomycin from a myriad of different matrices all formed primarily from various commercial bone cements and formulated in the clinics. Takeaways from the limited pool of published research indicates that large fractions (> 99%) of the infused vancomycin remain sequestered in the cement and are not bioavailable after solidification. Antibiotic fluence from samples exposed to a receiver solution ranged from 1 to 283 $\mu g/cm^2hr$ primarily depending on dose level. Most of the drug release happened very soon after immersion, and perhaps some variation in the initial fluence measurements depended on

when the first measurement was taken. The initial strength of the various antibiotic-loaded samples as produced was between 52 and 96 MPa. Simulated exposures in a fluid environment by submersion reduced the antibiotic-loaded strengths between 3% and 29%. Some strength measurements were noted below the ASTM F451 standard for acrylic bone cement although drug-releasing spacers likely have different requirements. The glassy behavior of the cured cement led to low permeability and a burst response, which were noted for other drugs formulated into cements.

Based on the aforementioned results, a study was performed on the thermophysical and viscoelastic properties of Pluronic F127 gels loaded with vancomycin (VAN), ciprofloxin (CIPRO), cefepime (CEFE), and gentamicin (GM) as a function of concentration as they form a softer, drug-infused gel using DSC and rheology. The rationale for the study was matrices with more molecular mobility and a lower glass transition temperature would be more conducive to drug permeability from its bulk. Variations in ΔH, $T_{micelle}$, and T_{gel} when increasing concentration of ternary additives were present. The largest decrease in $T_{micelle}$ was seen with 10% CEFE in 25% F127, while the smallest, ~2.5 °C, was seen with 2% CEFE. Notably, though $T_{micelle}$ and ΔH were invariant with CIPRO concentration, there was a ~2 °C decrease from the neat $T_{micelle}$ when CIPRO was already formulated with dextrose when mixed with the amphiphile, which had a greater influence on decreasing the endotherm energy from ~4.5 $J*mol^{-1}$ to ~3.9 $J*mol^{-1}$. The results showed that solubility and molecular size play a role in thermophysical and dynamic mechanical analysis of micellization and gelation.

A modified cell culture assay and bacterial growth inhibition protocol was developed to investigate gel-elution characteristics. The specific objectives of the cell culture analysis were to experimentally determine a “zone of inhibition” (ZoI) that would result from antibiotic-loaded

amphiphilic gels partially diffusing through agar and interacting with bacteria added to the culture plates, using standing microbiology techniques including microscopy and microplate reader absorbance. The adapted protocols required the removal of some fraction of the normal agar gel and replacing it with drug-infused amphiphilic gel plug. After incubation time that allowed the drug to permeate into the agar from the gel, a dead zone around the plug—as typically observed—was noted as a zone of inhibition with length or radial units and as a reduced absorbance. The spatial ZoI was resolved experimentally for the VAN (3.5-3.9 cm) and GM (3.5-5.7 cm) gels studied. Mass transport of the antibiotics from F127 hydrogels suppressed bacterial growth compared to neat samples and the data of the inflection time did not show a systematic trend with antibiotic concentration.

Two different kinetic models were applied to the absorbance data tracked by the plate readers including both the Gompertz and Boltzmann models. Both models incorporated time constants allowing for an assessment of the growth rate, although the Boltzmann model also allowed for an induction time before any growth was noted. Both models appeared to fit the data reasonably well, but both the modified assay and the modeling need further refinement to gauge the suppression quantitatively. Nonetheless, the gel in biopsy plug method seems to be a promising method to determine ZoI.

5.2 Future Work

5.2.1 Structural Evolution Characteristics

The data presented in this dissertation present a more complete picture of the interaction of antibiotics formulated with amphiphilic copolymers. While CEFE showed a concentration dependent suppression in the temperature at which gels form, which is in line with other researchers probing the perturbation of micelle formation as a result of small molecule addition,

VAN was invariant with concentration. CIPRO showed an initial effect on the endotherm energy and $T_{micelle}$, but the suppression was lost at higher concentration. GM showed an invariant effect on endotherm energy, but a similar response to CEFE on $T_{micelle}$. The difference was attributed to differences in both solubility and molecular weight of the different drugs. If VAN solubility (>1 KDa) was very low due to its larger molecular weight compared to the other drugs (300-500 Da), that could explain the invariance on $T_{micelle}$ with increasing concentration. More work on the true solubility of these antibiotics and Pluronics should be completed. While DSC and rheology provide insights on the energetics of micellization and gelation, respectively, a more detailed investigation into the structural evolution is needed to have a more complete picture on the molecular interactions occurring.

Scattering studies using Small Angle X-ray Scattering (SAXS) and/or Small Angle Neutron Scattering (SANS) would inform structural changes. Scattering studies were proposed as part of the original work, but the current pandemic has made controlled experimentation at the SAXS user facilities more of a challenge. SAXS would inform changes in the micelle lattice when loaded with antibiotics and SANS would improve the scattering contrast between the micelle core and shell to determine changes in the micelle lattice that are influenced by core size or shell interactions with antibiotics. It is unfortunate that there were essentially no opportunities to probe the drug-regulated micelle formation by SAXS due to the coronavirus pandemic and the challenges with remote access at the national laboratories.

5.2.2 Elution Characteristics and Determination of MIC

A deeper analysis is needed on the elution and antimicrobial properties of antibiotic-loaded gels. Here, the selection of a true antibiotic over an inhibitor like VAN might be a more useful assessment. Live/dead staining of the plug filled tissue culture plates seemed really

promising and opting for formulating a true antibiotic might show the elution characteristics in a functional assay more clearly. Also, more direct measurements of elution using tools, such as high-performance liquid chromatography (HPLC), may provide a more direct assessment of antibiotic mobility, and linking a functional MIC to the antibiotic elution from the gels might be possible. The Gompertz model with three parameters, one of which was a time constant, was useful in assessing the kinetics of bacterial growth particularly in the presence of inhibitors; but growth still happened from the onset of incubation. A more powerful kinetic model like the four-parameter Boltzmann model with two time constants might prove more capable of distinguishing between the responses of the gel in biopsy plug assessments based on antibiotic concentration, particularly if the permeation was so extensive that there was a much longer incubation time before the onset of bacterial growth. More modeling is needed even for the rudimentary analyses that have been done here.

Finally, some level of diffusion-based finite element modeling (FEM) would be useful in developing a predictive model for assessing the rates of release and the corresponding diameter of the zone of inhibition in an agar diffusion assay. Coupling the model with experimentally determined MIC and lag time could be used as an alternative method to develop standard curves for antimicrobial assays. This approach can also be extended to quantify other pharmaceuticals and Pluronic combinations.

Appendix

The Boltzmann sigmoidal and Gompertz model were deployed using Origin. The models were fit using data for control bacterial growth sample aliquots at one hour and six hours, and 1% VAN bacterial growth sample aliquots at one hour and six hours.

The Gompertz growth model for population studies in Origin uses the equation presented in Appendix Equation 1,

$$y = ae^{-\exp(-k(x-x_c))} \quad \text{Appendix Equation 1}$$

Where *y* is the expected value of growth as a function of time, and *x,* is time, *a* represents the maximum bacterial absorbance, *k* is a growth rate coefficient (which affects the slope of the curve), and x_c represents the time at the inflection.

The Boltzman sigmoidal model in Origin uses the equation presented in Appendix Equation 2,

$$y = \frac{A_1 - A_2}{1 + e^{(x-x_0)/dx}} + A_2 \quad \text{Appendix Equation 2}$$

Where *y* is the expected value of growth as a function of time, and *x,* is time, A_1 and A_2 represent the initial and final bacterial absorbance respectively, x_0 represents the time at the inflection, and *dx* is the time constant.

Origin reported the associated parameters and statistics for the respective models used on the sample data sets are presented in Appendix Tables 1 through 12.

Gompertz Fit Control Parameters

Sample	Parameters	Value	Standard Error	*t*-Value	Prob>|*t*|	Dependency
6 hr	a	1.418	0.021	68.82	3.17E-37	0.603
6 hr	xc	0.102	0.001	82.50	8.27E-40	0.257
6 hr	k	33.819	2.079	16.27	2.53E-17	0.522
1 hr	a	1.395	0.015	93.19	1.50E-41	0.631
1 hr	xc	0.064	0.001	56.72	1.78E-34	0.277
1 hr	k	25.775	1.124	22.94	7.48E-22	0.547

Appendix Table 1 Six-hour and one-hour aliquot control sample parameters determined by Gompertz Fit in Origin.

Gompertz Fit Control Statistics

Statistics	6 hr	1 hr
Number of Points	36	36
Degrees of Freedom	33	33
Reduced Chi-Sqr	0.00276	0.00167
Residual Sum of Squares	0.09124	0.0551
R-Square (COD)	0.99212	0.99315
Adj. R-Square	0.99164	0.99274
Fit Status	Succeeded(100)	Succeeded(100)

Appendix Table 2 Six-hour and one-hour aliquot control sample statistics of Gompertz model.

Gompertz Fit Control Model

Model	SGompertz	
Equation	y = a*exp(-exp(-k*(x-xc)))	
Plot	6 hr	1 hr
a	1.41781 ± 0.0206	1.39513 ± 0.01497
xc	0.10176 ± 0.00123	0.06415 ± 0.00113
k	33.81881 ± 2.07897	25.77522 ± 1.12377
Reduced Chi-Sqr	0.00276	0.00167
R-Square (COD)	0.99212	0.99315
Adj. R-Square	0.99164	0.99274

Appendix Table 3 Six-hour and one-hour aliquot control sample Gompertz model determined by Origin.

Boltzmann Control Fit Parameters

Samples	Parameters	Value	Standard Error	*t*-Value	Prob>|*t*|	Dependency
6 hr	A1	0.018	0.017	1.05	0.30043	0.523
6 hr	A2	1.372	0.014	99.89	1.66E-41	0.417

6 hr	x0	0.114	0.001	95.11	7.93E-41	0.446
6 hr	dx	0.018	0.001	16.86	1.77E-17	0.469
6 hr	span	1.354	0.024			
6 hr	EC50	1.120	0.001			
6 hr	EC10	1.077	0.003			
6 hr	EC20	1.092	0.002			
6 hr	EC80	1.149	0.002			
6 hr	EC90	1.166	0.003			
1 hr	A1	-0.047	0.029	-1.61	0.1162	0.881
1 hr	A2	1.364	0.009	155.27	1.26E-47	0.553
1 hr	x0	0.078	0.002	50.92	3.36E-32	0.823
1 hr	dx	0.027	0.001	21.98	7.12E-21	0.764
1 hr	span	1.410	0.033			
1 hr	EC50	1.081	0.002			
1 hr	EC10	1.020	0.004			
1 hr	EC20	1.042	0.003			
1 hr	EC80	1.122	0.002			
1 hr	EC90	1.146	0.002			

Appendix Table 4 Six-hour and one-hour aliquot control sample parameters determined by Boltzmann model.

Boltzmann Control Model Statistics

Statistics	**6 hr**	**1 hr**
Number of Points	36	36
Degrees of Freedom	32	32
Reduced Chi-Sqr	0.00192	7.36E-04
Residual Sum of Squares	0.06141	0.02357
R-Square (COD)	0.9947	0.99707
Adj. R-Square	0.9942	0.9968
Fit Status	Succeeded(100)	Succeeded(100)

Appendix Table 5 Six-hour and one-hour aliquot control sample statistics of Boltzmann model.

Boltzman Control Model

Model	**Boltzmann**	
Equation	y = A2 + (A1-A2)/(1 + exp((x-x0)/dx))	
Plot	6 hr	1 hr
A1	0.01827 ± 0.01736	-0.04674 ± 0.02894
A2	1.37213 ± 0.01374	1.36355 ± 0.00878
x0	0.11356 ± 0.00119	0.07792 ± 0.00153

dx	0.0181 ± 0.00107	0.02661 ± 0.00121
Reduced Chi-Sqr	0.00192	7.36E-04
R-Square (COD)	0.9947	0.99707
Adj. R-Square	0.9942	0.9968

Appendix Table 6 Six-hour and one-hour aliquot control sample Boltzmann model determined by Origin.

Gompertz Fit 1% VAN Parameters

Sample	Parameters	Value	Standard Error	*t*-Value	Prob>|*t*|	Dependency
6 hr	a	0.205	0.002	108.28	1.08E-43	0.235
6 hr	xc	0.020	0.001	17.83	1.65E-18	0.170
6 hr	k	53.648	4.199	12.78	2.52E-14	0.285
1 hr	a	0.109	0.001	77.23	7.21E-39	0.193
1 hr	xc	0.016	0.002	10.22	9.45E-12	0.186
1 hr	k	63.652	8.024	7.93	3.79E-09	0.280

Appendix Table 7 Six-hour and one-hour aliquot 1% VAN samples parameters determined by Gompertz model.

Gompertz Fit 1% VAN Statistics

Statistics	6 hr	1 hr
Number of Points	36	36
Degrees of Freedom	33	33
Reduced Chi-Sqr	8.22E-05	5.00E-05
Residual Sum of Squares	0.00271	0.00165
R-Square (COD)	0.96755	0.91479
Adj. R-Square	0.96558	0.90963
Fit Status	Succeeded(100)	Succeeded(100)

Appendix Table 8 Six-hour and one-hour aliquot 1% VAN samples statistics of Gompertz model.

Gompertz Fit 1% VAN Model

Model	SGompertz	
Equation	y = a*exp(-exp(-k*(x-xc)))	
Plot	6 hr	1 hr
a	0.20455 ± 0.00189	0.10868 ± 0.00141
xc	0.02011 ± 0.00113	0.01582 ± 0.00155
k	53.64831 ± 4.1988	63.65237 ± 8.02417
Reduced Chi-Sqr	8.22E-05	5.00E-05
R-Square (COD)	0.96755	0.91479

Adj. R-Square	0.96558	0.90963

Appendix Table 9 Six-hour and one-hour aliquot 1% VAN samples Gompertz model determined by Origin.

Boltzman 1% VAN Parameters

Sample	Parameter	Value	Standard Error	*t*-Value	Prob>|*t*|	Dependency
6 hr	A1	0	0	--	--	0
6 hr	A2	0.204	0.002	90.353	0.000	0.187
6 hr	x0	0.028	0.001	19.418	0.000	0.101
6 hr	dx	0.014	0.001	9.726	0.000	0.113
6 hr	span	0.204	0.002			
6 hr	EC50	1.028	0.001			
6 hr	EC10	0.997	0.003			
6 hr	EC20	1.009	0.003			
6 hr	EC80	1.048	0.003			
6 hr	EC90	1.060	0.004			
1 hr	A1	-0.578	2.392	-0.242	0.811	1.000
1 hr	A2	0.109	0.001	74.126	0.000	0.384
1 hr	x0	-0.028	0.089	-0.312	0.757	1.000
1 hr	dx	0.019	0.006	3.110	0.004	0.995
1 hr	span	0.687	2.393			
1 hr	EC50	0.973	0.086			
1 hr	EC10	0.932	0.095			
1 hr	EC20	0.947	0.092			
1 hr	EC80	0.999	0.081			
1 hr	EC90	1.015	0.077			

Appendix Table 10 Six-hour and one-hour aliquot 1% VAN samples parameters determined by Boltzmann model.

Boltzmann 1% VAN Statistics

Statistics	6 hr	1 hr
Number of Points	36	36
Degrees of Freedom	33	32
Reduced Chi-Sqr	1.25E-04	4.64E-05
Residual Sum of Squares	0.00413	0.00149

R-Square (COD)	0.95058	0.92323
Adj. R-Square	0.94759	0.91603
Fit Status	Succeeded(100)	Succeeded(100)

Appendix Table 11 Six-hour and one-hour aliquot 1% VAN samples statistics of Boltzmann model.

Boltzman 1% VAN Model

Model	**Boltzmann**	
Equation	y = A2 + (A1-A2)/(1 + exp((x-x0)/dx))	
Plot	6 hr	1 hr
A1	0 ± 0	-0.57784 ± 2.39201
A2	0.20352 ± 0.00225	0.10876 ± 0.00147
x0	0.02788 ± 0.00144	-0.02769 ± 0.08882
dx	0.01391 ± 0.00143	0.01938 ± 0.00623
Reduced Chi-Sqr	1.25E-04	4.64E-05
R-Square (COD)	0.95058	0.92323
Adj. R-Square	0.94759	0.91603

Appendix Table 12 Six-hour and one-hour aliquot 1% VAN samples Boltzmann model determined by Origin.

Bibliography

[1] Y. Yang, J. Wang, X. Zhang, W. Lu, Q. Zhang, A novel mixed micelle gel with thermo-sensitive property for the local delivery of docetaxel, J. Control. Release. 135 (2009) 175–182. https://doi.org/10.1016/j.jconrel.2009.01.007.

[2] A. Pitto-Barry, N.P.E. Barry, Pluronic® block-copolymers in medicine: from chemical and biological versatility to rationalisation and clinical advances, Polym. Chem. 5 (2014) 3291–3297. https://doi.org/10.1039/C4PY00039K.

[3] A.O. Miller, M.W. Henry, B.D. Brause, Prevention of joint infections, in: Manag. Periprosthetic Jt. Infect., Elsevier, 2017: pp. 3–23. https://doi.org/10.1016/B978-0-08-100205-6.00001-X.

[4] C. Otto-Lambertz, A. Yagdiran, F. Wallscheid, P. Eysel, N. Jung, Periprosthetic infection in joint replacement - Diagnosis and treatment, Dtsch. Arztebl. Int. 114 (2017). https://doi.org/10.3238/arztebl.2017.0347.

[5] P. Izakovicova, O. Borens, A. Trampuz, Periprosthetic joint infection: current concepts and outlook, EFORT Open Rev. 4 (2019) 482–494. https://doi.org/10.1302/2058-5241.4.180092.

[6] C. Li, N. Renz, A. Trampuz, Management of Periprosthetic Joint Infection, Hip Pelvis. 30 (2018) 138. https://doi.org/10.5371/hp.2018.30.3.138.

[7] P.-H. Hsieh, K.-C. Huang, C.-L. Tai, Liquid gentamicin in bone cement spacers: in vivo antibiotic release and systemic safety in two-stage revision of infected hip arthroplasty., J. Trauma. 66 (2009) 804–8. https://doi.org/10.1097/TA.0b013e31818896cc.

[8] A. Arivazhahan, Principles and Modes of Drug Administration, in: G.M. Raj, R. Raveendran (Eds.), Introd. to Basics Pharmacol. Toxicol. Vol. 1 Gen. Mol. Pharmacol. Princ. Drug Action, Springer Singapore, Singapore, 2019: pp. 69–79. https://doi.org/10.1007/978-981-32-9779-1_4.

[9] C. Perdikouri, E. Lidén, M. Diefenbeck, COMPARISON OF SYSTEMIC AND LOCAL ADMINISTRATION OF BISPHOSPHONATES IN AN ANIMAL BONE DEFECT MODEL: THE IMPORTANCE OF LOCAL DRUG DELIVERY, Orthop. Proc. 100-B (2018) 96. https://doi.org/10.1302/1358-992X.2018.16.096.

[10] C.A. Lipinski, F. Lombardo, B.W. Dominy, P.J. Feeney, Experimental and computational approaches to estimate solubility and permeability in drug discovery and development settings 1PII of original article: S0169-409X(96)00423-1. The article was originally

published in Advanced Drug Delivery Reviews 23 (1997), Adv. Drug Deliv. Rev. 46 (2001) 3–26. https://doi.org/10.1016/S0169-409X(00)00129-0.

[11] M. Mathew, V. Das Gupta, T. Zerai, Stability of ciprofloxacin in 5% dextrose and normal saline injections, J. Clin. Pharm. Ther. 19 (1994) 261–262. https://doi.org/10.1111/j.1365-2710.1994.tb00684.x.

[12] E.F. Berbari, S.S. Kanj, T.J. Kowalski, R.O. Darouiche, A.F. Widmer, S.K. Schmitt, E.F. Hendershot, P.D. Holtom, P.M. Huddleston, G.W. Petermann, D.R. Osmon, 2015 Infectious Diseases Society of America (IDSA) Clinical Practice Guidelines for the Diagnosis and Treatment of Native Vertebral Osteomyelitis in Adultsa, Clin. Infect. Dis. 61 (2015) e26–e46. https://doi.org/10.1093/cid/civ482.

[13] H.R. Seyyed Hosseinzadeh, M. Emami, F. Lahiji, A. Sina, A. Masoudi, S. Emami, The Acrylic Bone Cement in Arthroplasty, Arthroplast. - Updat. (2013). https://doi.org/10.5772/53252.

[14] K.-D. Kühn, What is Bone Cement?, in: Well-Cemented Total Hip Arthroplast. Theory Pract., Springer Berlin Heidelberg, Berlin, Heidelberg, 2005: pp. 52–59. https://doi.org/10.1007/3-540-28924-0_5.

[15] S.C. Scherping, A.D. Aaron, Orthopedic Infections, in: S.W. Wiesel, J.N. Delahay (Eds.), Essentials Orthop. Surg., Springer New York, New York, NY, 2007: pp. 84–105. https://doi.org/10.1007/978-0-387-38328-6_3.

[16] B.J. Love, Biomaterials: A Systems Approach to Engineering Concepts, Elsevier Inc., 2017.

[17] K. Anagnostakos, Therapeutic Use of Antibiotic-loaded Bone Cement in the Treatment of Hip and Knee Joint Infections, J. Bone Jt. Infect. 2 (2017) 29–37. https://doi.org/10.7150/jbji.16067.

[18] R. Gálvez-López, A. Peña-Monje, R. Antelo-Lorenzo, J. Guardia-Olmedo, J. Moliz, J. Hernández-Quero, J. Parra-Ruiz, Elution kinetics, antimicrobial activity, and mechanical properties of 11 different antibiotic loaded acrylic bone cement, Diagn. Microbiol. Infect. Dis. 78 (2014) 70–74. https://doi.org/10.1016/j.diagmicrobio.2013.09.014.

[19] Y. He, J.P. Trotignon, B. Loty, A. Tcharkhtchi, J. Verdu, Effect of antibiotics on the properties of poly(methylmethacrylate)-based bone cement., J. Biomed. Mater. Res. 63 (2002) 800–6. https://doi.org/10.1002/jbm.10405.

[20] E.H. Immergut, H.F. Mark, Plasticization and Plasticizer Processes, 1965. https://doi.org/10.1021/ba-1965-0048.

[21] K. Anagnostakos, P. Wilmes, E. Schmitt, J. Kelm, Elution of gentamicin and vancomycin from polymethylmethacrylate beads and hip spacers in vivo., Acta Orthop. 80 (2009) 193–7. https://doi.org/10.3109/17453670902884700.

[22] A.R. Bishop, S. Kim, M.W. Squire, W.E. Rose, H.-L.L. Ploeg, Vancomycin elution, activity and impact on mechanical properties when added to orthopedic bone cement, J. Mech. Behav. Biomed. Mater. 87 (2018) 80–86. https://doi.org/10.1016/j.jmbbm.2018.06.033.

[23] M. Nugent, A. McLaren, B. Vernon, R. McLemore, Strength of antimicrobial bone cement decreases with increased poragen fraction, Clin. Orthop. Relat. Res. 468 (2010) 2101–2106. https://doi.org/10.1007/s11999-010-1264-1.

[24] K. Kanellakopoulou, E.J. Giamarellos-Bourboulis, Carrier systems for the local delivery of antibiotics in bone infections., Drugs. 59 (2000) 1223–32. https://doi.org/10.2165/00003495-200059060-00003.

[25] R.G. Bitsch, J.P. Kretzer, S. Vogt, H. Büchner, M.N. Thomsen, B. Lehner, Increased antibiotic release and equivalent biomechanics of a spacer cement without hard radio contrast agents, Diagn. Microbiol. Infect. Dis. 83 (2015) 203–209. https://doi.org/10.1016/j.diagmicrobio.2015.06.019.

[26] M.J. Penner, C.P. Duncan, B.A. Masri, The in vitro elution characteristics of antibiotic-loaded CMW and Palacos-R bone cements, J. Arthroplasty. 14 (1999) 209–214. https://doi.org/10.1016/S0883-5403(99)90128-6.

[27] J. Jackson, F. Leung, C. Duncan, C. Mugabe, H. Burt, The use of bone cement for the localized, controlled release of the antibiotics vancomycin, linezolid, or fusidic acid: Effect of additives on drug release rates and mechanical strength, Drug Deliv. Transl. Res. 1 (2011) 121–131. https://doi.org/10.1007/s13346-011-0015-5.

[28] A. Andollina, G. Bertoni, F. Bertoni, C. Zolezzi, F. Trentani, P. Trentani, A. Maria Borrelli, D. Tigani, Vancomycin and meropenem in acrylic cement: elution kinetics of in vitro bactericidal action., Chir. Organi Mov. 91 (2008) 153–8. https://doi.org/10.1007/s12306-007-0025-0.

[29] A. Lilikakis, M.P.F. Sutcliffe, The effect of vancomycin addition to the compression strength of antibiotic-loaded bone cements, Int. Orthop. 33 (2009) 815–819. https://doi.org/10.1007/s00264-008-0521-3.

[30] V. Dubee, V. Zeller, L. Lhotellier, J.-M. Ziza, P. Mamoudy, N. Desplaces, Continuous high-dose vancomycin combination therapy for methicillin-resistant staphylococcal prosthetic hip infection: a prospective cohort study, Clin. Microbiol. Infect. 19 (2013) E98–E105.

[31] S.J. Dolin, Drugs and pharmacology, in: N.L. Padfield (Ed.), Total Intraven. Anesth., 2nd ed., Butterworth-Heinemann, Oxford, 2000: pp. 13–35.

[32] C. Mircioiu, V. Voicu, V. Anuta, A. Toduse, C. Celia, D. Paolino, M. Fresta, R. Sandulovici, I. Mircioiu, Mathematical Modeling of Release Kinetics from Supramolecular Drug Delivery Systems, Pharmaceutics. 11 (2019) 140.

[33] K.S. Estes, H. Derendorf, Comparison of the pharmacokinetic properties of vancomycin, linezolid, tigecyclin, and daptomycin, Eur. J. Med. Res. 15 (2010) 533. https://doi.org/10.1186/2047-783X-15-12-533.

[34] T. Gehrke, G. von Förster, L. Frommelt, Pharmacokinetic Study of a Gentamicin/Clindamicin Bone Cement Used in One-stage Revision Arthroplasty, in: Bone Cem. Cem. Tech., Springer Berlin Heidelberg, Berlin, Heidelberg, 2001: pp. 127–134. https://doi.org/10.1007/978-3-642-59478-6_11.

[35] D.O. Kendoff, T. Gehrke, P. Stangenberg, L. Frommelt, H. Bösebeck, Bioavailability of Gentamicin and Vancomycin Released from an Antibiotic Containing Bone Cement in Patients Undergoing a Septic One-Stage Total Hip Arthroplasty (THA) Revision: A Monocentric Open Clinical Trial, HIP Int. 26 (2016) 90–96. https://doi.org/10.5301/hipint.5000307.

[36] A.S. Lubin, D.R. Snydman, R. Ruthazer, P. Bide, Y. Golan, Predicting High Vancomycin Minimum Inhibitory Concentration in Methicillin-Resistant Staphylococcus aureus Bloodstream Infections, Clin. Infect. Dis. 52 (2011) 997–1002. https://doi.org/10.1093/cid/cir118.

[37] S.J. van Hal, T.P. Lodise, D.L. Paterson, The Clinical Significance of Vancomycin Minimum Inhibitory Concentration in Staphylococcus aureus Infections: A Systematic Review and Meta-analysis, Clin. Infect. Dis. 54 (2012) 755–771. https://doi.org/10.1093/cid/cir935.

[38] K.-H. Song, M. Kim, C.J. Kim, J.E. Cho, Y.J. Choi, J.S. Park, S. Ahn, H.-C. Jang, K.-H. Park, S.-I. Jung, N. Yoon, D.-M. Kim, J.-H. Hwang, C.S. Lee, J.H. Lee, Y.G. Kwak, E.S. Kim, S.Y. Park, Y. Park, K.S. Lee, Y.-S. Lee, H. Bin Kim, Impact of Vancomycin MIC on Treatment Outcomes in Invasive Staphylococcus aureus Infections, Antimicrob. Agents Chemother. 61 (2017). https://doi.org/10.1128/AAC.01845-16.

[39] R. Bettini, P. Colombo, G. Massimo, P.L. Catellani, T. Vitali, Swelling and drug release in hydrogel matrices: polymer viscosity and matrix porosity effects, Eur. J. Pharm. Sci. 2 (1994) 213–219. https://doi.org/10.1016/0928-0987(94)90025-6.

[40] M.V.S. Varma, A.M. Kaushal, A. Garg, S. Garg, Factors Affecting Mechanism and Kinetics of Drug Release from Matrix-Based Oral Controlled Drug Delivery Systems, Am. J. Drug Deliv. 2 (2004) 43–57. https://doi.org/10.2165/00137696-200402010-00003.

[41] J. Klekamp, J.M. Dawson, D.W. Haas, D. DeBoer, M. Christie, The use of vancomycin and tobramycin in acrylic bone cement, J. Arthroplasty. 14 (1999) 339–346. https://doi.org/10.1016/S0883-5403(99)90061-X.

[42] B.A. Masri, C.P. Duncan, C.P. Beauchamp, N.J. Paris, J. Arntorp, Effect of varying surface patterns on antibiotic elution from antibiotic-loaded bone cement, J. Arthroplasty. 10 (1995) 453–459. https://doi.org/10.1016/S0883-5403(05)80145-7.

[43] J. Gogia, J. Meehan, P. Di Cesare, A. Jamali, Local Antibiotic Therapy in Osteomyelitis,

Semin. Plast. Surg. 23 (2009) 100–107. https://doi.org/10.1055/s-0029-1214162.

[44] F.A. Al-Mulhim, M.A. Baragbah, M. Sadat-Ali, A.S. Alomran, M.Q. Azam, Prevalence of surgical site infection in orthopedic surgery: A 5-year analysis, Int. Surg. 99 (2014) 264–268. https://doi.org/10.9738/INTSURG-D-13-00251.1.

[45] C. Jigar, C. Harshil, Treatment of Prosthetic Joint Infection Following Total Knee Arthroplasty: Current Review OPEN ACCESS, 2018.

[46] V. Ajit Singh, B. Chun Haw, A. Haseeb, C. Shuan Ju Teh, Hand-mixed vancomycin versus commercial tobramycin cement revisited: A study on mechanical and antibacterial properties, J. Orthop. Surg. 27 (2019) 230949901983961. https://doi.org/10.1177/2309499019839616.

[47] A.U. Dan Daniels, D. Wirz, E. Morscher, Extreme Differences in Properties of Successful Bone Cements, in: Well-Cemented Total Hip Arthroplast. Theory Pract., Springer Berlin Heidelberg, Berlin, Heidelberg, 2005: pp. 79–85. https://doi.org/10.1007/3-540-28924-0_8.

[48] S. Kurtz, K. Ong, E. Lau, F. Mowat, M. Halpern, Projections of Primary and Revision Hip and Knee Arthroplasty in the United States from 2005 to 2030, J. Bone Jt. Surg. 89 (2007) 780–785. https://doi.org/10.2106/JBJS.F.00222.

[49] V.C. de Carvalho, P.R.D. de Oliveira, K. Dal-Paz, A.P. de Paula, C. da S. Félix, A.L.L. Munhoz Lima, Gram-negative osteomyelitis: clinical and microbiological profile, Brazilian J. Infect. Dis. 16 (2012) 63–67. https://doi.org/10.1016/S1413-8670(12)70276-3.

[50] D.U. Park, J.K. Yeom, W.J. Lee, K.M. Lee, Assessment of the levels of airborne bacteria, gram-negative bacteria, and fungi in hospital lobbies, Int. J. Environ. Res. Public Health. 10 (2013) 541–555. https://doi.org/10.3390/ijerph10020541.

[51] L.M. Mensah, B.J. Love, A meta-analysis of bone cement mediated antibiotic release: Overkill, but a viable approach to eradicate osteomyelitis and other infections tied to open procedures, Mater. Sci. Eng. C. 123 (2021) 111999. https://doi.org/10.1016/j.msec.2021.111999.

[52] S.H. Lee, C.L. Tai, S.Y. Chen, C.H. Chang, Y.H. Chang, P.H. Hsieh, Elution and mechanical strength of vancomycin-loaded bone cement: In vitro study of the influence of brand combination, PLoS One. 11 (2016) e0166545. https://doi.org/10.1371/journal.pone.0166545.

[53] H. van De Belt, D. Neut, W. Schenk, J.R. van Horn, H.C. van Der Mei, H.J. Busscher, Gentamicin release from polymethylmethacrylate bone cements and Staphylococcus aureus biofilm formation, Acta Orthop. Scand. 71 (2000) 625–629. https://doi.org/10.1080/000164700317362280.

[54] X. Huang, C.S. Brazel, On the importance and mechanisms of burst release in matrix-controlled drug delivery systems, J. Control. Release. 73 (2001) 121–136.

https://doi.org/10.1016/S0168-3659(01)00248-6.

[55] T.A. Ahmed, Pharmacokinetics of Drugs Following IV Bolus, IV Infusion, and Oral Administration, in: Basic Pharmacokinet. Concepts Some Clin. Appl., InTech, 2015. https://doi.org/10.5772/61573.

[56] J. Fan, I.A.M. de Lannoy, Pharmacokinetics, Biochem. Pharmacol. 87 (2014) 93–120. https://doi.org/10.1016/j.bcp.2013.09.007.

[57] A.R. Bishop, S. Kim, M.W. Squire, W.E. Rose, H.L. Ploeg, Vancomycin elution, activity, and impact on mechanical properties when added to orthopedic bone cement, J. Mec. Behav. Biomed. Mater. 87 (2018) 80–86.

[58] A.L. Thompson, A.N. Ball, B.J. Love, Controlled Release Characteristics of Aqueous PEO-PPO-PEO Micelles With Added Malachite Green, Erythrosin, and Cisplatin Determined by UV-Visible Spectroscopy, J. Surfactants Deterg. 21 (2018) 5–15. https://doi.org/10.1002/jsde.12001.

[59] Astm, Standard specification for acrylic bone cement, ASTM Int. (2010) DOI: 10.1520/F451-08. https://doi.org/10.1520/F0451-08.2.

[60] R.E. Duey, A.C.M. Chong, D.A. McQueen, J.L. Womack, Z. Song, T.A. Steinberger, P.H. Wooley, Mechanical properties and elution characteristics of polymethylmethacrylate bone cement impregnated with antibiotics for various surface area and volume constructs., Iowa Orthop. J. 32 (2012) 104–15. https://www.ncbi.nlm.nih.gov/pubmed/23576930 (accessed September 2, 2019).

[61] A. Klinder, S. Zaatreh, M. Ellenrieder, S. Redanz, A. Podbielski, T. Reichel, H. Bösebeck, W. Mittelmeier, R. Bader, Antibiotics release from cement spacers used for two-stage treatment of implant-associated infections after total joint arthroplasty, J. Biomed. Mater. Res. Part B Appl. Biomater. 107 (2019) 1587–1597. https://doi.org/10.1002/jbm.b.34251.

[62] K. Anagnostakos, C. Meyer, Antibiotic Elution from Hip and Knee Acrylic Bone Cement Spacers: A Systematic Review, Biomed Res. Int. 2017 (2017) 1–7. https://doi.org/10.1155/2017/4657874.

[63] S.K. Nandi, S. Bandyopadhyay, P. Das, I. Samanta, P. Mukherjee, S. Roy, B. Kundu, Understanding osteomyelitis and its treatment through local drug delivery system, Biotechnol. Adv. 34 (2016) 1305–1317. https://doi.org/10.1016/j.biotechadv.2016.09.005.

[64] M.. Veyries, G. Couarraze, S. Geiger, F. Agnely, L. Massias, B. Kunzli, F. Faurisson, B. Rouveix, Controlled release of vancomycin from Poloxamer 407 gels, Int. J. Pharm. 192 (1999) 183–193. https://doi.org/10.1016/S0378-5173(99)00307-5.

[65] W.A. Jiranek, A.D. Hanssen, A.S. Greenwald, Antibiotic-Loaded Bone Cement for Infection Prophylaxis in Total Joint Replacement, J. Bone Jt. Surg. 88 (2006) 2487–2500. https://doi.org/10.2106/JBJS.E.01126.

[66] A.O. Kshetry, N.D. Pant, R. Bhandari, S. Khatri, K.L. Shrestha, S.K. Upadhaya, A. Poudel, B. Lekhak, B.R. Raghubanshi, Minimum inhibitory concentration of vancomycin to methicillin resistant Staphylococcus aureus isolated from different clinical samples at a tertiary care hospital in Nepal, Antimicrob. Resist. Infect. Control. 5 (2016). https://doi.org/10.1186/s13756-016-0126-3.

[67] M.O. Avilés, L.D. Shea, Hydrogels to modulate lentivirus delivery in vivo from microporous tissue engineering scaffolds, Drug Deliv. Transl. Res. 1 (2011) 91–101. https://doi.org/10.1007/s13346-010-0011-1.

[68] G. Tiwari, R. Tiwari, S. Bannerjee, L. Bhati, S. Pandey, P. Pandey, B. Sriwastawa, Drug delivery systems: An updated review, Int. J. Pharm. Investig. 2 (2012) 2. https://doi.org/10.4103/2230-973X.96920.

[69] A. Rastogi, P.D. Bowman, S. Stavchansky, Evaluation of a perforated drug delivery system in mice for prolonged and constant release of a hydrophilic drug, Drug Deliv. Transl. Res. 2 (2012) 106–111. https://doi.org/10.1007/s13346-012-0062-6.

[70] J.A. Inzana, E.M. Schwarz, S.L. Kates, H.A. Awad, Biomaterials approaches to treating implant-associated osteomyelitis, Biomaterials. 81 (2016) 58–71. https://doi.org/10.1016/j.biomaterials.2015.12.012.

[71] C.A. Ford, J.E. Cassat, Advances in the local and targeted delivery of anti-infective agents for management of osteomyelitis, Expert Rev. Anti. Infect. Ther. 15 (2017) 851–860. https://doi.org/10.1080/14787210.2017.1372192.

[72] J.Y. Ferguson, M. Dudareva, N.D. Riley, D. Stubbs, B.L. Atkins, M.A. McNally, The use of a biodegradable antibiotic-loaded calcium sulphate carrier containing tobramycin for the treatment of chronic osteomyelitis, Bone Joint J. 96-B (2014) 829–836. https://doi.org/10.1302/0301-620X.96B6.32756.

[73] M.D. McKee, E.A. Li-Bland, L.M. Wild, E.H. Schemitsch, A Prospective, Randomized Clinical Trial Comparing an Antibiotic-Impregnated Bioabsorbable Bone Substitute With Standard Antibiotic-Impregnated Cement Beads in the Treatment of Chronic Osteomyelitis and Infected Nonunion, J. Orthop. Trauma. 24 (2010) 483–490. https://doi.org/10.1097/BOT.0b013e3181df91d9.

[74] N. Fleiter, G. Walter, H. Bösebeck, S. Vogt, H. Büchner, W. Hirschberger, R. Hoffmann, Clinical use and safety of a novel gentamicin-releasing resorbable bone graft substitute in the treatment of osteomyelitis/osteitis, Bone Joint Res. 3 (2014) 223–229. https://doi.org/10.1302/2046-3758.37.2000301.

[75] Z. Li, C. He, B. Yuan, X. Dong, X. Chen, Injectable Polysaccharide Hydrogels as Biocompatible Platforms for Localized and Sustained Delivery of Antibiotics for Preventing Local Infections, Macromol. Biosci. 17 (2017) 1600347. https://doi.org/10.1002/mabi.201600347.

[76] J. Hoque, B. Bhattacharjee, R.G. Prakash, K. Paramanandham, J. Haldar, Dual Function

Injectable Hydrogel for Controlled Release of Antibiotic and Local Antibacterial Therapy, Biomacromolecules. 19 (2018) 267–278. https://doi.org/10.1021/acs.biomac.7b00979.

[77] Z. Zhou, J. Seta, D.C. Markel, W. Song, S.M. Yurgelevic, X.W. Yu, W. Ren, Release of vancomycin and tobramycin from polymethylmethacrylate cements impregnated with calcium polyphosphate hydrogel, J. Biomed. Mater. Res. Part B Appl. Biomater. 106 (2018) 2827–2840. https://doi.org/10.1002/jbm.b.34063.

[78] N.A.K. Meznarich, K.A. Juggernauth, K.M. Batzli, B.J. Love, Structural Changes in PEO–PPO–PEO Gels Induced by Methylparaben and Dexamethasone Observed Using Time-Resolved SAXS, Macromolecules. 44 (2011) 7792–7798. https://doi.org/10.1021/ma2015358.

[79] D. Overstreet, A. McLaren, F. Calara, B. Vernon, R. McLemore, Local Gentamicin Delivery From Resorbable Viscous Hydrogels Is Therapeutically Effective, Clin. Orthop. Relat. Res. 473 (2015) 337–347. https://doi.org/10.1007/s11999-014-3935-9.

[80] A.L. Thompson, L.M. Mensah, B.J. Love, The effect of cisplatin on the nanoscale structure of aqueous PEO–PPO–PEO micelles of varying hydrophilicity observed using SAXS, Soft Matter. 15 (2019) 3970–3977. https://doi.org/10.1039/C9SM00071B.

[81] N.A.K. Meznarich, B.J. Love, The Kinetics of Gel Formation for PEO−PPO−PEO Triblock Copolymer Solutions and the Effects of Added Methylparaben, Macromolecules. 44 (2011) 3548–3555. https://doi.org/10.1021/ma200302s.

[82] A.L. Thompson, B.J. Love, Thermodynamic properties of aqueous PEO–PPO–PEO micelles with added methylparaben determined by differential scanning calorimetry, J. Colloid Interface Sci. 398 (2013) 270–272. https://doi.org/10.1016/j.jcis.2013.01.064.

[83] N. Patel, P. Lubanski, S. Ferro, M. Bonafede, S. Harrington, A. Evans, K. Stellrecht, T.P. Lodise, Correlation between vancomycin MIC values and those of other agents against gram-positive bacteria among patients with bloodstream infections caused by methicillin-resistant Staphylococcus aureus, Antimicrob. Agents Chemother. 53 (2009) 5141–5144. https://doi.org/10.1128/AAC.00307-09.

[84] A. Kabanov, J. Zhu, V. Alakhov, Pluronic block copolymers for gene delivery., Adv. Genet. 53 (2005) 231–61. http://www.ncbi.nlm.nih.gov/pubmed/16240996.

[85] Rb. Mustapha, S. Lafforgue, N. Fenina, J. Marty, Influence of drug concentration on the diffusion parameters of caffeine, Indian J. Pharmacol. 43 (2011) 157. https://doi.org/10.4103/0253-7613.77351.

[86] E.. Ricci, M.V.L.. Bentley, M. Farah, R.E.. Bretas, J.. Marchetti, Rheological characterization of Poloxamer 407 lidocaine hydrochloride gels, Eur. J. Pharm. Sci. 17 (2002) 161–167. https://doi.org/10.1016/S0928-0987(02)00166-5.

[87] I.R. Schmolka, AMPHOTERIC SURFACTANT GELS, 3925241, 1975.

[88] M. VADNERE, G. AMIDON, S. LINDENBAUM, J. HASLAM, Thermodynamic studies on the gel-sol transition of some pluronic polyols, Int. J. Pharm. 22 (1984) 207–218. https://doi.org/10.1016/0378-5173(84)90022-X.

[89] R.E. Goldstein, Model for phase equilibria in micellar solutions of nonionic surfactants, J. Chem. Phys. 84 (1986) 3367–3378. https://doi.org/10.1063/1.450272.

[90] G. Wanka, H. Hoffmann, W. Ulbricht, The aggregation behavior of poly-(oxyethylene)-poly-(oxypropylene)-poly-(oxyethylene)-block-copolymers in aqueous solution, Colloid Polym. Sci. 268 (1990) 101–117. https://doi.org/10.1007/BF01513189.

[91] R.K. Prud'homme, G. Wu, D.K. Schneider, Structure and Rheology Studies of Poly(oxyethylene−oxypropylene−oxyethylene) Aqueous Solution, Langmuir. 12 (1996) 4651–4659. https://doi.org/10.1021/la951506b.

[92] P. Alexandridis, V. Athanassiou, T.A. Hatton, Pluronic-P105 PEO-PPO-PEO Block Copolymer in Aqueous Urea Solutions: Micelle Formation, Structure, and Microenvironment, Langmuir. 11 (1995) 2442–2450. https://doi.org/10.1021/la00007a022.

[93] P. Alexandridis, J.F. Holzwarth, T.A. Hatton, Micellization of Poly(ethylene oxide)-Poly(propylene oxide)-Poly(ethylene oxide) Triblock Copolymers in Aqueous Solutions: Thermodynamics of Copolymer Association, Macromolecules. 27 (1994) 2414–2425. https://doi.org/10.1021/ma00087a009.

[94] C. Chaibundit, N.M.P.S. Ricardo, F. de M.L.L. Costa, S.G. Yeates, C. Booth, Micellization and Gelation of Mixed Copolymers P123 and F127 in Aqueous Solution, Langmuir. 23 (2007) 9229–9236. https://doi.org/10.1021/la701157j.

[95] C. Chaibundit, N.M.P.S. Ricardo, N.M.P.S. Ricardo, B.M.D. O'Driscoll, I.W. Hamley, S.G. Yeates, C. Booth, Aqueous Gels of Mixtures of Ionic Surfactant SDS with Pluronic Copolymers P123 or F127 †, Langmuir. 25 (2009) 13776–13783. https://doi.org/10.1021/la901584u.

[96] J. Jiang, C. Li, J. Lombardi, R.H. Colby, B. Rigas, M.H. Rafailovich, J.C. Sokolov, The effect of physiologically relevant additives on the rheological properties of concentrated Pluronic copolymer gels, Polymer (Guildf). 49 (2008) 3561–3567. https://doi.org/10.1016/j.polymer.2008.05.038.

[97] D.C. Pozzo, L.M. Walker, Small-angle neutron scattering of silica nanoparticles templated in PEO–PPO–PEO cubic crystals, Colloids Surfaces A Physicochem. Eng. Asp. 294 (2007) 117–129. https://doi.org/10.1016/j.colsurfa.2006.08.002.

[98] M. Scherlund, A. Brodin, M. Malmsten, Micellization and gelation in block copolymer systems containing local anesthetics, Int. J. Pharm. 211 (2000) 37–49. https://doi.org/10.1016/S0378-5173(00)00589-5.

[99] P.K. Sharma, M.J. Reilly, S.K. Bhatia, N. Sakhitab, J.D. Archambault, S.R. Bhatia, Effect

of pharmaceuticals on thermoreversible gelation of PEO–PPO–PEO copolymers, Colloids Surfaces B Biointerfaces. 63 (2008) 229–235. https://doi.org/10.1016/j.colsurfb.2007.12.009.

[100] I.R. Schmolka, Artificial skin I. Preparation and properties of pluronic F-127 gels for treatment of burns, J. Biomed. Mater. Res. 6 (1972) 571–582. https://doi.org/10.1002/jbm.820060609.

[101] L.-J. Chen, S.-Y. Lin, C.-C. Huang, Effect of Hydrophobic Chain Length of Surfactants on Enthalpy−Entropy Compensation of Micellization, J. Phys. Chem. B. 102 (1998) 4350–4356. https://doi.org/10.1021/jp9804345.

[102] R. Lumry, S. Rajender, Enthalpy-entropy compensation phenomena in water solutions of proteins and small molecules: A ubiquitous properly of water, Biopolymers. 9 (1970) 1125–1227. https://doi.org/10.1002/bip.1970.360091002.

[103] R. Basak, R. Bandyopadhyay, Encapsulation of Hydrophobic Drugs in Pluronic F127 Micelles: Effects of Drug Hydrophobicity, Solution Temperature, and pH, Langmuir. 29 (2013) 4350–4356. https://doi.org/10.1021/la304836e.

[104] A.M. Bodratti, P. Alexandridis, Formulation of poloxamers for drug delivery, J. Funct. Biomater. 9 (2018). https://doi.org/10.3390/jfb9010011.

[105] A.L. Thompson, B.J. Love, Thermodynamic properties of aqueous PEO–PPO–PEO micelles of varying hydrophilicity with added cisplatin determined by differential scanning calorimetry, J. Therm. Anal. Calorim. 127 (2017) 1583–1592. https://doi.org/10.1007/s10973-016-5411-0.

[106] E. Sikorska, D. Wyrzykowski, K. Szutkowski, K. Greber, E.A. Lubecka, I. Zhukov, Thermodynamics, size, and dynamics of zwitterionic dodecylphosphocholine and anionic sodium dodecyl sulfate mixed micelles, J. Therm. Anal. Calorim. 123 (2016) 511–523. https://doi.org/10.1007/s10973-015-4918-0.

[107] S. Giovagnoli, T. Tsai, P.P. DeLuca, Formulation and Release Behavior of Doxycycline–Alginate Hydrogel Microparticles Embedded into Pluronic F127 Thermogels as a Potential New Vehicle for Doxycycline Intradermal Sustained Delivery, AAPS PharmSciTech. 11 (2010) 212–220. https://doi.org/10.1208/s12249-009-9361-8.

[108] L.-S. Yap, M.-C. Yang, Evaluation of hydrogel composing of Pluronic F127 and carboxymethyl hexanoyl chitosan as injectable scaffold for tissue engineering applications, Colloids Surfaces B Biointerfaces. 146 (2016) 204–211. https://doi.org/10.1016/j.colsurfb.2016.05.094.

[109] R.G. Larson, 5.2.3 Fractals and Self-Similarity, in: Struct. Rheol. Complex Fluids, Oxford University Press, 1999: pp. 238–243. https://app.knovel.com/hotlink/pdf/id:kt00U0SEN1/structure-rheology-complex/fractals-self-similarity BT - Structure and Rheology of Complex Fluids.

[110] H.H. Winter, Can the gel point of a cross-linking polymer be detected by theG? -G? crossover?, Polym. Eng. Sci. 27 (1987) 1698–1702. https://doi.org/10.1002/pen.760272209.

[111] K. Bouchemal, F. Agnely, A. Koffi, G. Ponchel, A concise analysis of the effect of temperature and propanediol-1, 2 on Pluronic F127 micellization using isothermal titration microcalorimetry, J. Colloid Interface Sci. 338 (2009) 169–176. https://doi.org/10.1016/j.jcis.2009.05.075.

[112] J.C. Gilbert, C. Washington, M.C. Davies, J. Hadgraft, The behaviour of Pluronic F127 in aqueous solution studied using fluorescent probes, Int. J. Pharm. 40 (1987) 93–99. https://doi.org/10.1016/0378-5173(87)90052-4.

[113] Q. Gao, Q. Liang, F. Yu, J. Xu, Q. Zhao, B. Sun, Synthesis and characterization of novel amphiphilic copolymer stearic acid-coupled F127 nanoparticles for nano-technology based drug delivery system, Colloids Surfaces B Biointerfaces. 88 (2011) 741–748. https://doi.org/10.1016/j.colsurfb.2011.08.010.

[114] R. Nagarajan, K. Ganesh, Block copolymer self-assembly in selective solvents: theory of solubilization in spherical micelles, Macromolecules. 22 (1989) 4312–4325. https://doi.org/10.1021/ma00201a029.

[115] R. Nagarajan, Solubilization of hydrocarbons and resulting aggregate shape transitions in aqueous solutions of Pluronic® (PEO–PPO–PEO) block copolymers, Colloids Surfaces B Biointerfaces. 16 (1999) 55–72. https://doi.org/10.1016/S0927-7765(99)00061-2.

[116] J.E. Matthew, Y.L. Nazario, S.C. Roberts, S.R. Bhatia, Effect of mammalian cell culture medium on the gelation properties of Pluronic® F127, Biomaterials. 23 (2002) 4615–4619. https://doi.org/10.1016/S0142-9612(02)00208-9.

[117] G. Dumortier, J.L. Grossiord, F. Agnely, J.C. Chaumeil, A Review of Poloxamer 407 Pharmaceutical and Pharmacological Characteristics, Pharm. Res. 23 (2006) 2709–2728. https://doi.org/10.1007/s11095-006-9104-4.

[118] M. Callan, E. Jang, J. Kelly, K. Nguyen, C. Marmorat, M. Rafailovich, Characterization of Pluronic F127 for the Controlled DrugRelease Vancomycin in the Spinal Column, J. Undergrad. Chem. Eng. Res. 6 (2017) 9–19. https://cpb-us-e1.wpmucdn.com/you.stonybrook.edu/dist/f/2071/files/2017/04/1-Kim-F127-Pg-9-19-y289nt.pdf.

[119] W. LI, J. ZHOU, Y. XU, Study of the in vitro cytotoxicity testing of medical devices, Biomed. Reports. 3 (2015) 617–620. https://doi.org/10.3892/br.2015.481.

[120] A.L. Barry, M.B. Coyle, C. Thornsberry, E.H. Gerlach, R.W. Hawkinson, Methods of measuring zones of inhibition with the Bauer-Kirby disk susceptibility test, J. Clin. Microbiol. 10 (1979) 885–889. https://doi.org/10.1128/JCM.10.6.885-889.1979.

[121] H. Dickert, K. Machka, I. Braveny, The uses and limitations of disc diffusion in the

antibiotic sensitivity testing of bacteria, Infection. 9 (1981) 18–24. https://doi.org/10.1007/BF01640803.

[122] V.R. Krishnamurthi, I.I. Niyonshuti, J. Chen, Y. Wang, A new analysis method for evaluating bacterial growth with microplate readers, PLoS One. 16 (2021) e0245205. https://doi.org/10.1371/journal.pone.0245205.

[123] CLSI, Performance Standards for Antimicrobial Susceptibility Testing, in: Clinical and Laboratory Standards Institute (Ed.), CLSI Suppl. M100, 31st ed., 2021. http://em100.edaptivedocs.net/GetDoc.aspx?doc=CLSI M100 ED31:2021&sbssok=CLSI M100 ED31:2021 TABLE 2C&format=HTML#CLSI M100 ED31:2021 TABLE 2C.

[124] B. Gompertz, XXIV. On the nature of the function expressive of the law of human mortality, and on a new mode of determining the value of life contingencies. In a letter to Francis Baily, Esq. F. R. S. &c, Philos. Trans. R. Soc. London. 115 (1825) 513–583. https://doi.org/10.1098/rstl.1825.0026.

[125] C.J. JEFFERIES, P. BRAIN, K.G. STOTT, A.R. BELCHER, Experimental systems and a mathematical model for studying temperature effects on pollen-tube growth and fertilization in plum, Plant. Cell Environ. 5 (1982) 231–236. https://doi.org/10.1111/1365-3040.ep11572417.

[126] M.D. Rolfe, C.J. Rice, S. Lucchini, C. Pin, A. Thompson, A.D.S. Cameron, M. Alston, M.F. Stringer, R.P. Betts, J. Baranyi, M.W. Peck, J.C.D. Hinton, Lag Phase Is a Distinct Growth Phase That Prepares Bacteria for Exponential Growth and Involves Transient Metal Accumulation, J. Bacteriol. 194 (2012) 686–701. https://doi.org/10.1128/JB.06112-11.

[127] B. Li, Y. Qiu, H. Shi, H. Yin, The importance of lag time extension in determining bacterial resistance to antibiotics, Analyst. 141 (2016) 3059–3067. https://doi.org/10.1039/C5AN02649K.

[128] E. Desmond-Le Quéméner, T. Bouchez, A thermodynamic theory of microbial growth, ISME J. 8 (2014) 1747–1751. https://doi.org/10.1038/ismej.2014.7.

[129] A.L. Navarro-Verdugo, F.M. Goycoolea, G. Romero-Meléndez, I. Higuera-Ciapara, W. Argüelles-Monal, A modified Boltzmann sigmoidal model for the phase transition of smart gels, Soft Matter. 7 (2011) 5847. https://doi.org/10.1039/c1sm05252g.

[130] A. El Aferni, M. Guettari, T. Tajouri, Mathematical model of Boltzmann's sigmoidal equation applicable to the spreading of the coronavirus (Covid-19) waves, Environ. Sci. Pollut. Res. (2020). https://doi.org/10.1007/s11356-020-11188-y.